Frequency-specific functional network of the resting brain

安静時脳における周波数特異的な機能的ネットワーク

A dissertation presented

by

Shuntaro Sasai

笹井俊太朗

to

Division of Physical and Health Education
Graduate School of Education

in partial fulfillment of the requirements
for the degree of
Doctor of Philosophy
in the subject of
Education

The University of Tokyo

May, 2013

Acknowledgement

Many people supported me directly or indirectly to undertake and complete my PhD projects, and to produce this thesis. I could not have finished all of my doctoral works without their valuable guidance and assistance, and, for this, I would like to sincerely thank them.

First of all, I wish to thank my supervisor, Professor Gentaro Taga, for his enormous supports over five years in graduate school. He always provided suggestions, with enthusiasm, and guidance with my various projects. He also taught me the importance of thinking twice about my researches. He also demonstrated how he thinks about the world, how he generates his hypotheses, how he verifies the hypotheses, and how he reaches his conclusions, sometimes by taking a long time that seemed like endless time for me. Thanks to his distinguished and sympathetic guidance, I could have carefully finished all of the projects introduced in this thesis, while being aware of that the scientific findings are bred by a lot of failures and new inspirations drawn from substantial efforts.

I also wish to thank Drs. Hama Watanabe and Fumitaka Homae for also providing me with enormous assistances and advices. Dr. Watanabe taught me not only many things about science but also the importance of completing works on time. Although I'm still poor at finishing all of my works as scheduled, thanks to her assistance, I was able to execute my projects very smoothly. Dr. Homae is also brilliant scientist, and provided me enormous invaluable advice. I respect his attitude toward science: He can advance studies with a great deal of subtlety. His comments repeatedly impressed me and often helped me to improve my crude views on findings and rough appearances of research papers.

As a student of the division of physical and health education, I could stay in the wonderful circumstance to advance my projects. I would like to thank Drs. Masaya Hirashima, Kenji Morita, Fumiharu Togo, Daichi Nozaki, Tsukasa Sasaki and Yoshiharu Yamamoto for all of their helpful advice in the research meetings. Their expertise comments always provided good opportunities for me to rethink the meaning of my project. I would like to thank Ms. Kayo Asakawa for her technical and administrative

assistance. Mr. Ichiro Hidaka, Drs. Shinya Fujii, Hiroshi Kadota, Masanori Shimono and Toru Nakamura provided me with much advice concerning the data analyses. To my senior graduate students, I would like to thank Drs. Takuya Honda, Tsuyoshi Ikegami, Akifumi Kishi, Shoko Kasuga, and Atsushi Yokoi for their help and support in my projects. Needless to say, encouragement from my colleagues was essential to finish my projects. I would like to thank Takuji Hayashi, Makiko Imai, Nao Kanemaru, Moe Kato, Jinhyuk Kim, Yuko Kitagawa, Yoshio Kobayashi, Misato Matamura, Hiroki Ohashi, Yasuki Okamoto, Yasutaka Ojio, and Gaku Yamawaki for their encouragement.

I would like to thank Dr. Norihiro Sadato for his help. He gave me the opportunity to simultaneously measure NIRS and fMRI. He also provided a lot of helpful comments that advanced and strengthened my projects. Without generous support for my projects, I could not prosecute large parts of my PhD projects. In the simultaneous recording, fMRI scanning was conducted by Drs. Akihiro Sasaki and Hiroki Tanabe. I also would like to thank them for their help.

Finally, I would like to thank my parents and my wife. They always quietly accepted the inconvenient fact that I was always crazy to do something they could not understand, and supported me to tackle my own problems in the PhD project. I would like to give a special thanks to them for their encouragement and assistance that they had provided for me to complete my study and my thesis.

Table of contents

List of Figures

List of Tables

Chapter 1 General introduction

1.1 Background

1.1.1 Motivation

From ancient times, humans have asked themselves, "who are we?" The answer to this question has been sought in the field of metaphysical philosophy. In his book *Discourse on Method*, René Descartes advocated the idea of self with his statement, “Cogito ergo sum,” or, “I think therefore I am” (Cottingham et al., 1985). In 1861, Pierre Paul Broca observed that patients who suffered a stroke in the left frontal lobe often lost their ability to speak, but they could still understand language (Broca, 1861). This finding of Broca supported the idea that the brain plays an important role in our ability to form language, and this indicated where the brain’s language functions are distributed. Broca’s observation encouraged subsequent investigations on the relationship between the mind and the brain. This research field has evolved into the modern discipline of neuroscience. Neuroscience has established a strong position in the study of human nature, which has accumulated a plethora of evidence that supports the idea that the brain takes charge of behavior, faculty of mind, and consciousness. Thus, I believe that humans can get closer to answering, “who are we?” by using scientific methods to determine the operational principles of the brain.

1.1.2 How do we study the brain?

How can we determine an operational principle for the brain? Classically, the relationship between the mind and brain has been investigated by using the “subtraction” method, which is the basis

for the idea of functional brain mapping (Raichle and Snyder, 2007). This method exploits a simple premise on the relationship between mental operations and brain regions: a brain region that takes charge of a specific mental operation must be activated by execution of the mental operation. For example, when we open our eyes, we passively develop visual awareness of external objects. In this case, the idea of functional brain mapping implies that there is a brain region that processes visual information from the eyes and produces awareness of visual objects. The reverse relationship is also implied: when we close our eyes, we lose visual awareness of external objects and the corresponding brain region no longer processes information from the external environment. The functional brain mapping hypothesis also implies that the activity in a brain region increases as the information processing increases to perform the mental function. Finally, we can investigate which part of our brain participates in visual processing through experimentation: when we open and close our eyes, the activity in the brain region playing a role in visual processing should increase and decrease, respectively. In fact, functional magnetic resonance imaging (fMRI) signals obtained from the occipital cortical areas, or the primary visual areas, show significant increases and decreases when participants open and close their eyes (Fig. 1.1). This method of pairing tasks or behaviors with certain stimuli has been used frequently in attempts to construct one-to-one correspondence maps between mental operations and brain regions. As a result, we now have much available evidence that shows different brain region activations in response to different stimulus categories, including, among others, places and faces. These data support the localization of the brain function theory, which states that different brain regions participate in specialized functions.

This methodology has three premises as follows: 1) each mental operation is performed by

Figure 1.1. Subtraction method with fMRI (reproduced from Fox and Raichle, 2007). Functional MRI signals measured within the occipital cortex are increased through eye opening and decreased through eye closure. The time series expressed by the red line in the left figure is the fMRI signal obtained from the occipital cortex, depicted in the right figure, while the time series indicated by the blue line represents the expected increase of the fMRI signal from baseline. According to the idea of functional brain mapping, this fMRI signal fluctuation reflects the function of the occipital cortex: to process visual information from the eyes.

a specific brain region; 2) execution of the mental operation causes only activation of that brain region; and, 3) only the execution of that mental function determines the extent of activation. In other words, this methodology hypothesizes that the brain is composed of simple units that have only stimulus-response functions and takes a role in limited mental operations. However, many evidences indicate that these three premises are too simplistic. For example, by using fMRI and positron emission tomography (PET), it was demonstrated that several brain regions increase their activity in response to tasks requiring attention to the external environment, but some brain regions decrease their activity during the same tasks (Raichle et al., 2001). Furthermore, inter-trial variability exists among the magnitudes of event-related activities measured by fMRI during sensory perception tasks. In terms of localizing brain function, the inter-trial variability is thought to result from noise produced through the measurement of brain activity, and this is typically removed by averaging the deviations among trials.

Nevertheless, the inter-trial variability in fMRI signal responses has some relevancy to sensory perception (Boly et al., 2007, 2008; Pessoa et al., 2002; Pessoa and Padmala, 2005; Ress and Heeger, 2003; Wagner et al., 1998). For example, Ress and Heeger (2003) found that the magnitude of an fMRI signal response predicted the visual contrast perception. Considering these evidences contradicting the premises of functional brain mapping, it may be unreasonable to determine an operational principle for the brain based solely on the localization of brain function theory.

What theories or ideas might compensate for the shortcomings of functional brain mapping? Studying the intrinsic dynamics of neurons presents a reasonable methodology. Cortical neurons demonstrate stimulus-induced activity that includes inter-trial variability (Fellous et al., 2004; Vogel et al., 1989). For example, Fellous et al. (2004) demonstrated that inter-trial variability in active neurons cannot always be attributed to random noises due to the experimental environment, but, instead, such variability might be produced by trial-to-trial differences of an intrinsic neural response to the stimulus. In their study, while activity was recorded from the single neuron in the middle temporal area (MT) in macaques, two switching Gabor patches were presented to the monkeys with randomized inter-switching intervals (30–300 msec). Although the recorded neurons largely fired when the two Gabor patches switched, sometimes they did not show any response at the timing of switching. Then, the experimenters switched the Gabor patches with a specific sequence of inter-switching timings (Fig. 1.2A). They observed that neurons can fire only once within a specific time window during the course of switching timings (Fig. 1.2B–D). This finding could not be attributed to random noises, such as the trial-to-trial variability in the timing of Gabor patch switching, and, therefore, this indicates the existence of an intrinsic mechanism that determines the timing of neural activity.

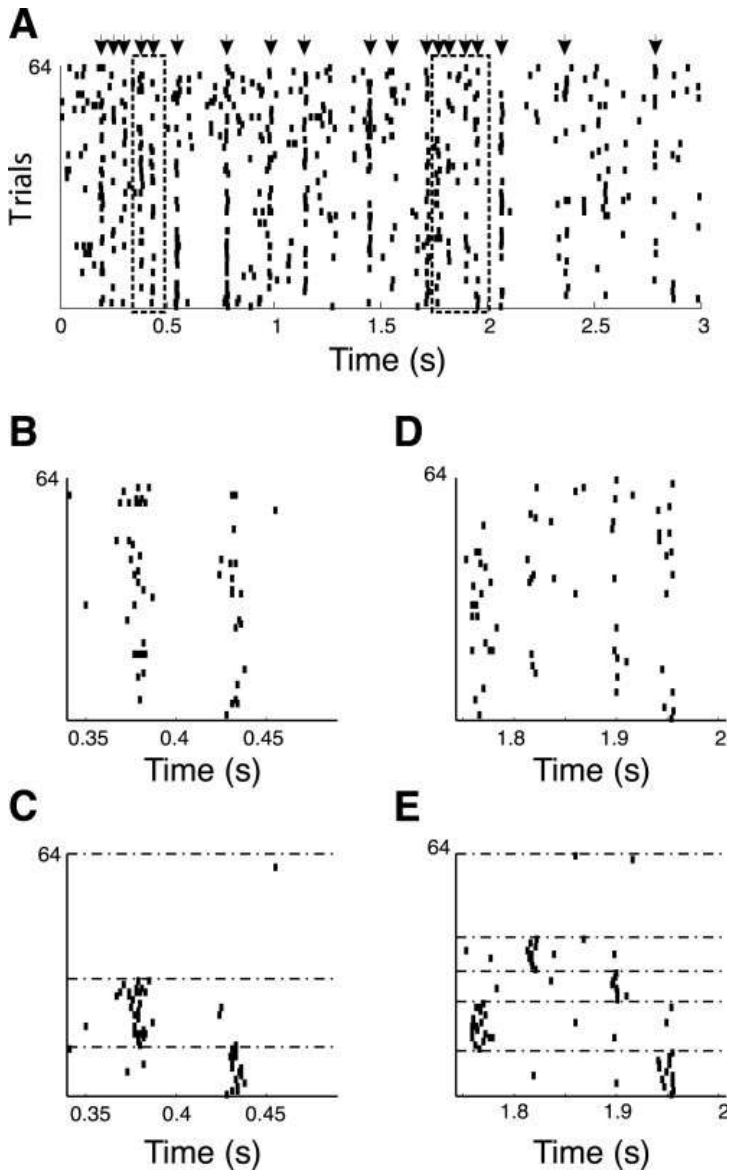

Figure 1.2. Non-random spike patterns in MT neurons (reproduced from Fellous et al., 2004). (A) Raster plots of spikes of MT neurons when monkeys viewed alternating sequences of Gabor patches. Arrows indicate the timing of spikes at the event (switching of Gabor patches). (B) and (D) correspond to two periods surrounded by broken lines in (A). By reordering plots in these periods, it was revealed that neurons can be active just once in these windows as shown in (C) and (E).

It is difficult to investigate such intrinsic neural mechanisms by using behavioral tasks because they should introduce task-specific neural activity. Therefore, many efforts have focused on ongoing and spontaneous brain activity. Spontaneous activity is defined as a brain activity that is observed without controlled tasks and stimuli, and it can be observed at different spatial scales of the brain: from a single neuron to the whole brain. For example, Steriade et al. (1993) found that cortical neurons in the cat association, motor, and visual areas demonstrate spontaneous bi-phasic membrane potential transitions. The higher phase was called the up-state of the membrane potential, and the lower phase was called the down-state. During the up-state, neurons discharged spontaneously. The interval duration for the transition between the up-state and the down-state was longer than the duration of an action potential of a single neuron, indicating that these two membrane potential states are not attributed to inputs from other neurons but are rather intrinsically generated. Furthermore, neural activities measured at larger spatial scales, such as the electrophysiological time series acquired by using electroencephalography (EEG), showed different power spectra corresponding to distinct sleep-wake states (Aeschbach et al., 1999; Cajochen et al., 2002; Dijk et al., 1990, 1997). These findings suggest that the brain intrinsically has different states of activity depending on sleep-wake states. Therefore, I propose that we can examine the intrinsic order of brain activity by focusing on spontaneous activity.

How important is an intrinsic rule of brain activity? Is it necessary to use such a focus to understand an operational principle of the brain? From a viewpoint of energy consumption, spontaneous brain activity is not functionally meaningless noise, and it is important for understanding an operational principle of the brain. Interestingly, most of the energy consumed in the brain is used with spontaneous activity (Ames, 2000; Attwell and Laughlin, 2001; Fox and Raichle, 2007; Lennie,

2003; Raichle and Mintun, 2006; Shulman et al., 2004). For example, Lennie (2003) shows that increases in energy consumption by controlled tasks and stimuli may be at most 15% (Fig. 1.3). Therefore, in terms of energy consumption, ongoing activity appears more important than task participation.

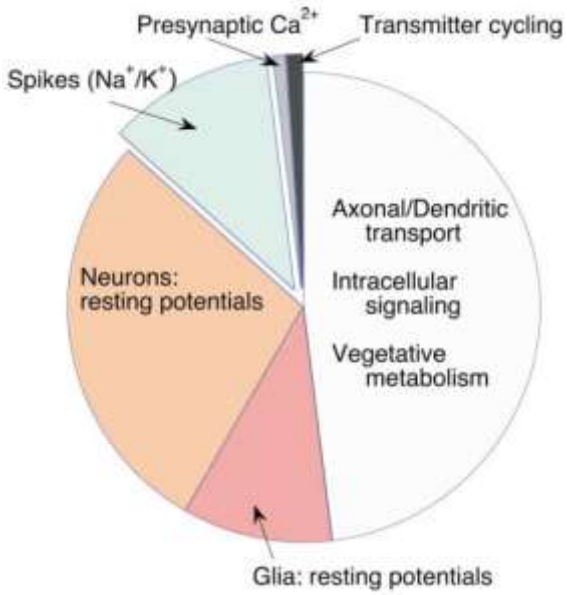

Figure 1.3. Composition of total energy consumption in the human cortex (adapted from Lennie, 2003). Lennie (2003) calculated the fraction of energy consumption depending on spiking activity. Energy consumption attributed to spikes is shown as the separated segment of the pie chart, which is under 15% of total energy consumption in the cortex.

As shown in the success of functional brain mapping, the usage of tasks is useful to investigate brain functions. However, while there are brain activities that are explicitly controlled by tasks under experimental conditions, there should also be activities that occur implicitly. When we conduct some tasks, our brains are required not only to generate explicit mental processes that are

controlled by experimental conditions and are accompanied by conscious experiences, but they are also required to produce implicit processes that are not explicitly conditioned and are operated under consciousness. For example, when we are instructed to see an apple in front of us, our brain must extract the boundary between the apple and the background by specifying other objects in the environment. So, while there are neural activities that generate the conscious experience of the apple, there should also be neural activities playing a role in the extraction of the boundary of the apple. Thus, an adequate theory for an operation principle of the brain must explain both the explicit and implicit processes.

1.1.3 A part and the whole

To understand an operational principle of the brain, it is essential to study its intrinsic architecture by focusing on spontaneous brain activity. This chapter summarizes my understanding of spontaneous brain activity.

Functional brain mapping studies have revealed many facts regarding the localization of cerebral functions. Nevertheless, because functional brain mapping studies have focused only on the brain activity that changes in relation to specific tasks or stimuli, they have ignored the intrinsic features of brain activity. Therefore, it is necessary to investigate brain activity without controlled tasks or stimuli in order to study the intrinsic operational mechanisms of the brain.

What is the intrinsic order ruling brain dynamics? To answer this question, it is necessary to observe the brain's anatomical structure. Neurons are interconnected through synapses and form a complex network structure. Considering this structural constraint, it is likely that individual neurons do not operate independently, but, rather, they interact with other neurons through structural

interconnections. In fact, the findings from several studies support this hypothesis. For example, many sensory neurons respond to a stimulus presenting within a specific location on the body surface called a receptive field. Neurons in the primary somatosensory area (postcentral gyrus) that have similar receptive fields form a columnar distribution that is called a cortical column (Mountcastle 1957). Neurons within the same cortical column have more recursive synaptic connections with neurons in the same column than with neurons in different columns (Gilbert and Wiesel, 1983; Hubel and Wiesel, 1962). Moreover, the ratio of the synapses corresponding to a visual input is only about 15% of all synapses existing in a primary visual area (Douglas et al., 1995). Considering the fact that neural activities occur spontaneously, this result indicates that not only afferent (visual) inputs, but also synaptic inputs, through the interconnections with other neurons area contribute to neural activities in the primary visual area. These findings further indicate that we should not completely depend on the theory of localization when considering an operational principle of the brain, and the brain's functions are generated through interactions among neurons.

It has shown that there are many neurons that have long axons projecting to other brain regions. Interaction through axons also occurs not only within cortical columns, but also between columns and among whole brain regions (Van Essen et al., 1992). For example, spontaneous brain activity does not occur independently among brain regions, but it occurs simultaneously among multiple brain regions. The primary motor cortices of the left and right hemispheres are interconnected by the corpus callosum, which is a bundle of long axons. These regions are activated by using a bilateral finger tapping task (Fig. 1.4A). Biswal et al. (1995) discovered that the fMRI time series acquired from these brain regions during the resting state are strongly correlated to each other (Fig. 1.4B). This correlation, which is called functional connectivity, demonstrates the fact that, although

there is no explicit task such as the bilateral finger tapping task activating bilateral primary motor cortices with the same time course, the bilateral primary motor cortices are intrinsically constrained to show coherent activities. Functional connectivity, which is defined as statistical dependency of brain activities between different brain regions, has been reported with many subsequent fMRI studies among several sets of brain regions that are thought to play a role in similar brain functions (Damoiseaux et al., 2006; De luca et al., 2006; Fox et al., 2005; Greicius et al., 2003; Lowe et al., 1998). Therefore, functional connectivity may reflect the intrinsic order of brain dynamics as well as the intrinsic functional organization in the brain. Furthermore, the existence of functional connectivity suggests the idea that each brain region does not function independently, but, rather, there is functioning through interactions with other regions.

Is the interaction through functional connectivity really functionally significant? Many brain regions are active during tasks that demand attention to the external environment (Raichle et al., 2001). Nevertheless, during the resting state, functional connectivity can be observed among the same brain regions that increase their activity during the attention task (Fox et al., 2006). When humans orient their attention to a location in the external space, two mental operations can be involved. The first operation is top-down attention, which allocates attention to the external object voluntarily. The second operation is bottom-up attention, which allocates attention to a salient object involuntarily. These two attention mechanisms activate two different sets of brain regions. Spatial orientation accompanying top-down attention activates the dorsal attention system, and is comprised of the bilateral intraparietal sulcus and the junction of the precentral and superior frontal sulcus (Astafiev et al., 2003; Corbetta and Shulman, 2002; Shulman et al., 2003). On the other hand, spatial orientation induced by bottom-up attention activates the ventral attention system, and is comprised of the right

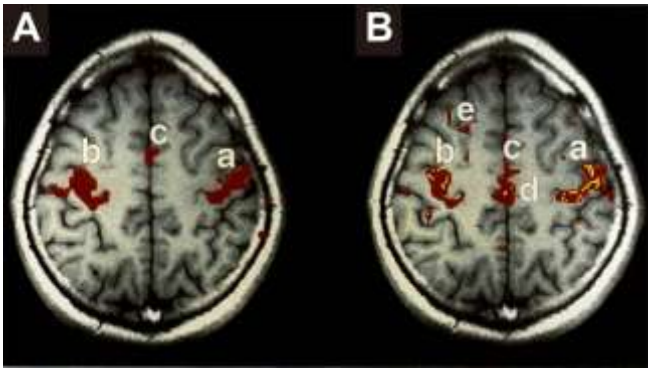

Figure 1.4. Task-induced activation and correlation of spontaneous activity (reproduced from Biswal et al., 1995). (A) Brain regions activated by bilateral left and right finger movement are localized within bilateral left and right somatomotor cortices that are indicated by characters (a) and (b). (B) By extracting fMRI time series from region (a) and calculating the correlation between the time series and those in overall measured regions, significant correlations were found in regions (b), (c), (d), and (e). Regions (b) and (c) are the same regions as those activated by the finger movement task.

temporal-parietal junction and the right ventral frontal cortex (Astafiev et al., 2003; Astafiev et al., 2004). Fox et al. (2006) found that spontaneous activities occurring within the brain regions in these two attention systems show significant correlations with other regions in the same system, but not with regions in the other system. In other words, these findings suggest that there are two different spatial orientation systems that are separated by "dis-connection" of functional connectivity. Brain regions constituting these two attention systems show increased activity during attention tasks and represent the "task-positive system." On the other hand, there are brain regions that represent the "task-negative system" (also known as the default mode system) that show significant decreases of activity with task demands (Fox et al., 2005; Greicius et al., 2003; Raichle et al., 2001). Fox et al. (2005) demonstrated that spontaneous brain activities in brain regions consisting of the task-negative system also show significant correlations among regions within the system, but show negative correlations with regions

located in the task-positive system. While task-positive and task-negative systems show increase and decrease in activity during tasks, those systems show opposite patterns of activities during the resting state: the task-positive system shows decrease during the resting state, while the task-negative system shows increase (Fox et al., 2005). Furthermore, it has been shown that brain regions forming the task-negative system show significant activation during task-unrelated thought and mind wandering (Mason et al., 2007). Considering that task-unrelated thought increases error of task execution (Smallwood et al., 2008), opposite behaviors of brain activities between the task-positive and task-negative systems may reflect the fact that these systems play opposite brain functions. These findings suggest that functional connectivity forms the mesoscopic functional system in the brain.

Thus, the interaction among brain regions is performed autonomously, and this plays an important role in producing brain function that is the basis of human behavior. Nevertheless, there are some degrees of functional localization within the brain, and this idea is supported by many findings of functional brain mapping studies. What hypotheses can resolve the two apparent paradoxical ideas? One hypothesis might be that the brain combines these two mechanisms to generate its functions. For example, when we see an apple in front of us, different visual attributes like shape, color, texture, and depth are processed simultaneously in different cortical regions. Because we do not see these attributes separately, but, rather, we experience “an apple” itself, our brain must unify the information for these different attributes into one integrated attribute. Theoretical and empirical evidence supports the idea that integration among brain regions occurs through interactions at multiple levels from cortical columns to the entire brain (Damasio 1990; Mesulam, 1990; Tononi et al., 1994; Varela et al., 2001). It should be noted that this idea focuses on a balance between functional specialization and interactions among brain regions. Unlike with task-induced activity, interaction among brain regions is an intrinsic

order of brain activity, which is supported by findings from resting state functional connectivity studies (Fox et al., 2005, 2006). Moreover, many studies indicate the relevance between functional connectivity observed during the resting state and human behavior (Cole et al., 2012; Gießing et al., 2013; Kelly et al., 2008; Mennes et al., 2011). For example, it was discovered by using fMRI that continuous maintenance of attention correlates significantly with spontaneous activity in task-positive and task-negative systems (Kelly et al., 2008). Furthermore, Fox and Greicius (2010) showed that abnormalities exist in the intensity and spatial structure of functional connectivity in patients with neurological disorders (Table 1.1). These observations indicate that the brain produces its functions through the balance between functional segregation in each brain region, and its integration via the interaction.

Table 1.1. Group differences in resting state functional connectivity patterns observed in various brain diseases or conditions (reproduced from Fox and Greicius, 2010).

Disease/condition	References	Findings
Alzheimer's	(Li et al., 2002; Greicius et al., 2004; Wang et al., 2006a,b, 2007; Allen et al., 2007; Supekar et al., 2008)	Decreased correlations within the DMN including hippocampi, decreased anticorrelations with the DMN, and reduced local connectivity as reflected in clustering coefficients
PIB positive	(Hedden et al., 2009; Sheline et al., 2010)	Decreased correlations within the DMN
Mild cognitive impairment	(Li et al., 2002; Sorg et al., 2007)	Decreased correlations within the DMN and decreased anticorrelations with the DMN
Fronto-temporal dementia	(Seeley et al., 2007a, 2008)	Decreased correlations within the salience network
Healthy aging	(Andrews-Hanna et al., 2007; Damoiseaux et al., 2008)	Decreased correlations within the DMN Decreased correlations within the somatomotor network
Multiple sclerosis	(Lowe et al., 2002; De Luca et al., 2005)	Decreased connectivity within the DMN and within the somatomotor network (esp. premotor cortex)
ALS	(Mohammadi et al., 2009)	Variable: Decreased corticolimbic connectivity (esp. with dorsal anterior cingulate), increased connectivity within the DMN (esp. anterior cingulate), increased connectivity within the DMN (esp. subgenual prefrontal cortex), decreased connectivity between DMN and caudate
Depression	(Anand et al., 2005a,b, 2009; Greicius et al., 2007; Bluhm et al., 2009a)	Decreased corticolimbic connectivity
Bipolar	(Anand et al., 2009)	Decreased connectivity within the DMN
PTSD	(Bluhm et al., 2009c)	Variable: Decreased or increased correlations within the DMN. Decreased, increased or unchanged correlations and anticorrelations between the DMN and other systems.
Schizophrenia	(Liang et al., 2006; Liu et al., 2006, 2008; Bluhm et al., 2007, 2009b; Salvador et al., 2007; Zhou et al., 2007; Jafri et al., 2008; Whitfield-Gabrieli et al., 2009)	
Schizophrenia 1° relatives	(Whitfield-Gabrieli et al., 2009)	Increased connectivity within the DMN
ADHD	(Zhu et al., 2005, 2008; Cao et al., 2006; Tian et al., 2006; Zang et al., 2007; Castellanos et al., 2008; Wang et al., 2009)	Variable: reduced connectivity within the DMN, reduced anticorrelations with the DMN, increased connectivity in the salience network
Autism	(Cherkassky et al., 2006; Kennedy and Courchesne, 2008; Monk et al., 2009; Weng et al., 2010)	Decreased connectivity within the DMN (although hippocampus is variable and connectivity may be increased in younger patients)
Tourette syndrome	(Church et al., 2009)	Delayed maturation of task-control and cingulo-opercular networks
Epilepsy	(Waites et al., 2006; Lui et al., 2008; Bettus et al., 2009; Zhang et al., 2009a,b)	Variable: decreased connectivity in multiple networks including the medial temporal lobe, decreased connectivity within the DMN (esp. in patients with generalized seizures)
Blindness	(Liu et al., 2007; Yu et al., 2008)	Decreased connectivity within the visual cortices and between visual cortices and other sensory and multimodal regions
Chronic pain	(Greicius et al., 2008; Cauda et al., 2009b,c, 2010)	Variable: Increased/decreased connectivity within the salience network, decreased connectivity in attention networks
Neglect	(He et al., 2007)	Decreased connectivity within the dorsal and ventral attention networks
Coma/vegetative state	(Boly et al., 2009; Cauda et al., 2009a; Vanhaudenhuyse et al., 2010)	Progressively decreased DMN connectivity with progressive states of impaired consciousness
Generalized anxiety disorder	(Etkin et al., 2009)	Increased connectivity between amygdala and frontoparietal control network and decreased connectivity between amygdala and salience network

DMN = default mode network including regions in the posterior cingulate/precuneus, lateral parietal cortex, medial temporal lobes, and medial prefrontal cortex. Salience network includes regions in the dorsal anterior cingulate and bilateral fronto/insular cortices; dACC = dorsal anterior cingulate cortex; PIB = Pittsburg compound B, a marker of amyloid plaque accumulation in the brain. PTSD = post-traumatic stress disorder; ALS = amyotrophic lateral sclerosis; ADHD = attention deficit hyperactivity disorder. Note: some references (Greicius et al., 2004; He et al., 2007) reflect "near-rest" conditions in which task-related variance has been minimized and other references (Zhu et al., 2005, 2008; Cao et al., 2006; Zang et al., 2007) reflect local changes in spontaneous BOLD fluctuations as opposed to correlations in these fluctuations between separate regions.

1.1.4 Network theory

As I have shown, we can take the following as a working hypothesis for an operational principle in normal brain function: although each brain region performs specialized functions, the brain works as a functional whole through interactions among brain regions. Information processing, specialized within individual brain regions, has been investigated with the subtracting method. How then can we examine the brain as a functional whole through interactions among local regions? Systems that contain many components and perform many interactions among the components often behave in similar ways. Such a behavior can be characterized by the network theory. The network theory is a theoretical framework for the spatial pattern of interactions among components (Boccaletti et al., 2006; Newman, 2003; Strogatz, 2001). This theoretical framework can apply to many systems, even when their components and interactions differ. For example, the propagation efficiency of information between different network components on the World Wide Web, human relationships, and the brain can be analyzed by a specific index in the network theory, despite the fact that their interactions are performed in different ways. Since each component in the brain is connected with others, there may be more than one possible information transmission pathway between two arbitrary components in the brain. If we can ignore the time spent on each interaction in the network, then the most efficient propagation is borne by the most direct channels of communication (i.e. the pathway with the smallest number of synaptic transmission in the brain network). By regarding each system component as a network node, and interactions between components as edges, a maximum efficiency pathway between a given pair of two components in the network can be found mathematically. Since the transmission efficiency between domains is considered as the inverse proportion to the number of the interactions contained in the shortest path (Fig. 1.5A), the transmission efficiency between domains

can be expressed as the reciprocal. The network average of this index is called *global efficiency*, and it can measure the information propagation efficiency of the entire network quantitatively (Latora and Marchiori, 2001).

The localization of communication within a network can be investigated in the framework of the network theory. It is necessary to give mutual interactions among the subsets of components in order to improve the propagation efficiency inside the same subsets and to increase the independency between different subsets by removing interactions in order to limit the communication between different subsets. In a network theory, the localization of the communication within the subset in a network is dealt with quantitatively by searching for these structural aspects. The minimum unit inducing such localization in a network is the triangle (Fig. 1.5A). Therefore, the index that investigates the extent to which each network node is a triangular vertex can be used as a simple index for the localization of communication, and it is called the *clustering coefficient* (Watts and Strogatz, 1998). Even so, communication localization is not always borne with three components like social groups in human relationships or cortical columns in the brain. A common aspect of these sub-network architectures is a high-density interconnection within each subset and sparse connections between different subsets. In the network theory, a mesoscopic communication unit is called a "module" or a "community" (Fig. 1.5B). The extent of community structure in a network is called *modularity* (Newman, 2004, 2006), and this serves as an index for communication localization in a network.

A famous example of ubiquitous communication characteristics in a network is the "small-world phenomenon." By counting the shortest path lengths between a pair of citizens in the United States, there are, on average, six citizens interconnected between any two given citizens (Milgram, 1967). This phenomenon has been observed in other networks, including human and animal

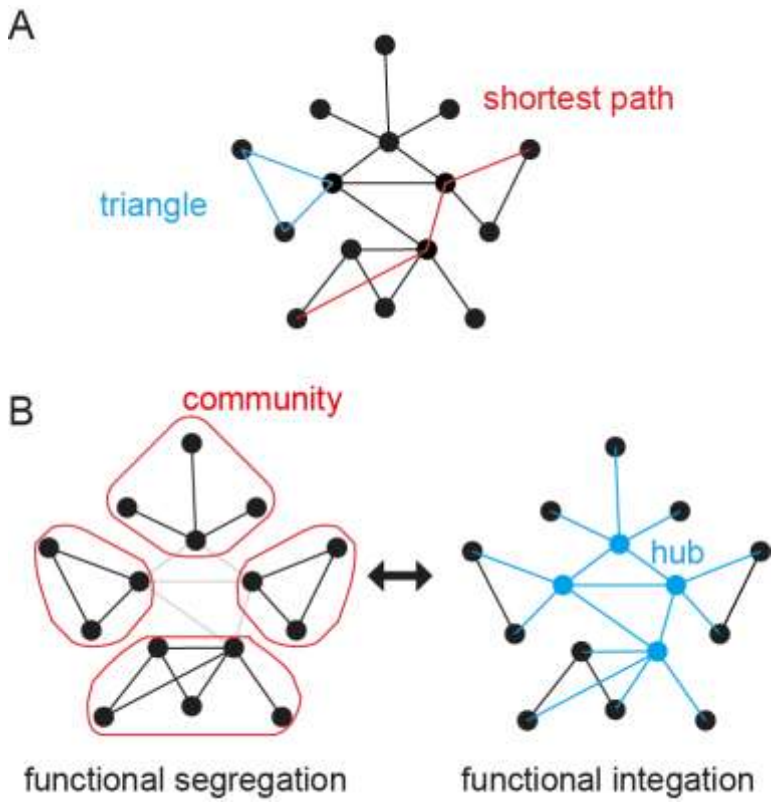

Figure 1.5. Network structures and the implications on information segregation and integration. (A) Shortest path and triangle (adapted from Rubinov and Sporns, 2010). The shortest path between two nodes is defined as a pathway on the network with the least number of other nodes that are traversed by the path (red). A triangle is defined as three nodes linked by the edges of each other (blue). (B) Communities are defined as sets of nodes where nodes in the same community are densely interconnected with each other, while nodes in different communities are sparsely connected. Node sets that are surrounded by red lines are communities. A hub is defined as a node with a larger number of edges than other nodes, and it is indicated as a blue node. Generally, the mean plus the standard deviation of the number of edges connected to nodes in the network is used as the criteria for a "large number of edges" in the network. Coexistence of communities and hubs indicates that the network can simultaneously achieve both local, separated information processing within communities and global, network-level integration of processed information through edges connected to hubs (blue edges). While local information processing takes charge of the segregation of function in the network, global information integration enables the network to behave as a functional whole (adapted from Sporns, 2013).

brain networks, and it is characterized by a high degree of global efficiency and a clustering coefficient (Humphries and Gurney, 2008). Collectively, the system-level characteristics that ubiquitously emerge on a system are determined by its spatial architecture.

Since brain regions are connected anatomically, we can construct the network of the brain using our knowledge of anatomical connections. It is also possible to construct a network by considering the functional connectivity between brain regions as a network edge (Bullmore and Sporns, 2009). By considering functional connectivity as an edge, we can investigate the spatial organization of the brain as a network constructed from anatomical connections. Even if a cerebral anatomical connection exists, it is unclear whether the connection plays an important role in communicating information. Since functional connectivity is defined as a correlation in brain activity between regions, it guarantees that informational dependence exists between the correlated brain regions. Furthermore, an anatomical connection does not necessarily exist between the brain regions linked by functional connectivity. Even if two brain regions are not directly connected by synapses, but interact through indirect, polysynaptic connections, functional connectivity can occur if the interaction is strong. In fact, it was shown that there are significant differences in the spatial connection patterns in networks between their anatomical connections and those made from functional connectivity (Honey et al., 2007, 2009). Therefore, in order to investigate the information processing that takes place within the brain, it is necessary to investigate the network character by considering functional connectivity as an edge.

A brain network based on functional connectivity is called a functional connectivity network (FCN). It was shown that a FCN contains community structures that may perform specialized information processing functions (Dosenbach et al., 2007, 2010; Power et al., 2011; Spreng et al., 2013). Because brain regions forming each community corresponds to the sets of regions that show

similar activation profiles to a specific task, each community is considered as a mesoscopic functional unit (also called as a functional system) within the brain (Corbetta and Shulman, 2002; Corbetta et al., 1995; Dosenbach et al., 2006). There are some brain regions, however, that have many functional connectivity with other regions. These high-throughput regions represent the "hub" of the FCN (Achard et al., 2006; Buckner et al., 2009; van den Heuvel et al., 2008b; Tomasi and Volkow, 2011a,b). It is thought that the hub plays an important role in mediating communication for information transfer between different brain regions and in unifying the information processed in multiple brain regions. The fact that a community and hub exist simultaneously in the FCN strongly suggests the brain has a fundamental architecture that locally processes information within functional units as both a brain region and a community (functional segregation), and it concurrently integrates processed information into unifying information across the entire brain (functional integration) (Fig. 1.5B).

1.1.5 Time scale of brain activity

In previous sections, I introduced evidence that supports the idea that the brain is an autonomous, information-processing organ with an intrinsic operational order. While each brain region and community functions as a functional unit for information processing, and performs a specific function, the information processed in each structure is integrated in hub regions.

This hypothesis is derived from the studies of network properties of FCN, which is the network consisting of functional connectivity among different brain regions. Generally, functional connectivity is defined by estimating statistical dependencies between two time series of brain activities that have multiple time scales. Different time scales in the brain activities may have different functional roles. For example, the brain must process information at different time scales to properly

comprehend the external environment. To understand conversation, the brain must identify three to six syllables uttered per second as one word, and must understand the meaning expressed in sentences, which consists of multiple words (Honey et al., 2012). Furthermore, electrophysiological signals have several time scale components that span five orders of magnitude in frequency (Buzsáki and Draguhn, 2004) and have a power spectrum following power-law distributions (He et al., 2010; Miller et al., 2009). Do the frequency components in brain activity relate to information processing in the brain? He et al. (2010) showed that task performance modulates the power spectrum in several brain regions, and this changes the coefficients of power-law distributions, suggesting that different frequency components have different functional relevancies. Furthermore, there is considerable evidence that supports the idea that the frequency-specific coherence observed in electrophysiological signals has specific functional properties (Fries, 2009; Siegel et al., 2012). For example, using magnetoencephalography (MEG), it was shown that long-range interactions within the gamma-band are enhanced among several brain regions during tasks that require spatially selective attention (Siegel et al., 2008). Activity within the beta-band relates to visual detection tasks (Gross et al., 2004).

Hemodynamic fluctuations measured during the resting state contain various frequency components (Baria et al., 2011; He, 2011; Obrig et al., 2000; Schroeter et al., 2004; Zuo et al., 2010a). Frequency-specific changes in power were observed in fMRI signals acquired during task performance and at rest (Baria et al., 2011). This suggests that the time scale of brain activity changes with the state of information processing. In the field of psychology, human personality can be described with the index called the “Big Five” personality traits (John and Srivastava, 1999). Relevancies between some of these traits and power spectrums have been observed: individual differences between extraversion and neuroticism show a positive correlation with the individual variability of band-limited power

within 0.01–0.027 Hz and a negative correlation with those within 0.027–0.073 Hz (Wei et al., 2012). Dosenbach et al. (2006) conducted fMRI studies with a unique blocked design that consisted of a number of tasks, all of which required attention to the external environment (Fig. 1.6). In this task design, a task-set system should instantiate and maintain different task sets in response to the task instructions, and this should process the relevant information to execute each task. The authors observed short-term activity related to the failure in each task and the prolonged activity spanning from the beginning of the task until the end. These findings indicate the brain works on several time scales to process information according to the time scales of the cognitive functions. Thus, a theory of operational principle of the brain must explain the spatial structure and temporal characteristics of brain activity.

Until now, most functional neuroimaging studies have investigated the spatial and temporal characteristics of brain activity independently. Are there relationships between the spatial orders and time scales of brain activity? If so, we should investigate these dimensions of brain activity simultaneously. Some fMRI studies provided evidence suggesting the existence of the dependency between functional connectivity and time scales of hemodynamic fluctuations measured during the resting state. Generally, fMRI studies estimate functional connectivity as temporal correlation in the "low frequency" range (< 0.10 Hz) (Biswal et al., 1995; Cordes et al., 2001; Fox et al., 2005; Fox and Raichle, 2007). On the other hand, Wu et al. (2008) used fMRI to demonstrate the frequency-dependency of functional connectivity within this frequency range. They extracted frequency components using band-pass filters whose widths of pass bands were narrower than those generally used in estimating functional connectivity (pass band: 0.01–0.10 Hz). Then, they calculated functional connectivity within each narrower frequency band. They found that spontaneous brain

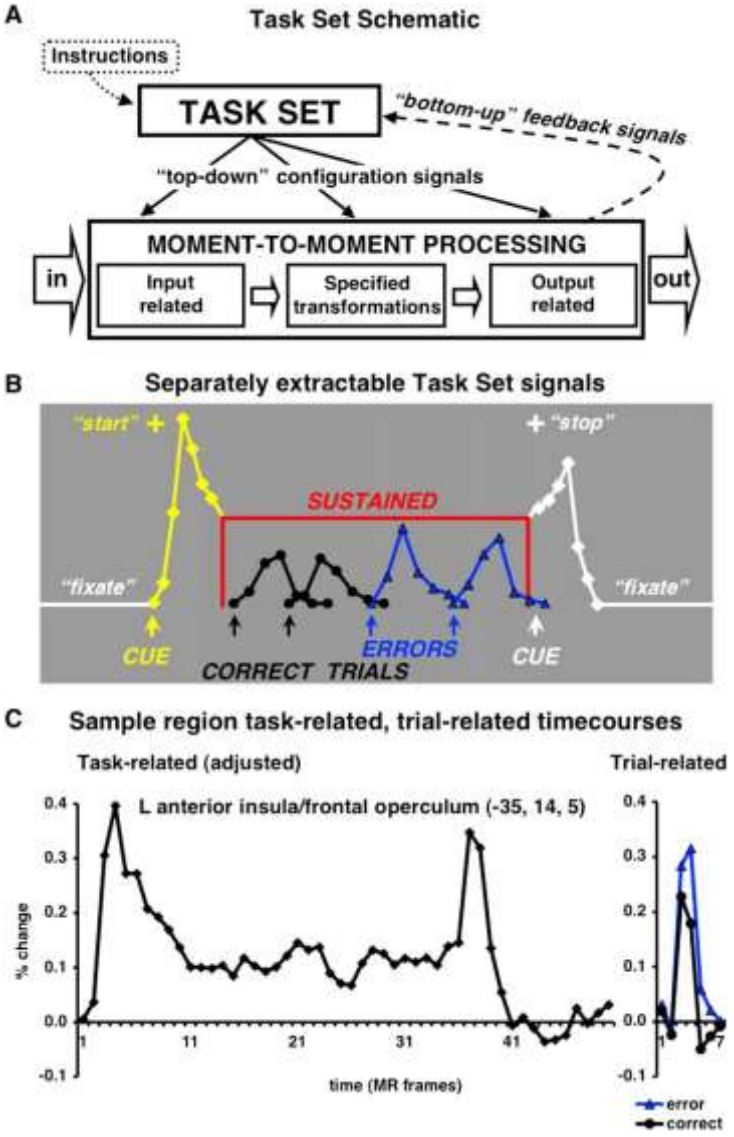

Figure 1.6. Multiplexed brain activity during attentional tasks (reproduced from Dosenbach et al., 2006). (A) A scheme of task set control. In the repetitive attention tasks, a "task-set system" in the brain must start and maintain the state of the brain in order to engage in a series of tasks, while that system also must perform moment-to-moment processing. (B) Depending on the time scales of processes in the series of tasks, the brain should show several activities with different time scales. For example, there should be transient activities relating to task-initiation and task-termination (yellow and white) and activities coding correct and error to each task (black and blue). Also, there should be a long-lasting, sustained activity relating to maintenance of the state of the brain to engage the set of tasks during the task period (red). (C) fMRI study found both sustained (left) and transient (right) activities (Dosenbach et al., 2006).

activity fluctuating within 0.01–0.06 Hz mainly contributes to functional connectivity within cortico-cortical systems (Fig. 1.7A). They also found that the frequency-dependency of functional connectivity within sub-cortical systems was different from that in the cortico-cortical systems: functional connectivity within sub-cortical systems was strong within a wider frequency range (0.01–0.14 Hz) (Fig. 1.7B). Furthermore, Chang and Glover (2010) demonstrated that the frequency-dependency of functional connectivity in the same functional system is different from the frequency-dependency of functional connectivity between two different functional systems (task-positive and task-negative systems).

These findings indicate that interactions among different brain regions occur on a time scale that is specific to the pair of brain regions. This suggests that the spatial architecture of the FCN can vary with the time scales of brain activity. Honey et al. (2007) conducted a simulation study to investigate the relationship between anatomical connection and functional connectivity. They modeled spontaneous fMRI signal fluctuation in each brain region as a non-linear oscillator and enabled interactions between these oscillators if an actual anatomical connection existed between the brain regions. By simulating spontaneous brain activity and calculating frequency-specific functional connectivity, they observed that the functional connectivity estimated from signal fluctuations in the ultra-low frequency band (<0.01 Hz) was identical to the anatomical connection; functional connectivity estimated in frequency ranges higher than 0.01 Hz had similar, but different, spatial patterns as compared to anatomical connections. This suggests that while spatial structure in functional connectivity is constrained by anatomical connections, we must attend to the time scales of brain activity in order to capture the spatial characteristics in the functional interactions among brain regions that are not present in the anatomical connections.

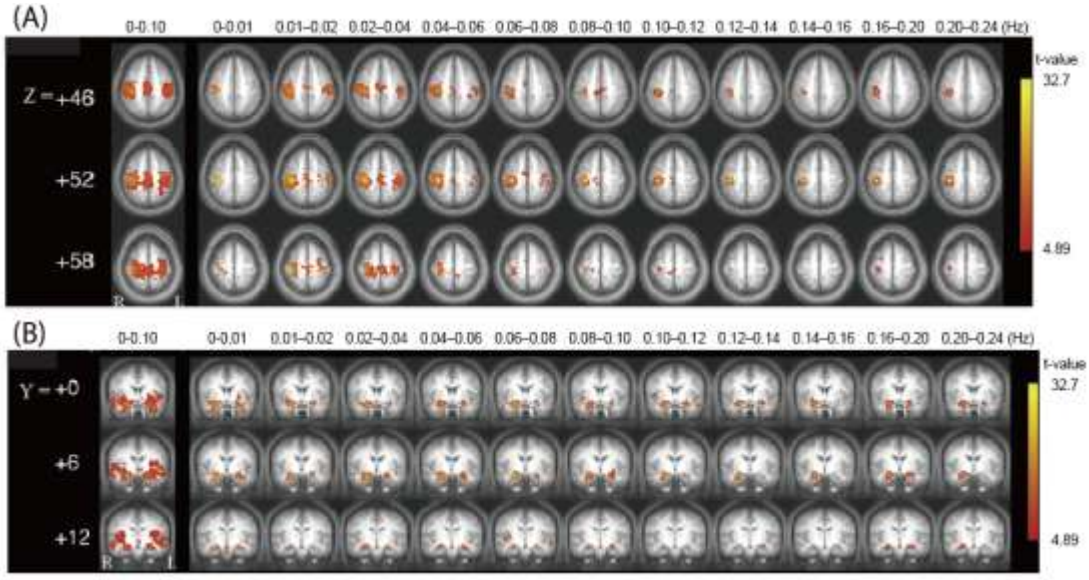

Figure 1.7. Frequency-dependency of functional connectivity is different depending on the combination of brain regions (adapted from Wu et al., 2008). (A) Band-limited correlation with the left sensorimotor cortical region of interest (ROI) is shown. Correlation was calculated as follows. First, fMRI signals obtained during rest were processed with 12 band-pass filters (0–0.10, 0–0.01, 0.01–0.02, 0.02–0.04, 0.04–0.06, 0.06–0.08, 0.08–0.10, 0.10–0.12, 0.12–0.14, 0.14–0.16, 0.16–0.20, and 0.20–0.24 Hz). Then, correlation between a time series extracted from a ROI located in the left sensorimotor cortex and time series in whole brain voxels were calculated in each frequency band. A significant correlation between bilateral sensorimotor cortices was found within 0.01–0.06 Hz. (B) Band-limited correlation with left amygdala. Method to derive the result is the same as used in (A). Significant correlation between bilateral amygdalae was found within 0.01–0.14 Hz.

1.2 Methodology for functional connectivity

1.2.1 Methods used for studies of functional connectivity

Functional connectivity has been studied using fMRI because it measures localized brain activity across all brain regions. Although EEG and MEG also provide non-invasive measures of cortico-cortical interactions, the signal localization in the brain is worse for these methods than for fMRI. Therefore, we must predict the signal sources mathematically.

Blood oxygenation level-dependent (BOLD) contrasts acquired by fMRI are generated by the regional differences of deoxygenated hemoglobin within local brain regions (Ogawa and Lee, 1990; Ogawa et al., 1990a,b). When neural activity occurs in a local brain region, the concentration of oxygen within the brain region decreases. This generates the high concentration gradient of oxygen between brain tissue and capillaries within the brain region compared to the equilibrium state. The high gradient of oxygen concentration causes more oxygen to unload from the passing oxygenated hemoglobin. However, because neural activity increases cerebral blood flow by controlling vasodilation, the relative amounts of deoxygenated hemoglobin during neural activities are lower than the amount when neurons are not active. Therefore, when brain activity occurs in a local brain region, we acquire increased BOLD contrast in the brain region (Murphy et al., 2013).

Similar to fMRI, near infrared spectroscopy (NIRS) is a method that measures the changes of both oxygenated and deoxygenated hemoglobin concentrations associating with neural activities. NIRS also has a higher spatial resolution than EEG and MEG. Since Jöbsis (1977) first introduced NIRS to measure hemodynamic fluctuations in the cerebral cortex, this method has developed an important role in investigating spontaneous (Elwell et al., 1999; Hoshi et al., 1998; Obrig et al., 2000; Schroeter et al., 2004; Toronov et al., 2000; Toronov and Webb, 2001) and task-related hemodynamic

fluctuations (Chance et al., 1993; Franceshini et al., 2003; Hoshi and Tamura, 1993; Kato et al., 1993; Villringer et al., 1993). Because NIRS requires less physical restraint of subjects than does fMRI, hemodynamic fluctuations can be measured in populations (Taga et al., 2000 for sleeping state of infant) and conditions where fMRI is difficult to use (Ikegami and Taga, 2008; Karim et al., 2012, 2013; Suda et al., 2010). Recently, it was shown that NIRS can be used to estimate functional connectivity during the resting state in adults and infants (Homae et al., 2010, 2011; Lu et al., 2010; Mesquita et al., 2010; White et al., 2009; Zhang et al., 2010b). Considering the advantage of a higher temporal resolution with NIRS than with fMRI, NIRS can obtain more information on hemodynamic fluctuations in a time domain, and it may be more suitable for investigating the relationship between the time scale of the brain activity and functional connectivity. Nevertheless, NIRS has poorer spatial resolution than fMRI. Furthermore, while NIRS can measure hemodynamic fluctuations only in the superficial regions of the cerebral cortex, fMRI can obtain signals from all brain regions, including deep brain regions. Therefore, NIRS cannot be used to investigate the spatial structure of a FCN covering the entire brain.

Although the task-related signal changes in NIRS and fMRI are observed with simultaneous recordings with these neuroimaging tools (Cui et al., 2011; Hoge et al., 2005; Kleinschmidt et al., 1996; Schroeter et al., 2006; Strangman et al., 2002; Toronov et al., 2001; Toyoda et al., 2008), the consistency between signals obtained during the resting state with NIRS and fMRI is unclear. Because NIRS signals are potentially affected by blood flow in tissues between the scalp and the brain, some researchers question whether NIRS can accurately measure hemodynamic fluctuations produced by neural activity (Takahashi et al., 2011).

1.2.2 Data analysis for estimation of functional connectivity

Functional connectivity is defined as a statistical dependency of brain activities obtained in different brain regions (Aertsen et al., 1989; Friston et al., 1993). Most general and simple measures of statistical dependency are reflected by the temporal correlation between two fMRI signals obtained in different brain regions (Biswal et al., 1995; Cordes et al., 2000; Fox et al., 2005; Greicius et al., 2003). While the linear index-like correlation is a useful measure of functional connectivity, nonlinear indices such as mutual information (Inouye et al., 1995; Jeong et al., 2001; Na et al., 2002) and phase synchronization (Mizuhara et al., 2005; Mormann et al., 2000; Tass et al., 1998; Varela et al., 2001) have been applied mainly in the studies of functional connectivity with electrophysiological data. Furthermore, there are many variations of the indices depending on the focus of studies. For example, to characterize frequency-dependency of functional connectivity, correlation has been used with a combination of narrow band-pass filters (Wu et al., 2008). Also, coherence and partial coherence (Sun et al., 2003), frequency-based mutual information (Salvador et al., 2005b, 2007), and wavelet correlation (Achard et al., 2006) have been used as indices of functional connectivity in the frequency domain.

In order to characterize the distributions of functional connectivity in the brain (functional connectivity map), functional connectivity must be estimated among whole brain regions. There are largely two categories of methods to characterize functional connectivity maps: model-dependent and model-free methods (van den Heuvel and Hulshoff, 2010). Model-dependent methods utilize a priori information such as functional or anatomical profiles of brain regions in order to determine a region of interest (ROI). For example, while ROI can be selected as a region showing a specific activation profile to interested tasks (Biswal et al., 1995; Cordes et al., 2000; Dosenbach et al., 2007, 2010; Fox et al.,

2005; Greicius et al., 2003; Power et al., 2011), it can also be determined as one anatomical area by referring to atlases such as the Automated Anatomical Labeling system (AAL) (Achard et al., 2006; Salvador et al., 2005a, 2005b, 2007, 2008). With the model-dependent method, the functional connectivity map is generally estimated by calculating the correlation between a seed signal extracted from one a priori ROI and signals of whole brain voxels (Biswal et al., 1995; Cordes et al., 2000; Fox et al., 2005; Greicius et al., 2003). On the other hand, the model-free method has been also introduced to characterize functional connectivity without a priori selection of a seed ROI. Most successfully applied methods are independent component analyses (Beckmann et al., 2005; Calhoun et al., 2001; Damoiseaux et al., 2006; De Luca et al., 2006; van de Ven et al., 2004). Also, principal component analysis (Friston, 1993, 1998) and hierarchical clustering (Cordes et al., 2002) have been used as data-driven methods to detect the distribution of functional connectivity in the brain. Usages of model-dependent and model-free methods have successfully reproduced consistent findings on the functional connectivity maps in the brain.

FCN is defined as a network consisting of a number of brain regions interconnected with each other by functional connectivity. Unlike the method for estimating the functional connectivity map, we must identify many-to-many statistical dependencies among different brain regions to construct the network in order to investigate network properties such as measurements of functional segregation and integration (see 1.1.4 Network theory). Although there are some fMRI studies that calculated correlation among all brain voxels (Buckner et al., 2009; Cecchi et al., 2007; Eguíluz et al., 2005; Hayasaka and Laurienti, 2010; van den Heuvel et al., 2008b), many studies constructed FCN by estimating functional connectivity among sets of ROIs to decrease the computational demand (Achard et al., 2006; Dosenbach et al., 2007, 2010; Fair et al., 2007, 2008, 2009; Power et al., 2011; Salvador et

al., 2005b, 2007, 2008; Supekar et al., 2008).

1.3 Overview of the composition of the thesis

In order to comprehend the operational mechanisms of the brain, the three following aspects must be focused on: 1) the brain is not a stimulus-responsive unit, but an autonomous organ with its own intrinsic rules of dynamics; 2) brain function is generated through the spatial architecture of a FCN that concurrently segregates information between communities and integrates that information over the entire brain via hubs; and, 3) normal brain function requires information processing over multiple time scales. Until now, the intrinsic organization of the FCN has been investigated by measuring spontaneous hemodynamic fluctuations and estimating as statistical dependency of the fluctuations within 0.01–0.10 Hz among several brain regions. However, it is unclear whether spatial structure in the FCN is dependent on the time scale of spontaneous hemodynamic fluctuations. Considering the existence of frequency-dependency of functional connectivity within 0.01–0.10 Hz (Chang and Glover, 2010; Wu et al., 2008), I hypothesized that there are frequency-specific topologies of FCN in the narrower frequency bands than the wider frequency band (0.01–0.10 Hz) where functional connectivity has been calculated (Fig. 1.8). Therefore, the purpose of this thesis was to investigate this hypothesis.

This thesis is organized into five chapters including this chapter. As you already read, I introduce the background and purpose of this thesis as a general introduction in Chapter 1. In Chapter 2, I introduce Study 1 where I investigated the frequency-character of functional connectivity by conducting resting state measure measurements of NIRS. In this study, NIRS was used to measure resting state hemodynamic fluctuations in limited brain regions over the frontal, temporal, and occipital

cortices, bilaterally, to determine frequency-specific characteristics in functional connectivity. Frequency-specificity of functional connectivity within 0.01–0.10 Hz was investigated by calculating band-limited correlation and coherence among all NIRS channels because these measures are the simplest indices of statistical dependency. I discuss the results in Study 1 to conclude this chapter with providing the statement: frequency-specificity of functional connectivity is different depending on the pair of brain regions.

In Chapter 3, I introduce Study 2 where I investigated the relationship between functional connectivity estimated by using NIRS and fMRI during the resting state. Although NIRS has sufficiently high temporal resolution (sampling rate: ~10 Hz) to characterize hemodynamic responses to neural activities (~15 sec), measurement of brain regions of NIRS are limited to surfaces of cerebral cortex. Therefore, while usage of NIRS is suitable to characterize the frequency-dependency of functional connectivity, it is not useful to investigate the relationship between the structure of FCN consisting of whole brain regions and time scales of hemodynamic fluctuations. In contrast, while fMRI has a lower sampling rate (~0.5 Hz) than NIRS, usage of fMRI enables us to investigate the functional connectivity among whole brain regions. However, it is unclear whether signals obtained by NIRS and fMRI share hemodynamic information contributing to functional connectivity. Thus, before conducting the examination of frequency-specificity of functional connectivity with fMRI data, I conducted simultaneous recording of NIRS and fMRI during the resting state and investigated the relationship between signals obtained by NIRS and fMRI with special emphasis on the consistency of functional connectivity. I discuss the results in Study 2 to conclude this chapter with providing the statement: NIRS and fMRI can produce consistent functional connectivity.

In Chapter 4, I introduce Study 3 where I investigated if spatial patterns of functional

connectivity are different in distinct narrow frequency bands between 0.01–0.10 Hz by examining the relationship between the spatial architectures of the FCN and time scales of fMRI signals obtained during rest. Specifically, I investigated the different network topologies reflecting functional segregation and integration among identified frequency-specific FCNs. I discuss the results in Study 3 to conclude this chapter with providing the statement: frequency-specific topologies of FCN exist in the brain.

Finally, in Chapter 5, I express my viewpoint on the contribution of this thesis to the scientific and methodological breakthroughs in the field of neuroimaging by summarizing the results of the above-mentioned three studies. Furthermore, I discuss topics relevant to the thesis and future issues: functions of frequency-specific FCNs, relationships between different frequency-specific FCNs, the way frequency-specific FCNs work in real-time, and possible electrophysiological backgrounds of frequency-specific FCNs.

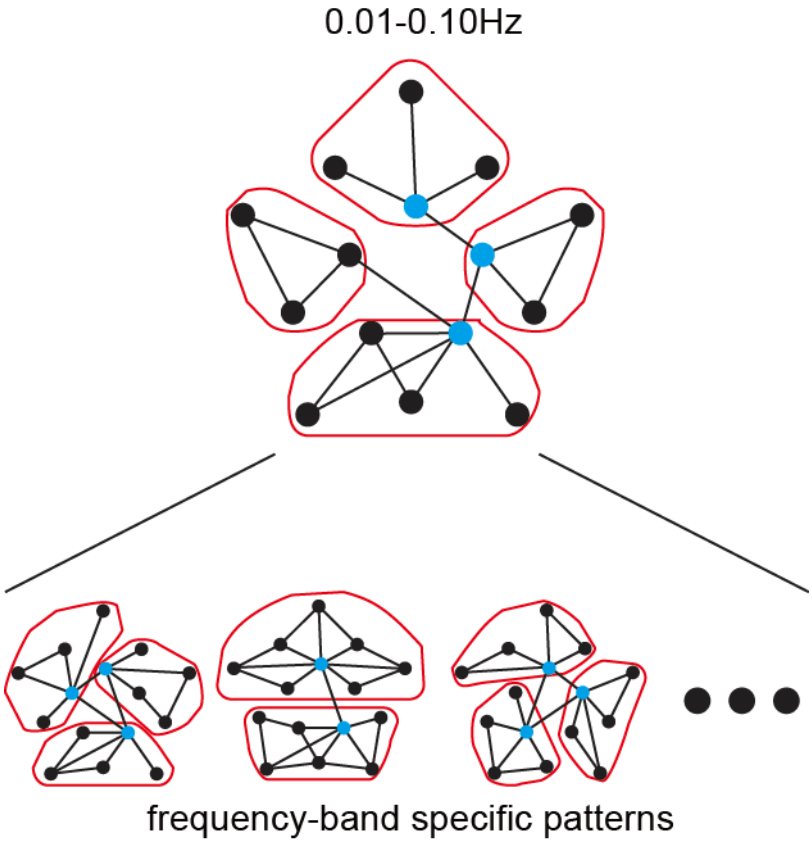

Figure 1.8. Hypothesis of this thesis. Black nodes are nodes representing different brain regions. Blue nodes are hub nodes. Areas surrounded by red lines are communities. Generally, functional connectivity has been estimated by estimating the correlation of hemodynamic fluctuations within 0.01–0.10 Hz. However, some studies showed the existence of frequency-dependency of functional connectivity within this frequency band. Thus, I hypothesized that there are different spatial patterns of FCNs within narrower frequency bands than the wider frequency band (0.01–0.10 Hz) where functional connectivity has been estimated. The purpose of this thesis was to clarify the spatial patterns of FCN in narrow frequency bands within 0.01–0.10 Hz.

Chapter 2 Frequency-specific functional connectivity in the brain during resting state as revealed by NIRS (Study 1)

2.1 Introduction

It is known that spontaneous fluctuations of brain activity exist even in the absence of overt tasks or stimuli (Fox and Raichle, 2007). This phenomenon is detectable in blood oxygenation level-dependent (BOLD) signals measured by functional magnetic resonance imaging (fMRI) (Biswal et al., 1995; see Fox and Raichle, 2007 for review) and hemoglobin oxygenation signals measured by near infrared spectroscopy (NIRS) (Elwell et al., 1999; Hoshi et al., 1998; Obrig et al., 2000; Toronov et al., 2000 for resting state in adults; Schroeter et al., 2004 for resting state in elderly subjects; Taga et al., 2000 for sleeping state in infants). It is also demonstrated that there are strong correlations among BOLD signal fluctuations of distinct regions of the brain in the low frequency range (<0.1 Hz) in the resting state (Biswal et al., 1995). This correlation, termed "resting state functional connectivity," has been well reproduced in many studies using fMRI. Moreover, distributed cortical regions showing such functional connectivity have been seen to constitute "resting state networks" (RSNs), including sensory, motor, sensory association, and default mode networks (Damoiseaux et al., 2006; De Luca et al., 2006; Fox and Raichle, 2007; Lowe et al., 1998). Some studies using NIRS also successfully demonstrated functional connectivity (Lu et al., 2010; White et al., 2009; Zhang et al., 2010b). Although these studies showed the first demonstration of NIRS applicability to detect functional connectivity, brain regions measured in these studies were limited to selected cortical regions such as sensorimotor, auditory, and visual regions. A NIRS study of infants showed functional connectivity of the global cortical network

during the sleeping state (Homae et al., 2010). However, global network properties of functional connectivity among diverse regions of the cortex in adults have not been well studied using NIRS.

Functional connectivity is characterized by a temporal correlation between two raw time series with "low frequency," separable from respiratory (0.1–0.5 Hz) and cardiovascular (0.6–1.2 Hz) signal frequencies by using fMRI (Cordes et al., 2001). Several fMRI studies with frequency component analyses using coherence or mutual information have shown that functional connectivity is predominantly subtended by low frequency components of the data (<0.3 Hz) (Achard et al., 2006; Salvador et al., 2005b, 2008; Sun et al., 2003). One fMRI study of decomposition of signals into various frequency bands within a low frequency range (0–0.24 Hz) demonstrated that correlations in the cortical networks concentrated within ultra-low frequencies (0.01–0.06 Hz) (Wu et al., 2008). On the other hand, NIRS has a higher time resolution (sampling rate: ~10 Hz) than fMRI (sampling rate: ~1 Hz), which prevents aliasing of higher frequency activity such as respiratory and cardiovascular activity into low-frequency signal fluctuations (Elwell et al., 1999; Lu et al., 2010; Obrig et al., 2000; White et al., 2009). Enhanced time resolution of NIRS-detected oxygenated hemoglobin (oxy-Hb) and deoxygenated hemoglobin (deoxy-Hb) changes should provide more information about the hemodynamics of neurovascular coupling (Obrig and Villringer, 2003 for review). Studies using NIRS demonstrated that spontaneous oscillations of cerebral hemodynamics include two distinguishable frequency components at low frequency (~0.10 Hz) and a very low frequency (~0.04 Hz) (Obrig et al., 2000; Schroeter et al., 2004). Although the mechanism underlying these signal fluctuations remains unknown, simultaneous recordings of cerebral hemoglobin oxygenation, heart rate, and mean arterial blood pressure showed that the systemic signal contribution to the hemodynamic changes in the frequency range (0.04–0.15 Hz) was 35% for oxy-Hb and 7% for deoxy-Hb (Katura et al., 2006),

suggesting that low-frequency fluctuations largely reflect hemodynamic responses to regional neural activities. Moreover, analysis of functional connectivity using NIRS is conducted by calculating the correlation between raw time series of measurement signals, and no information is lost through preprocessing of raw data. Despite the limited number of NIRS measurement channels, this limitation should provide a reasonable compromise for mesoscopic characterization of networks of functional connectivity in the cerebral cortex. Thus, I performed a NIRS study to explore the frequency-specific features of functional connectivity between diverse regions of the cerebral cortex, which has not been investigated by other NIRS studies in adults.

2.2 Material and methods

2.2.1 Participants

A total of 21 healthy adults (13 women and 8 men; range, 20–36 years old) participated in this experiment. All participants were awake with their eyes closed during the measurements. Ethical approval was obtained for this study from the ethical committee of the Graduate School of Education, University of Tokyo, and informed consent was obtained from all participants prior to initiation of the experiments.

2.2.2 Data acquisition

I used a near-infrared optical topography instrument (ETG-100; Hitachi Medical Corporation, Tokyo, Japan) to measure the time series of spontaneous changes in oxy-Hb and deoxy-Hb during a 16-min period with 0.1-s time resolution. The instrument generated two wavelengths of near-infrared (NIR) light (780 nm and 830 nm). I evaluated relative changes in the

oxy-Hb and deoxy-Hb signals from an arbitrary 0 baseline at the start of the measurement period based on the Lambert-Beer law (Maki et al., 1995; Reynolds et al., 1988). Since the precise optical path length was unknown, the unit used to measure these values was molar concentration multiplied by length (mM·mm). The distance between the incident and the detection fibers was 3 cm, and each pair of adjacent incident and detection fibers defined a single measurement channel. The 10 emitters and 8 detectors were plugged into a holder and arranged into a 1 × 18 array, resulting in 16 measurement channels (Fig. 2.1A). Arrays were positioned over the bilateral prefrontal, temporal, and occipital regions by referring to the international 10-20 system of electrode placement (Fig. 2.1B). I also conducted measurements on a spherical phantom made of silicone rubber, which was considered to have similar properties of optical absorption as the human head region (Hitachi Medical Corporation, Tokyo, Japan).

2.2.3 Data analysis

To remove long-term drift of baseline and higher-frequency cardiac or respiratory activity (Lu et al., 2010; White et al., 2009), I used a band-pass Fourier filter (0.009–0.10 Hz) on the raw time series of the oxy-Hb and deoxy-Hb signals. After this process, I calculated the cross-correlations of signals between all of the channel pairs for each participant. The top 30% of participant-averaged coefficients, which corresponds to a threshold of $r > 0.6$, were mapped as functional connectivity.

In order to investigate the frequency specificity of functional connectivity, I decomposed the raw signals into band-pass filtered signals with narrow frequency bands (0.009–0.02, 0.02–0.04, 0.04–0.06, 0.06–0.08, and 0.08–0.10 Hz) instead of using a broadband band-pass Fourier filter (0.009–0.10 Hz). After this procedure, I applied the above-described cross-correlation analysis for each

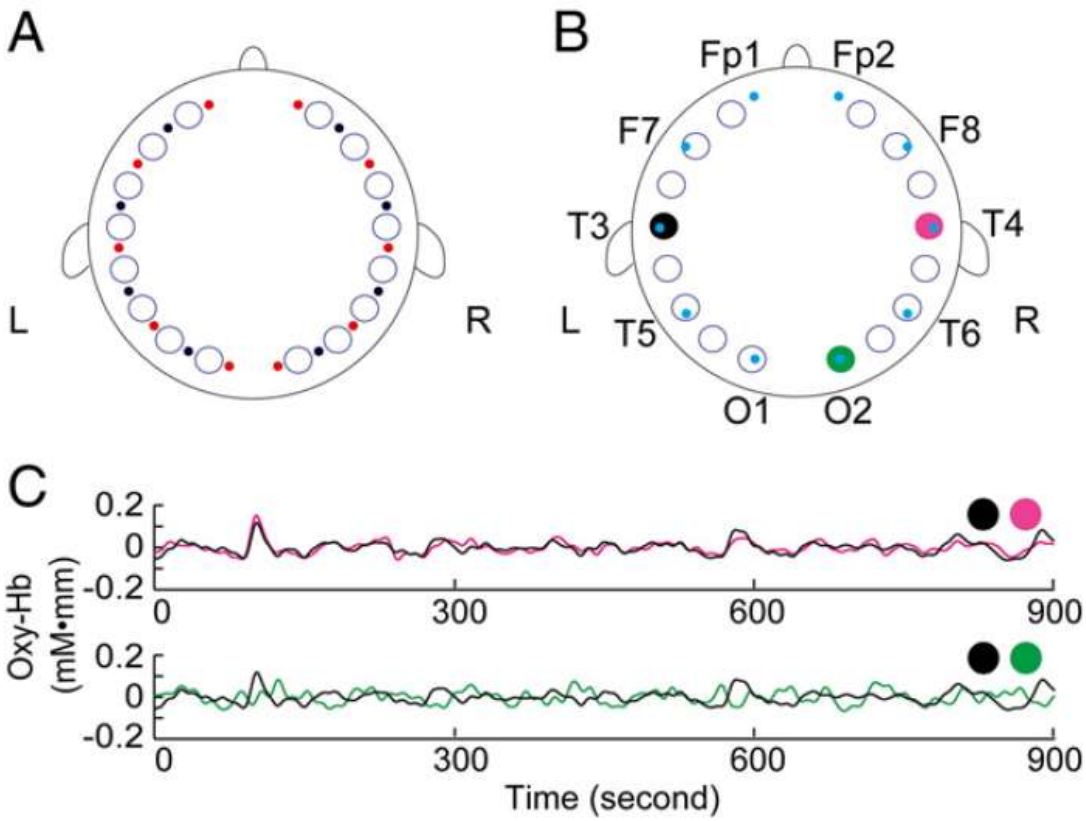

Figure 2.1. Channel configuration and measured signals. (A) Configuration of emitters (red dots), detectors (black dots), and measurement channels (blue circles) of the NIRS system. (B) Configuration of 16 measurement channels (blue circles) of NIRS based on the international 10–20 system (cyan dots). (C) Representative examples of continuous data of a participant. The black, pink, and green lines show the data of the measurement channel filled with the same colors in B. The pair in the top has a high temporal correlation. In the bottom, the correlation between the two channels was lower than that in the top.

dataset and mapped participant-averaged functional connectivity exceeding the same threshold.

I then aimed to further clarify coherence of the functional connectivity at the network level. To this aim, squared coherence between all of the channel pairs for each participant was calculated. I applied Welch's averaged modified periodogram method (using a 2,048-point Fourier transform, Hanning window, and 1,024-point overlap) to estimate the cross-spectral density and power spectral density, both of which were used to calculate the squared coherence. Then, participant-averaged squared coherence was calculated for each channel pair. To characterize the frequency properties of functional connectivity between distinct cortical regions, I selected three connectivity groups: (1) homologous connectivity between interhemispheric homologous regions of the frontal, temporal, and occipital cortices; (2) fronto-posterior connectivity, which consists of long-distance connections between bilateral prefrontal and bilateral occipital cortices; and, (3) control connectivity, which consists of arbitrarily chosen connections. Each connectivity group consisted of eight channel pairs and averaged squared coherence was obtained for each connectivity group.

To reveal the specific feature of each connectivity group in each frequency band, I analyzed the effects of factors between frequency bands and between connectivity groups. I selected two frequency bands for this analysis: (1) very low frequency (VLF) (0.009–0.02 Hz) and (2) low frequency (LF) (0.06–0.08 Hz). Averaged coherence values of each connectivity group in these two frequency bands were calculated and converted to z scores using Fischer’s z transformation. I performed two-way analysis of variance (ANOVA) with both frequency bands (VLF and LF) and connectivity groups (homologous connectivity, fronto-posterior connectivity, and control connectivity) as two factors. Ryan’s tests were applied as post-hoc tests.

2.3 Results

Figure 2.1C shows an example of a single participant's time series data. While the signal changes of the measurement channels on the homologous regions of the bilateral temporal cortices appeared to be correlated, those on the left temporal cortex and on the right occipital cortex appeared to be non-correlated. Participant-averaged temporal correlations of continuous oxy-Hb signals between all of the measurement channel pairs revealed functional connectivity between interhemispheric homologous regions of the frontal, temporal, and occipital cortices (homologous connectivity) (Fig. 2.2A). I also observed both short-distance ipsilateral connectivity and long-distance contralateral connectivity. However, no long-distance connectivity within the hemisphere was observed. The deoxy-Hb signal results showed a high correlation between interhemispheric homologous regions (Fig. 2.2C).

To reveal the frequency-specificity of the functional connectivity, I applied five distinct band-pass filters to the raw time series and performed correlation analyses for the filtered data (Fig. 2.2B for oxy-Hb signals and Fig. 2.2D for deoxy-Hb signals). The decomposition of signals into narrower frequency bands revealed that the functional connectivity observed in the broadband frequency band of filtering (0.009–0.10 Hz) was found in the lower frequency bands (0.009–0.02 Hz and 0.02–0.04 Hz) in both signals. In contrast, in the higher frequency band (0.04–0.06 Hz, 0.06–0.08 Hz, and 0.08–0.10 Hz), only oxy-Hb signals showed functional connectivity between the prefrontal regions of both hemispheres and the wide regions of the temporal and occipital cortices of the ipsilateral and contralateral hemispheres. The findings of the oxy-Hb signals demonstrated that homologous connectivity was subtended in the broader frequency bandwidth (0.009–0.10 Hz), while the fronto-posterior connectivity was present in the narrower bandwidth (0.04–0.10 Hz).

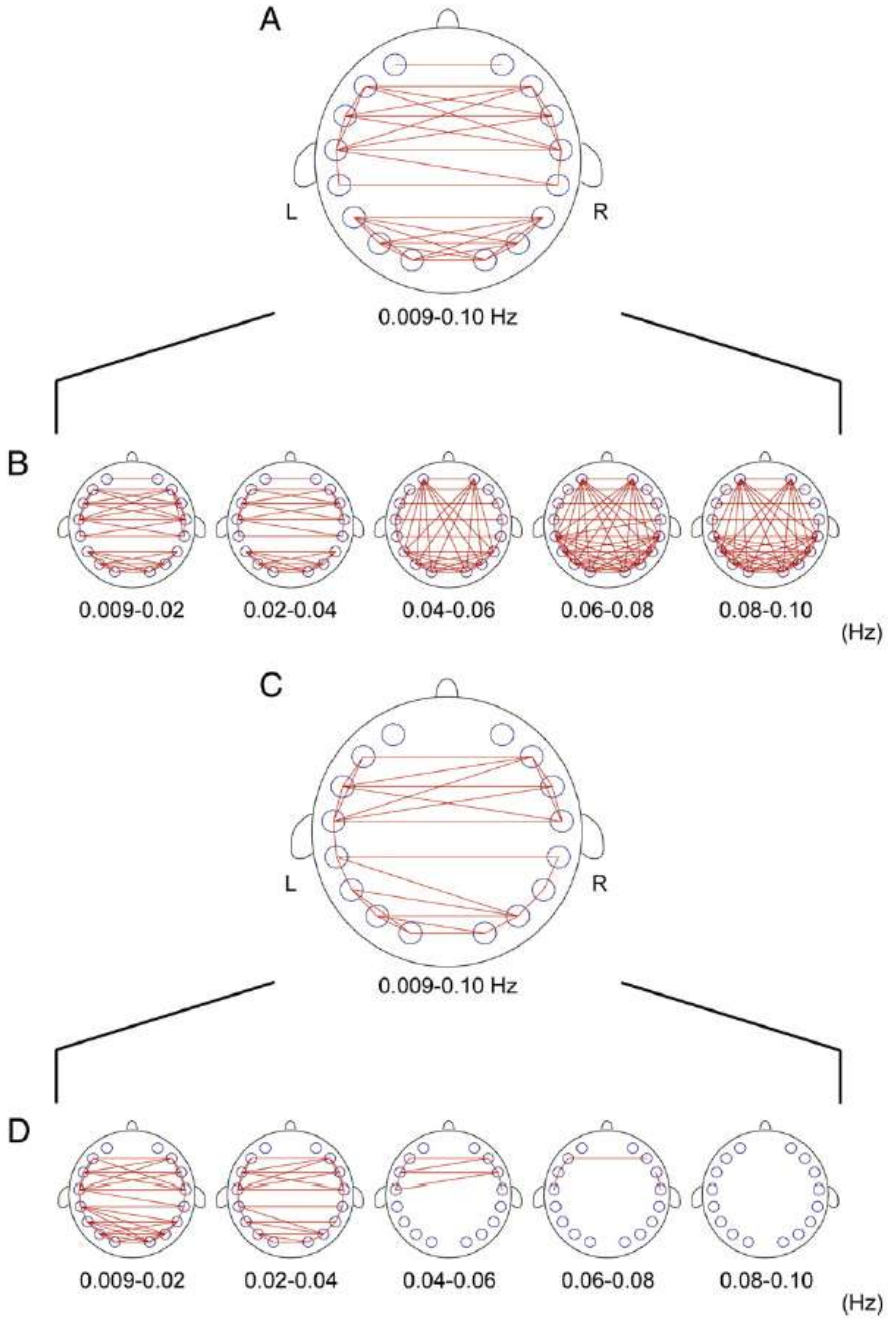

Figure 2.2. Frequency-specificity of the functional connectivity maps. (A) Functional connectivity based on oxy-Hb signals in a broad band (0.009–0.10 Hz). (B) Frequency-specific functional connectivity maps based on oxy-Hb signals with narrow frequency bands. (C) Functional connectivity based on deoxy-Hb signals in a broad band. (D) Frequency-specific functional connectivity maps based on deoxy-Hb signals with narrow frequency bands. The lines show correlations that were higher than 0.6 (averaged across all participants).

The result of averaged coherence of the three different groups of functional connectivity (Fig. 2.3A) in oxy-Hb signals showed that the averaged coherence of the homologous connectivity was high over a wide frequency range (~0.10 Hz), while the coherence of the fronto-posterior connectivity was high only within a specific frequency range (0.04–0.10 Hz) (Fig. 2.3B). The coherence of the control pairs was lower than that of the homologous and fronto-posterior connectivity over the wide frequency range (0.009–0.10 Hz). Thus, the results confirmed correlation analysis findings that fronto-posterior connectivity occurred within a specific narrow frequency range, whereas the homologous connectivity extended over a broad frequency range in oxy-Hb signals.

Results of analysis of variance (ANOVA) to examine the effect of both frequency bands (VLF and LF) and connectivity groups (homologous connectivity, fronto-posterior connectivity, and control connectivity) to coherence are shown in Figure 2.3C. A significant main effect was observed for the connectivity groups ($F(2,40) = 114.714$, $p < 0.001$), while no significant effect was found for the frequency bands (Fig. 2.3C). In addition, there were significant interactions between the connectivity groups and the frequency bands ($F(2,40) = 10.752$, $p < 0.001$). With regard to the interaction, there were significant simple main effects of the connectivity groups on VLF ($F(2,80) = 91.295$, $p < 0.001$) and LF ($F(2,80) = 51.581$, $p < 0.001$). Post-hoc multiple comparisons for the connectivity groups on VLF and LF revealed that the mean z score of the homologous and fronto-posterior connectivity was greater than that for control connectivity ($p < 0.001$ for homologous and $p < 0.01$ for fronto-posterior on VLF and all $p < 0.001$ on LF) and that for homologous connectivity was greater than that for fronto-posterior connectivity in both frequency bands ($p < 0.001$ for all). It was also revealed that while there was no significant effect of the connectivity groups on the frequency bands, there were significant simple main effects of the frequency bands on fronto-posterior connectivity ($F(1,60) = 17.164$, $p <$

0.001), revealing that the mean z score in LF was greater than that in VLF for fronto-posterior connectivity.

Figure 2.4 shows the averaged coherence of three different functional connectivity groups in terms of the deoxy-Hb signals. The results show that the average coherence of the homologous connectivity was high in the low frequency range (0.009–0.10 Hz), while the coherence of fronto-posterior connectivity and control pairs was low over the same frequency range (Fig. 2.4A). The results of two-way ANOVA to examine the effect of both frequency bands and connectivity groups on coherence are shown in Figure 2.4B. Significant main effects were observed for the connectivity groups ($F(2,40) = 93.983$, $p < 0.001$) and for the frequency bands ($F(1,20) = 19.885$, $p < 0.001$). In addition, there was a significant interaction between the frequency bands and the connectivity groups ($F(2,40) = 27.541$, $p < 0.001$). With regard to this interaction, there were significant simple main effects of the connectivity groups on VLF ($F(2,80) = 118.922$, $p < 0.001$) and LF ($F(2,80) = 21.762$, $p < 0.001$). Post-hoc multiple comparisons for the connectivity groups on VLF and LF revealed that there were significant differences between the mean z score of homologous connectivity and those of the other two connectivity groups ($p < 0.001$ for all). Between fronto-posterior and control connectivity, a significant but weak difference ($p < 0.05$) in VLF and no significant difference in LF were observed. There were also significant simple main effects of the frequency bands on homologous connectivity ($F(1,60) = 68.663$, $p < 0.001$), revealing that the mean homologous connectivity z score in VLF was greater than that in LF.

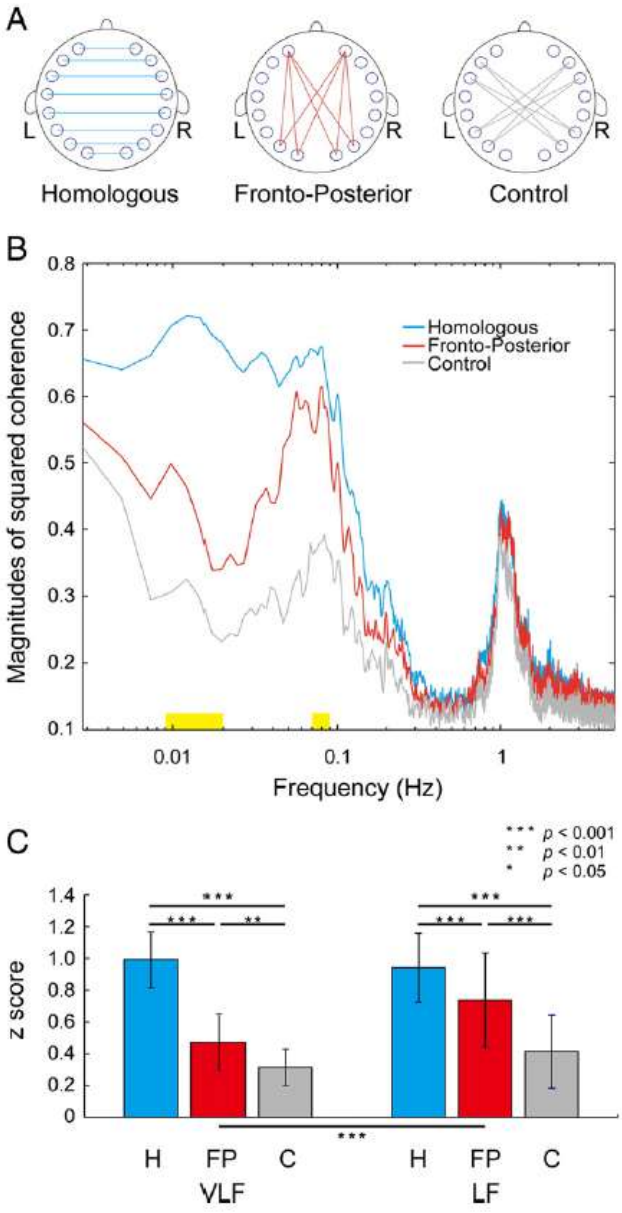

Figure 2.3. Averaged squared coherence for the connectivity groups in oxy-Hb signals. (A) Configurations of selected connectivity groups. (B) Magnitudes of participant-averaged squared coherence for each connectivity group. Yellow bars indicate the range of very low frequency (VLF) (0.009–0.02 Hz) and low frequency (LF) (0.06–0.08 Hz). (C) Result of statistical analysis using two-way ANOVA (factor 1: connectivity groups, factor 2: frequency bands). The terms of 'H', 'FP', and 'C' represent homologous, fronto-posterior and control connectivities, respectively. Error bars indicate standard deviations. Significant differences between connectivity groups and between frequency bands are shown (*$p < 0.05$, **$p < 0.01$, ***$p < 0.001$, post-hoc tests).

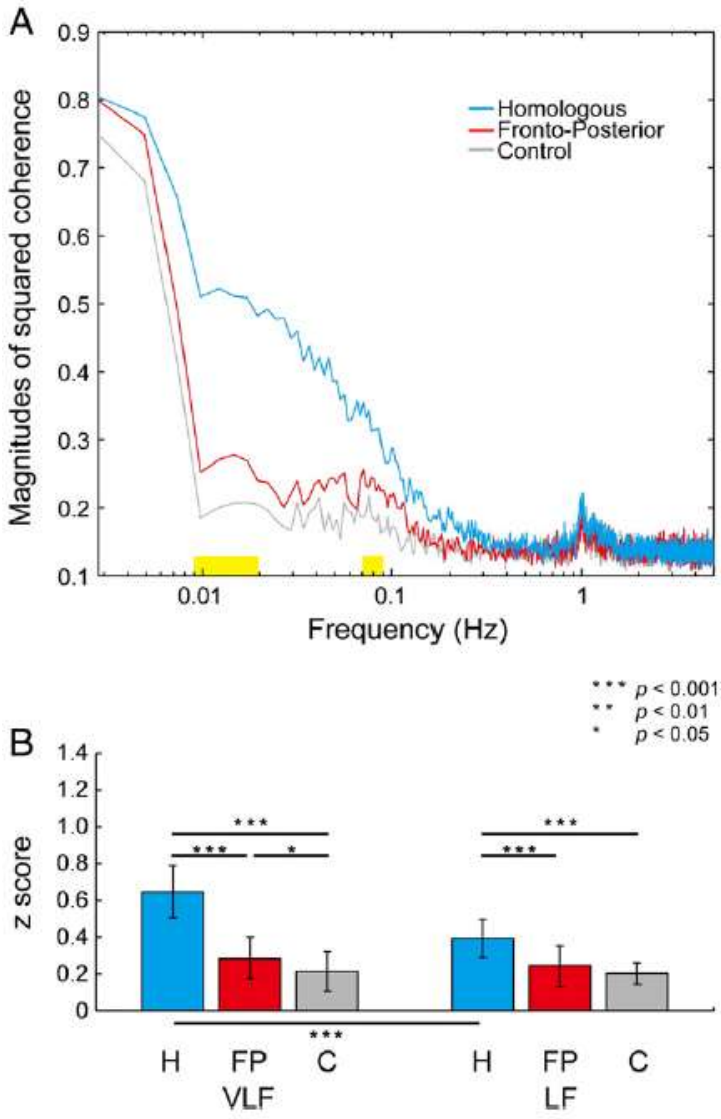

Figure 2.4. Averaged squared coherence for the connectivity groups in deoxy-Hb signals. (A) Magnitudes of participant-averaged squared coherence for each connectivity group. Yellow bars represent the same frequency bands as described in Fig. 2.3. (B) Result of statistical analysis using two-way ANOVA (factor 1: connectivity groups, factor 2: frequency bands). See Fig. 2.3 for abbreviations of.connectivity groups and frequency bands. Error bars indicate standard deviations. The differences between connectivity groups and between frequency bands are shown (*p < 0.05, **p < 0.01, ***p < 0.001, post-hoc tests).

To investigate the effect of signal fluctuations caused by measurement device instabilities and/or non-physiological artifacts on low-frequency coherence, I conducted an additional measurement on a spherical phantom with equal absorption in the human head region; also, the same analysis, with respect to measured signals as applied to the human participant data (see section 2.2), was undertaken. All of the connectivity groups showed relatively high coherence in an ultra-low frequency band (~0.009 Hz), which possibly reflected baseline signal drifts that are not related to neural activity. The results confirmed that there was no high coherence in the two connectivity groups of channel pairs (homologous and fronto-posterior connectivity) generated by the NIRS device in the range of the broadband filter (0.009–0.10 Hz) (see Fig. 2.S1 in supplementary materials).

2.4 Discussion

In this study, I investigated the frequency characteristics of functional connectivity among the prefrontal, temporal, and occipital regions of the cortex during the resting state by using NIRS. To fulfill the aims, correlation analysis of narrow or broadband pass-filtered data was performed (Fig. 2.2). The oxy-Hb signal results indicated that functional connectivity between distinct regions of the cortex showed distinct properties in the frequency domain. In particular, interhemispheric homologous connectivity showed high correlation in the wide frequency range (0.009–0.10 Hz), whereas fronto-posterior connectivity showed high correlation only in the specific frequency band (0.04–0.10 Hz). Frequency-specific characteristics were confirmed by coherence analysis (Fig. 2.3). Collectively, our findings showed that there was frequency-specific functional connectivity of the global cortical networks, including fronto-posterior connectivity.

It is generally assumed that extremely low frequency signals are caused by measurement

device instabilities, non-physiological artifacts, and/or temporal durations of NIRS measurement. Coherency analyses using the spherical phantom showed that coherence of the selected channel pairs was very high at frequencies less than 0.009 Hz and that the values were comparable to those measured in human participants (Fig. 2.S1). In contrast, coherence in the phantom measurement was sufficiently low at frequencies greater than 0.009 Hz (Fig. 2.S1). These results for both oxy-Hb and deoxy-Hb signals showed that while the extremely low frequency signal changes were largely affected by measurement artifacts and/or durations of measurement, the signal changes faster than 0.009 Hz could not be attributed to non-physiological noise.

Hemoglobin concentration changes in the cerebral cortex detected by NIRS may include not only responses to regional neural activities but also to signals unrelated to regional neural activities, such as systemic regulation of the cardiovascular system or respiratory fluctuation. In our study, I confined analyses and interpretation to a low frequency region below 0.10 Hz. Since frequency bands corresponding to respiratory frequency and cardiac pulsations are higher than 0.10 Hz (respiratory fluctuation, ~0.2 Hz; cardiac pulsation, ~1 Hz) (Elwell et al., 1999; Obrig et al., 2000), it is unlikely that our results were affected by these signals. It is also unlikely that the measured signals simply reflected skin blood flow fluctuation since a previous study reported that this possibility can be largely excluded on the basis of a measurement using different inter-optode distance (Obrig et al., 2000). On the other hand, I cannot fully exclude the possibility that some portions of the low frequency range hemoglobin signal changes were contaminated by heart rate and blood pressure fluctuations. However, a study investigating the causal relationship between hemoglobin concentration changes, heart rate, and mean arterial blood pressure by using transfer entropy as measures of information transfer demonstrated that these systemic signals can account for only 35% of the information carried by

oxy-Hb changes in a frequency range of 0.04–0.15 Hz (Katura et al., 2006). Furthermore, our finding of significantly higher coherence in homologous and fronto-posterior connectivity compared to that in control connectivity (Fig. 2.3C) cannot be accounted for only by systemic effects and/or extracerebral tissue contributions, which should appear all over the cortical regions. Thus, our findings indicate that higher coherence of hemodynamic changes between specific cortical regions in the low frequency range reflects higher coherence of neural activity between these regions.

One of the possible underlying mechanisms of generating functional connectivity, such as homologous connectivity, is represented by covariance of neural activity through direct structural connection. Several studies have suggested that distinct regions among which hemodynamic fluctuations show high correlation are connected directly through neuroanatomical structures. For example, the white matter pathways between the functionally linked brain areas of the resting state network were reconstructed using diffusion tensor imaging (Greicius et al., 2009; van den Heuvel et al., 2009). Another study demonstrated that interhemispheric functional connectivity was lost after complete section of the corpus callosum for treatment of intractable epilepsy (Johnston et al., 2008). Furthermore, the correlation coefficient of a given functional connectivity is negatively associated with physical distance (Wu et al., 2008). All this evidence strongly suggests that functional connectivity reflects underlying neuroanatomical connectivity. Intriguingly, spontaneous neuronal activities of interhemispheric human auditory cortices show high correlation at slow firing rates (<0.10 Hz) but no correlation at fast firing rates (>1 Hz) during wakeful rest (Nir et al., 2008). These findings, overall, suggest that homologous connectivity reflects a correlation of spontaneous neuronal activities in a wide frequency range through direct structural connection.

On the other hand, taking into consideration that the time scale of typical hemodynamic

responses to a single event (10–20 s) corresponds to the frequency band, including LF, the high coherency of the fronto-posterior connectivity in the LF range may reflect simultaneous transient activity of these regions. Furthermore, given the fact that the prefrontal region serves executive control over selecting actions or thoughts in relation to internal goals, fronto-posterior connectivity may serve as the hub of functional network in the resting state.

In line with the results of oxy-Hb signals, the average coherence of homologous connectivity based on deoxy-Hb signals was high in a wide frequency range (0.009–0.10 Hz). In contrast, the fronto-posterior connectivity based on deoxy-Hb signals was very low even in the LF band. Such discrepancies between the oxy-Hb and deoxy-Hb signal results may be attributable to the difference in the nature of hemodynamic responses to transient neural activity and/or the difference in signal-to-noise ratios in the NIRS measurement. To examine the former assumption, it would be helpful to investigate the effect of transient and sustained stimuli on functional connectivity defined by each hemoglobin signal. Interestingly, the fMRI study on functional connectivity frequency analysis showed correlation concentrates within 0.01–0.06 Hz (Wu et al., 2008), which seems compatible with the deoxy-Hb data in the present study. Future studies of simultaneous measurements using fMRI and NIRS will provide additional insight into this issue.

NIRS requires fewer physical constraints than fMRI. Thus, applying NIRS to investigate functional connectivity enables us to extend its focus toward other cases from current experimental conditions for which application of fMRI is not suitable, such as the investigation of patients, children, and infants. For example, a NIRS study successfully demonstrated that resting state functional connectivity of human infants during sleep varies dynamically along the developmental course (Homae et al., 2010). The present study showed that NIRS was applicable for investigating the spatiotemporal

properties of functional connectivity, thus promoting further study of structural and functional networks of the brain in various populations with NIRS.

2.5 Supplementary materials

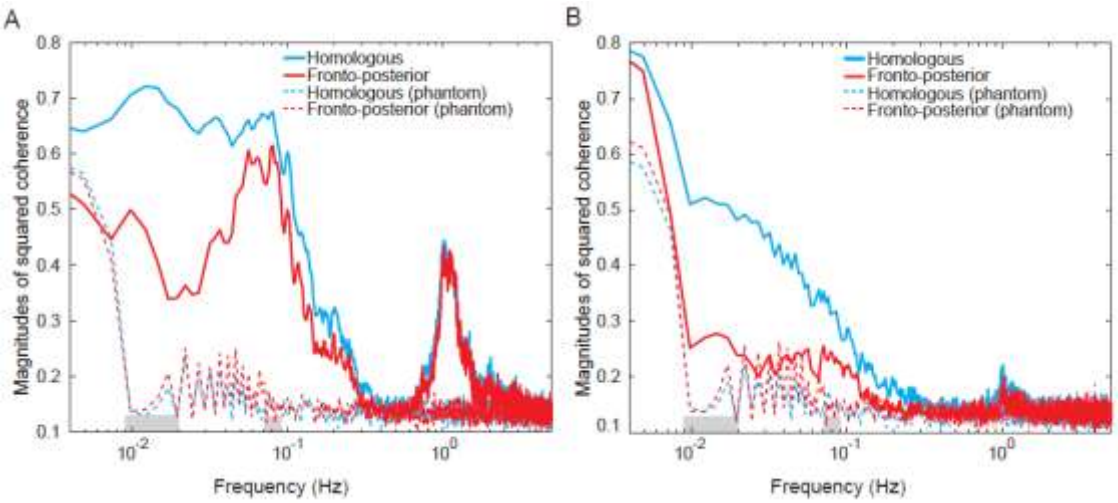

Figure 2.S1. The effect of measurement device instabilities and/or non-physiological artifacts on coherence. Phantom measurements were conducted on a head made of silicone rubber using the same procedures as performed in human participants. Average coherence of each connectivity: (A) oxy-Hb and (B) deoxy-Hb. Line colors represent connectivity groups: homologous connectivity (blue) and fronto-posterior connectivity (red). Bold and broken lines indicate human and phantom measurements, respectively.

Chapter 3 A NIRS–fMRI study of the resting state network (Study 2)

3.1 Introduction

The brain typically operates in a coordinated manner even during the resting state. Functional magnetic resonance imaging (fMRI) demonstrates that there is a strong correlation among blood oxygenation level-dependent (BOLD) signal fluctuations of distinct regions of the brain in the low frequency range (<0.1 Hz) in the resting state (Biswal et al., 1995). This correlation, termed resting state functional connectivity, has often been observed between functionally related brain regions, including sensory, motor, sensory association, attention, and task-negative regions (Fox and Raichle, 2007). When I regard this connectivity as the "edge" and the brain regions linked by the connectivity as the "node," the spontaneous brain activity constitutes unique network architectures, termed resting state networks (RSNs) (De Luca et al., 2006; Fox and Raichle, 2007; Lowe et al., 1998). These network architectures are consistent across healthy individuals (Damoiseaux et al., 2006), and they are suggested to reflect intrinsic functional architecture of the brain (Fox and Raichle, 2007).

Near infrared spectroscopy (NIRS) is a technique for measuring changes in local oxygenated and deoxygenated hemoglobin (oxy-Hb and deoxy-Hb) concentrations. Studies using NIRS have successfully observed functional connectivity during the resting state in both adult and infant participants (Homae et al., 2010, 2011; Lu et al., 2010; Mesquita et al., 2010; White et al., 2009; Zhang et al., 2010b). One NIRS study also demonstrated that functional connectivity estimated using oxy-Hb and deoxy-Hb signals obtained during the resting state has different frequency characteristics (Sasai et al., 2011). Moreover, higher temporal resolution of NIRS has revealed a temporal relationship of

signals obtained at different brain regions in combination with analysis of phase synchronization (Taga et al., 2000, 2011). These results support that NIRS is a useful neuroimaging technique for acquisition of information pertaining to functional connectivity. Considering that NIRS is less physically demanding and relatively easy to use compared to other neuroimaging techniques, application of NIRS may allow easy RSN data collection even in cases where fMRI would be difficult to use.

Because both fMRI and NIRS signals measured during the resting state may reflect spontaneous brain activity, NIRS signals in diverse regions of the cortex during the resting state should show a high correlation with BOLD signals in regions adjacent to each of the NIRS measurement positions. Furthermore, despite the fact that NIRS can detect cortical activity only in superficial cortical regions, I can hypothesize that the NIRS signals measured in separate regions of the cortex can capture information reflecting different RSNs that include not only superficial regions, but also deep brain regions such as the default mode network (Buckner et al., 2008; Raichle et al., 2001). However, although the simultaneous use of these techniques during stimulation or task execution has shown a high correlation between the two different signals in the corresponding cortical regions (Cui et al., 2011; Hoge et al., 2005; Kleinschmidt et al., 1996; Schroeter et al., 2006; Strangman et al., 2002; Toronov et al., 2001; Toyoda et al., 2008), it is not well understood whether this relationship is also true during the resting state. Moreover, although previous studies have simultaneously recorded NIRS signals within limited regions and BOLD signals of the whole brain during the resting state (Duan et al., 2012; Tong and Frederick, 2010), the investigators did not compare the NIRS signals in diverse regions of the cortex and the BOLD signals. Thus, the aim of this study was to establish the NIRS–fMRI relationship to study functional connectivity with a special focus on the RSNs.

To solve the above-mentioned issue, I designed and conducted step-by-step analyses. First,

I had to determine the relative locations of NIRS measurement channels on the participant's brain to determine the brain regions where NIRS acquires its signals. However, I could only obtain the probabilistic anatomical cranio-cerebral correlation to represent the anatomical location of the NIRS measurement channels (Okamoto et al., 2004) because NIRS probes are located outside of the head. Thus, I obtained structural MRI of all participants while they were wearing NIRS probes and determined the accurate positional relationships between their brain regions and the NIRS probes, which constituted 14 channels and were located on bilateral frontal, temporal, and occipital cortices.

Second, I aimed to confirm that NIRS signals obtained from a channel during the resting state reflected the spontaneous hemodynamic fluctuations within the adjacent brain regions. Previous studies of simultaneous recordings of NIRS and fMRI have revealed that NIRS signals induced by several stimuli show high correlation with the BOLD signals obtained from adjacent brain regions to the NIRS measurement channels (Cui et al., 2011; Hoge et al., 2005; Kleinschmidt et al., 1996; Schroeter et al., 2006; Strangman et al., 2002; Toronov et al., 2001; Toyoda et al., 2008). In theory, with or without tasks, NIRS signals should reflect the concentration changes of oxy-Hb and deoxy-Hb within regions close to the NIRS channels. However, this theoretical deduction has not been confirmed for NIRS signals obtained during the resting state. To test this, I investigated whether I could find the local maximum of correlation coefficients between NIRS and BOLD signals simultaneously obtained during the resting state in the brain region close to each NIRS channel. However, because photons travel in a "banana shape" between the emitter and the detector (Okada et al., 1997; van der Zee et al., 1990), NIRS signals can be affected not only by changes in hemoglobin concentration within adjacent brain regions but also by those changes within non-brain regions such as skin and large pial veins (Gagnon et al., 2012a, 2012b; Kohno et al., 2007; Obrig et al., 2000; Saager and Berger, 2008; Tachtsidis et al.,

2008; Takahashi et al., 2011; Tonorov et al., 2000; Yamada et al., 2009; Zhang et al., 2007). Therefore, to evaluate whether the concentration changes of oxy-Hb and deoxy-Hb in the brain tissues are major substitutes of the NIRS signals obtained during the resting state, I sorted highly correlating voxels with NIRS signals by tissue types of the voxels (gray matter, white matter, cerebrospinal fluid [CSF], skull, and skin), and I calculated the proportion of the voxels within brain tissues (gray and white matter) against those within non-brain tissues (skull and skin).

Finally, I aimed to clarify whether RSNs estimated using fMRI data sets could be reproduced using NIRS signals. One of the techniques to estimate RSNs in the fMRI data sets is based on the calculation of cross-correlation between a BOLD time series extracted from a region of interest (ROI) as a seed and those of whole brain voxels. If NIRS signals include information characterizing RSNs contained in the seed BOLD signals, RSNs estimated using the BOLD signals extracted from ROIs should be reproduced using NIRS signals obtained from the ROIs. Thus, I investigated this issue by calculating correlation maps using BOLD and corresponding NIRS signals as seed signals.

If NIRS signals obtained from diverse regions of the cortex are probed to reflect the time series characterizing the major RSNs obtained by fMRI, it becomes possible to acquire the time series that represent RSNs solely by conducting NIRS measurements of the selected regions of the brain. By taking advantage of the high temporal resolution, we can address the temporal relationship between different RSNs (Chang and Glover, 2010; Kang et al., 2011; Majeed et al., 2011) using NIRS. Considering that NIRS measurements are relatively easy to use and less physically demanding, application of NIRS would facilitate in the collection of data on the RSNs not only in normal experimental environments but also in other situations, such as those involving a whole sleep period or social interaction and in particular populations such as infants and patients. Thus, using the

above-mentioned step-by-step analyses, I investigated whether sparse NIRS signals obtained from diverse regions of the cortex can represent the time series for major RSNs obtained by fMRI.

3.2 Materials and methods

The outline of the analysis conducted in this study is shown in Fig. 3.1.

3.2.1 Participants

A total of 28 healthy adults (15 men and 13 women; age range, 22–44 years) participated in this study. All participants were awake with their eyes closed during the measurements. The protocol was approved by the ethical committee of the National Institute for Physiological Sciences, Okazaki, Japan. Informed consent was obtained from all participants prior to initiation of the experiments.

3.2.2 Data acquisition

3.2.2.1 NIRS

A near-infrared optical topography instrument (ETG-4000; Hitachi Medical Corporation, Tokyo, Japan) was used to measure the time series of spontaneous changes in oxy-Hb and deoxy-Hb during a 20-min period with 0.1-s time resolution (Fig. 3.1, “NIRS data acquisition”). The instrument generated two wavelengths of near-infrared light (695 nm and 830 nm). I evaluated relative changes in the oxy-Hb and deoxy-Hb signals from an arbitrary baseline (set to 0) at the beginning of the measurement period based on the Lambert–Beer law. The unit used to measure these values was molar concentration multiplied by length (mM·mm). The distance between the incident and the detection fibers was 3 cm. The 8 emitters and 8 detectors were plugged into a holder, on which vitamin tablets

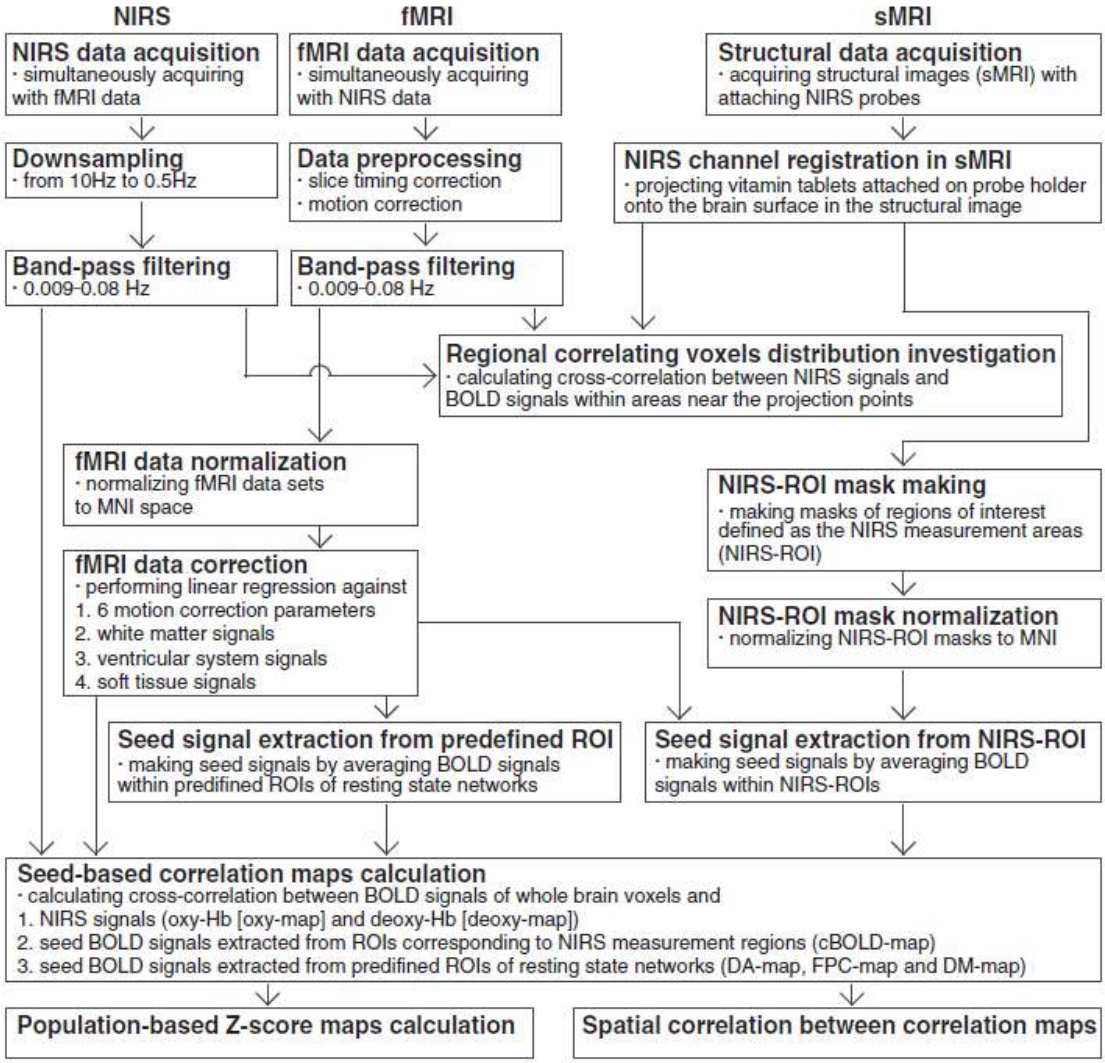

Figure 3.1. Outline of all analyses

were attached to identify the positions of NIRS channels in MRI images (Fig. 3.2A), and they were arranged into two 1 × 8 arrays, resulting in 14 measurement channels (Fig. 3.2B). Arrays were positioned over the bilateral frontal, temporal, and occipital regions by referring to the international 10–20 System of Electrode Placement (Fig. 3.2C). NIRS data were simultaneously obtained with fMRI

imaging for all participants, with each participant lying supine in an MRI scanner. The appearance of simultaneous recording with NIRS and fMRI is shown in Fig. 3.2D. A pillow was placed under the occiput to fix the participant's head and to avoid compressing the NIRS probes (Fig. 3.2E).

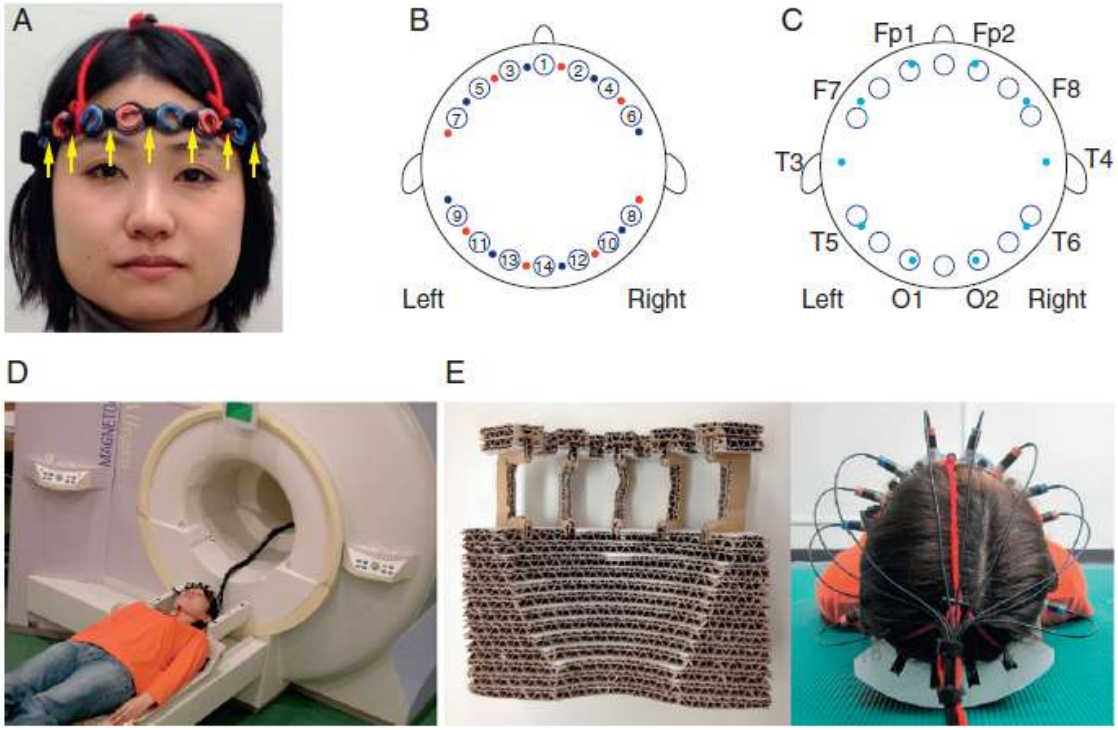

Figure 3.2. Experimental conditions, materials, and channel configurations. (A) Probe holder. Yellow arrows indicate attached vitamin tablets (black balls). (B) Configuration of emitters (red dots), detectors (black dots), and measurement channels (blue circles) of the NIRS system. Each channel was indexed by its unique number. (C) Configuration of 14 measurement channels (blue circles) of NIRS based on the international 10–20 system (cyan dots). (D) Appearance of simultaneous recording with NIRS and fMRI. (E) A pillow was used to fix the participant's head in the MRI scanner and to avoid compressing NIRS probes.

3.2.2.2 MRI

Functional and structural MRI images were acquired using a 3-Tesla MR scanner (Allegra; Siemens; Fig. 3.1, "fMRI data acquisition" and "Structural data acquisition"). First, a time series of 610 volumes was acquired for each session using T2*-weighted gradient-echo echo-planar imaging (EPI) sequence. Each volume consisted of 34 slices, each of which was 3.5 mm thick, with a 17% gap. The time interval between two successive acquisitions of the same slice (TR) was 2000 ms with a flip angle (FA) of 76° and an echo time (TE) of 30 ms. The field of view (FoV) was 192 × 192 mm and the in-plane matrix size was 64 × 64 pixels. Additionally, to acquire a fine structural whole brain image, magnetization-prepared rapid-acquisition gradient-echo (MPRAGE) images were obtained (TR = 2500 ms; TE = 4.38 ms; FA = 8°; FoV = 230×230 mm; one slab; number of slices per slab = 192; voxel dimensions = 0.9 × 0.9 × 1.0 mm).

3.2.3 Data preprocessing

3.2.3.1 NIRS

Both oxy-Hb and deoxy-Hb signals were downsampled to the fMRI acquisition frequency of 0.5 Hz by applying an anti-aliasing (lowpass) FIR filter in MATLAB (MathWorks, Inc., Natick,MA, USA) because these signals were measured with a 20-times higher sampling rate on fMRI data sets (10 Hz; Fig. 3.1, "Downsampling"). Spontaneous low frequency fluctuations are contaminated by various other signals originating mainly from non-neural sources. In order to remove the long term trends, which include respiratory and cardiac noises that are generally included outside the frequency band, I used a Butterworth band-pass filter (0.009–0.08 Hz) and performed zero-phase digital filtering by processing the data in both the forward and reverse directions in MATLAB (Fig. 3.1, "Band-pass

filtering").

3.2.3.2 fMRI

Functional MRI volumes were motion-corrected and slice-timing corrected using the SPM8 package (Wellcome Department of Imaging Neuroscience, London, UK) (Fig. 3.1, "Data preprocessing"). These functional volumes were neither spatially smoothed nor normalized. Subsequently, all data sets were processed with the same band-pass filter that was applied to NIRS signals (Fig. 3.1, "Band-pass filtering").

3.2.4 Registration of NIRS channels in the structural MRI

I defined projection points from each vitamin tablet onto the brain surface as the location of each NIRS channel (Fig. 3.1, "NIRS channel registration in sMRI"). Simulation studies demonstrated that I can assume that the photon traveling pathways are a "banana shape" between the incident and detection probes (Okada et al., 1997; van der Zee et al., 1990). Taking into account this property, the projection points were determined as follows. First, by visually searching vitamin tablets in the structural MRI images (Fig. 3.3A), I manually identified the position of each tablet in the structural image of each participant. Second, as shown in Fig. 3.3B, in order to determine a plane that mostly includes optical paths from the emitter to the detector for a NIRS channel, an optical path plane was estimated using a corresponding tablet and the two adjacent tablets on both sides. This plane was determined by minimizing a sum of squares of the distances between the plane and all voxels inside the three tablets. This procedure was used to determine planes for channels 1–5 and 10–14, whereas a plane for an adjacent channel was used for channels 6–9. Third, to determine a projection line from the

position of a tablet to the cortical surface, a bisector of the angle formed by the three median points of the section of the tablets on the optical path plane was chosen as a projection line for channels 1–5 and 10–14. On the other hand, by assuming that the curvature of the probe holder was constant along channels 4 and 6 and channels 5 and 7, a projection line was determined using the bisector angle and the plane of the adjacent channel for channels 6–9. Fourth, the projection point for each NIRS channel was defined as the intersection of the projection line of each channel and the surface of a gray matter mask, which was estimated from the structural image of each participant using the segmentation tool in SPM8. After the projection points were determined for all channels in each individual's data set by the above-mentioned procedure, I calculated the Montreal Neurological Institute (MNI) coordinates of the projection points. Subsequently, the mean and standard deviation of the MNI coordinates across all participants was calculated for each channel. Automated anatomical labeling (AAL) was applied to the mean MNI coordinate of each channel to obtain the most likely estimate (Tzourio-Mazoyer et al., 2002). I also applied the AAL system to the MNI coordinate of each channel for the data of each individual, and I evaluated the anatomical variability of a channel position across all participants.

3.2.5 Evaluation of regions where hemodynamic fluctuations were detected as NIRS signals during the resting state

I aimed to investigate the regions where hemodynamic fluctuations are detected as NIRS signals obtained during the resting state by finding the correlated voxels in the simultaneously acquired fMRI data (Fig. 3.1, “Regional correlating voxels distribution investigation”). A previous study using multiple tasks showed that NIRS signals mainly correlate with BOLD signals of the voxels adjacent to the projection points of channel markers located between emitters and detectors attached to brain

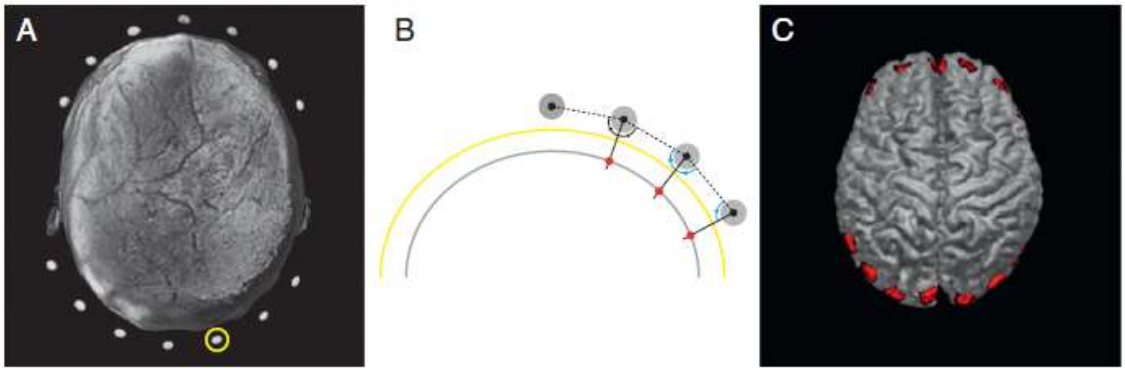

Figure 3.3. Determination of the cortical positions of vitamin tablets representing NIRS channels on the head. (A) Representative example of a structural image. One of fourteen vitamin tablets is surrounded by the open yellow circle. (B) Determination of the cortical projection points of vitamin tablets. Yellow and grey lines represent the skull and brain surfaces, respectively. Red dots are the determined projection points. Projection points were determined by projecting bisectors (black lines) of the angle formed by the three median points (black dots) of the section of the tablets on the optical path plane (filled grey circles) to the cortical surface. Angles with the same color have the same measure (black and cyan). (C) Representative example of determined ROIs corresponding to NIRS channels in the structural image. Red regions represent ROIs.

surfaces (Cui et al., 2011). Therefore, I assumed that NIRS signals should detect hemodynamic fluctuations in adjacent regions to the projection points of vitamin tablets for all measurement channels, even if there were many correlated voxels with NIRS signals distributed across broad brain regions. From this point of view, I identified the local best-correlated voxels (LBCV) with NIRS signals (Cui et al., 2011), and I investigated the spatial distributions of correlating voxels around the probe positions.

3.2.5.1 Distribution of the LBCV by referring to the projection point

After the preprocessing step, fMRI data sets were coregistered with the structural image of each participant using DARTEL in SPM8 (Ashburner, 2007). Subsequently, I calculated the

cross-correlation between each Hb signal obtained at each channel and BOLD signals from the whole head voxels. For each measurement channel, the nearest voxel from the projection point, which satisfied the following two conditions, was identified: (1) the correlation value for the voxel had a local maximum and (2) the correlation value was above 0.1 (Cui et al., 2011). Subsequently, the distance between the projection point and LBCV for each measurement channel was calculated.

3.2.5.2 Tissue level distribution

Because photons may travel across several tissues of a participant's head, highly correlated voxels (HCV) with NIRS signals can be located outside of brain tissues. To investigate whether HCVs were located within brain tissues, I identified the tissue type of HCVs. To do so, I estimated the mask of the brain tissue and the non-brain tissue using the New Segmentation method prepared in SPM8. By applying this method to the individual structural images, six types of masks were used (grey matter, white matter, CSF, skull, soft tissue, and air/background). Therefore, by combining the coregistered masks, I divided the voxels of fMRI data into two types of tissues: (1) brain tissue consisting of grey and white matter, and (2) non-brain tissue consisting of skull and soft tissue. After all, I investigated the locations of the top 100 ranked voxels within a 3-cm radius from the projection points and identified the types of tissues (brain tissue and non-brain tissue) of these voxels.

3.2.6 Whole brain distribution of correlated voxels with NIRS signals obtained during the resting state

After investigating the local relationship between NIRS and fMRI signals, I focused on examination of the spatial distribution of correlated voxels over the whole brain. Because fMRI studies

have repeatedly reported the existence of specific patterns of correlated voxels among several spatially separated brain regions, the NIRS signal can also correlate with BOLD signals from voxels other than those in adjacent areas to the channel. Therefore, I investigated whether the NIRS signal obtained at each measurement channel consistently reproduced the spatial pattern of the seed-based correlation map calculated with the BOLD signal of the ROIs corresponding to that NIRS measurement region. Furthermore, some NIRS probes were located near the brain regions included in the sets of brain regions specific to some RSNs (dorsal attention [DA], fronto-parietal control [FPC], and default mode [DM] networks), which have been reported consistently across various fMRI studies. Therefore, I also focused on determination of whether the NIRS signal obtained near the brain regions specific to the RSN determined the consistent RSN across participants.

3.2.6.1 Noise signal regression

After the above preprocessing steps, fMRI data sets were normalized to the MNI space using DARTEL in SPM8 (Fig. 3.1, "fMRI data normalization"). It is known that some types of noises are included in BOLD signals within the pass band of a band-pass filter (0.009–0.08 Hz). Therefore, multi-regression analysis was conducted to eliminate residual noises within the pass band of the filter from the fMRI data sets (Fig. 3.1, "fMRI data correction"). Generally, fluctuations due to scanner instabilities, subject motion, respiration and cardiac effects, and the coherent signal fluctuations across the brain (global signal) are considered to contaminate BOLD signals in the frequency band. In many studies, these contaminating signals are estimated by utilizing MRI data-inherent information and removed using a general linear model (GLM) technique (Fox et al., 2005). However, the regression of the global signal has been shown to introduce spurious anti-correlated RSNs (Anderson et al., 2011;

Murphy et al., 2009). To avoid this, Anderson et al. (2011) proposed an alternate method for correcting the global signal that makes use of an optimally phase-shifted waveform extracted from soft tissues of the face and calvarium, as well as regressors obtained from subject motion parameters, white matter, ventricles, and physiological waveforms (a method termed phase-shifted soft tissue correction [PSTCor]). To avoid generating spurious anti-correlation, in this study I also applied phase-shifted soft tissue time series as a regressor for the global signal correction instead of using the global signal. Although the original method proposed by Anderson et al. included some additional physiological waveforms, I selected 18 components for the regressors by estimating the following procedures:

1. Signals within white matter: These signals are largely independent from BOLD signal changes in cortical and sub-cortical gray matter, but they exhibit fluctuations due to scanner instabilities, subject motion, and respiration (Windischberger et al., 2002). I applied the white matter time series as a nuisance regressor and obtained it from the mean time series of voxels within two bounding boxes in each hemisphere of each participant defined by MNI coordinates (left hemisphere: $-38 < x < -28$, $-23 < y < -13$, $26 < z < 35$; right hemisphere: $28 < x < 38$, $-23 < y < -13$, $26 < z < 35$) that were determined based on the method used in a previous report (Fox et al., 2009).
2. Signals within ventricle: Physiological artifacts, including respiration and cardiac effects, are also present in the CSF (Dagli et al., 1999; Windischberger et al., 2002). After normalizing the functional images of all participants into the MNI space, voxels commonly contained in CSF-segmented images made by SPM8 for all participants were identified. Among these voxels, I selected those within the anterior horn of the lateral ventricle and extracted the

regressor as the mean time series within the selected voxels.

3. Signals within soft tissues: Soft tissue time series were applied as regressors to correct the coherent signal fluctuations across the brain. The soft tissue restriction mask was created for each participant to contain voxels within the face and calvarium.

4–9. Time series of motion correction parameters: In addition to the three aforementioned regressors, I also applied the time series of motion parameters from the automated realignment procedure (i.e., the realign step from preprocessing as described above) as nuisance regressors. Three of six corresponded to parameters of x, y, and z translation, whereas the other three corresponded to those of x, y, and z rotation.

10–18. The temporal derivatives of the upper nine components were used.

Before processing functional data sets with these 18 regressors, the first 3 time series of regressors were phase shifted to achieve optimal correlation with the mean gray matter signal (Anderson et al., 2011). After these three signals were phase shifted, temporal derivatives of 1–3 were also prepared to achieve optimal correlation with the mean gray matter signal. No phase shifting was performed for motion parameters because these were measured at zero lag from image data and showed the highest correlation coefficients at the lag. Finally, these 18 parameters were regressed out from filtered BOLD time series of all voxels using a GLM technique.

3.2.6.2 Estimation of correlation maps

The three types of seed-based correlation maps calculated with different seed signals were estimated:

1. NIRS (oxy-Hb and deoxy-Hb) time series: both preprocessed oxy-Hb and deoxy-Hb signals of all channels were used.

2. BOLD time series extracted from the brain regions selected as corresponding voxels to NIRS measurement regions in each participant's structural image: I estimated 14 ROIs corresponding to the NIRS measurement channels in each participant's structural image to obtain the corresponding BOLD time series to the NIRS signals (Fig. 3.1, "NIRS-ROI mask making"). Because NIRS signals, in theory, are generated by changes in the amount of photons traveling from an emitter to a detector, the corresponding fMRI signal to the NIRS signal can be related to the average BOLD signal in all voxels along the photon-traveling pathway. However, because the exact shape of the pathway was unknown, I used a spherical region underneath each channel marker (vitamin tablets attached on a probe holder, see Fig. 3.2B) as an approximation of a ROI, which was determined using the following processes with the anatomical image of each participant before normalizing the MNI space. First, the spherical region around the projection point of each channel was determined, which showed the radius of the sphere was 7.5 mm. Second, by removing any portion of the sphere that fell outside the gray matter mask and keeping only the voxels inside the gray matter, I determined 14 ROIs in the structural image for each participant (Fig. 3.3C). Subsequently, by normalizing these ROIs to the MNI space and identifying commonly included voxels between these ROIs and the functional volumes (Fig. 3.1, "NIRS-ROI mask normalization"), I extracted and averaged fMRI signals inside these voxels (Fig. 3.1, "Seed signal extraction from NIRS-ROI"). Thus, for each NIRS time series, I obtained a corresponding BOLD time series. The anatomical name of each ROI was determined in the MNI space by referring to the anatomical location of the centroid that was calculated as the

centroid of all centroids of the ROIs estimated in individual data sets.

3. BOLD time series used to produce each predefined RSN: Seed regions of BOLD time series used to estimate the predefined RSNs were extracted from ROIs in the MNI space (Fig. 3.1, "Seed signal extraction from predefined ROI"). The MNI coordinates reported by previous reports (Fox et al., 2005; Vincent et al., 2008; Table 3.1) were used to define the dorsal attention, the fronto-parietal control, and the default mode networks.

Table 3.1. Locations of predifined ROIs of three resting state networks

Network	name of ROI used in the previous study	corresponding name in the AAL	MNI coordinates		
			x	y	z
Dorsal attention	lMT+	Occipital_Mid_L	-45	-69	-2
Fronto-parietal	raPFC	Frontal_Mid_R	34	52	10
Default	vmPFC	Frontal_Med_Orb_L	0	51	-7

All MNI coordinates have reported in the previous studies (Fox et al., 2005; Vincent et al., 2008). Abbreviations: r/R = right, l/L = left, MT+ = middle temporal area, aPFC = anterior prefrontal cortex, vmPFC = ventromedial prefrontal cortex, Mid = middle, Med = medial part, Orb = orbital part

By calculating the cross-correlation at lag 0 between the BOLD time series of voxels from the whole brain and the above-mentioned seed time series, I obtained three types of correlation maps (maps calculated with NIRS signals [oxy-map and deoxy-map], corresponding BOLD signals [cBOLD-map], and RSNs [DA-map, FPC-map, and DM-map]) for each participant's data (Fig. 3.1, "Seed-based correction maps calculation"). All maps were processed using Fisher's Z transformation. Subsequently, a Student's t-statistic map (random effects analysis; uncorrected) was computed for each data set (Fig. 3.1, "Population based Z-score maps calculation"). Because distributions of p-values were different between maps calculated with seed signals acquired with different devices, I applied a threshold for each map based on the distribution of p-values.

3.2.6.3 Similarity of correlation maps

To evaluate the similarity of spatial distribution between the oxy-map, deoxy-map, and cBOLD-map for each measurement channel, I computed the standard Pearson correlation coefficient over all gray matter voxels within the cerebral cortex in each participant (Fox et al., 2006; Vincent et al., 2007; Fig. 3.1, "Spatial correlation between correlation maps"). Statistical significance was tested using a two-tailed *t*-test over subjects (random effects analysis) against the null hypothesis of no spatial correlation. The false discovery rate (FDR) method was used to correct for multiple comparisons, and significant connections were defined at $p < 0.05$ after FDR correction (Benjamini and Yekutieli, 2001).

It is likely that NIRS signals measured within the cortical region of RSNs include the information characterizing the spatial distribution of correlation coefficients in those RSN maps. To investigate this hypothesis, I also quantitatively compared spatial correlation between the maps and performed *t*-tests against 0, considering the individual data as random effects. To correct for multiple comparisons and significant connections, the false discovery rate (FDR) correction was adopted.

3.3 Results

3.3.1 Registration of NIRS channels in the structural MRI

The anatomical locations of NIRS channels are summarized in Table 3.2. The mean MNI coordinates of centroids across all participants are shown for each NIRS channel. The standard deviation of centroids of each NIRS channel represents the positional variations of centroids across the participants. The mean of the standard deviations across all channels was 9 mm. Each channel was anatomically labeled by applying AAL to the averaged MNI coordinates. All but two channels were located in different regions defined by AAL, whereas channels 11 and 13 were located within the same

region (Occipital_Mid_L). Therefore, these two channels were renamed as Occipital_Mid_Ant_L and Occipital_Mid_Post_L, respectively. Generally, the centroids of a channel across all participants were not consistently located within the same brain region in the AAL system due to the spatial variability across the participants. The four most likely anatomical locations of each channel are shown in Table 3.3.

Table 3.2. Locations of gravity points of normalized ROIs corresponding to NIRS channels

number of channel	anatomical location of gravity point	MNI coordinates			
		position			
		x	y	z	SD
1	Frontal_Sup_Medial_L	-1.9	59.3	5.4	8.4
2	Frontal_Sup_R	20.1	64.5	5.4	5.9
3	Frontal_Sup_L	-24.5	61.3	4.1	5.8
4	Frontal_Mid_R	40.6	53.2	2.4	6.9
5	Frontal_Mid_Orb_L	-43.4	47.4	-6.9	5.4
6	Frontal_Inf_Tri_R	51.4	32.7	1.2	7.4
7	Frontal_Inf_Orb_L	-47.9	23.7	-14.2	9.3
8	Temporal_Mid_R	54.0	-64.0	-0.5	10.4
9	Temporal_Mid_L	-56.1	-62.2	6.7	10.0
10	Occipital_Mid_R	41.2	-81.5	5.5	10.2
11	Occipital_Mid_Ant_L	-43.4	-82.0	9.1	10.5
12	Occipital_Sup_R	20.3	-94.9	6.2	12.6
13	Occipital_Mid_Post_L	-24.5	-95.1	9.8	11.2
14	Calcarine_L	-3.0	-93.6	8.8	12.2

The most likely anatomical labels are shown. Anatomical labels were determined by using the Automated Anatomical Labeling (AAL) (Tzourio-Mazoyer et al., 2002). All values are in millimeters. 'SD' stands for standard deviation. Abbreviations: L = Left hemisphere, R = Right hemisphere, Sup = Superior, Mid = Middle, Inf = Inferior, Ant = Anterior, Post = posterior, Orb = Orbital part, Tri = Triangular part.

Table 3.3. Proportion of centroids of ROIs across participants

ch	1st	%	2nd	%	3rd	%	4th	%
1	Frontal_Sup_Medial_L	70.4	Frontal_Sup_Medial_R	14.8	Frontal_Med_Orb_R	7.4	Cingulum_Ant_L	7.4
2	Frontal_Sup_R	92.3	Frontal_Sup_Orb_R	3.8	Frontal_Sup_Medial_R	3.8		
3	Frontal_Sup_L	74.1	Frontal_Mid_L	14.8	Frontal_Sup_Orb_L	11.1		
4	Frontal_Mid_R	75.0	Frontal_Mid_Orb_R	21.4	Frontal_Inf_Tri_R	3.6		
5	Frontal_Mid_Orb_L	60.7	Frontal_Inf_Orb_L	28.6	Frontal_Inf_Tri_L	7.1	Frontal_Mid_L	3.6
6	Frontal_Inf_Tri_R	82.1	Frontal_Inf_Orb_R	17.9				
7	Temporal_Pole_Sup_L	55.6	Frontal_Inf_Orb_L	40.7	Frontal_Inf_Tri_L	3.7		
8	Temporal_Mid_R	57.1	Temporal_Inf_R	39.3	Occipital_Mid_R	3.6		
9	Temporal_Mid_L	82.1	Occipital_Inf_L	7.1	Angular_L	7.1	Temporal_Inf_L	3.6
10	Occipital_Mid_R	78.6	Occipital_Inf_R	21.4				
11	Occipital_Mid_L	85.7	Occipital_Inf_L	10.7	Temporal_Mid_L	3.6		
12	Occipital_Sup_R	44.0	Calcarine_R	20.0	Cuneus_R	16.0	Occipital_Mid_R	12.0
13	Occipital_Mid_L	78.6	Occipital_Sup_L	10.7	Occipital_Inf_L	10.7		
14	Calcarine_L	48.0	Cuneus_L	44.0	Occipital_Sup_L	4.0	Lingual_L	4.0

The four most likely anatomical labels are shown. Anatomical labels were determined by using the Automated Anatomical Labeling (AAL) (Tzourio-Mazoyer et al., 2002). Abbreviations: L = Left hemisphere, R = Right hemisphere, Sup = Superior, Mid = Middle, Med = medial part, Inf = Inferior, Ant = Anterior, Post = posterior, Orb = Orbital part, Tri = Triangular part.

3.3.2 Evaluation of regions where hemodynamic fluctuations are detected as NIRS signals obtained during the resting state

The representative examples of both resampled oxy-Hb and deoxy-Hb signals are shown in Fig. 3.4. The descriptive statistics of LBCVs are shown in Table 3.4. Based on these data, the average distance across all channels was 5.3 mm for oxy-Hb and 5.6 mm for deoxy-Hb, whereas the standard deviations were 0.6 and 0.4, respectively. This result demonstrates that most of the LBCVs were located within the radius of two voxels from the projection point. Although most of the averaged correlation coefficients were higher than 0.3 for oxy-Hb and lower than -0.3 for deoxy-Hb, the absolute values in Frontal_Inf_Tri_R and Frontal_Inf_Orb_L were slightly lower than those in the other brain regions (Table 3.4).

To investigate the distribution of regions where hemodynamic changes affect the obtained NIRS signals at the brain tissue level, HCVs (top 100 ranked voxels within a 3-cm radius from the

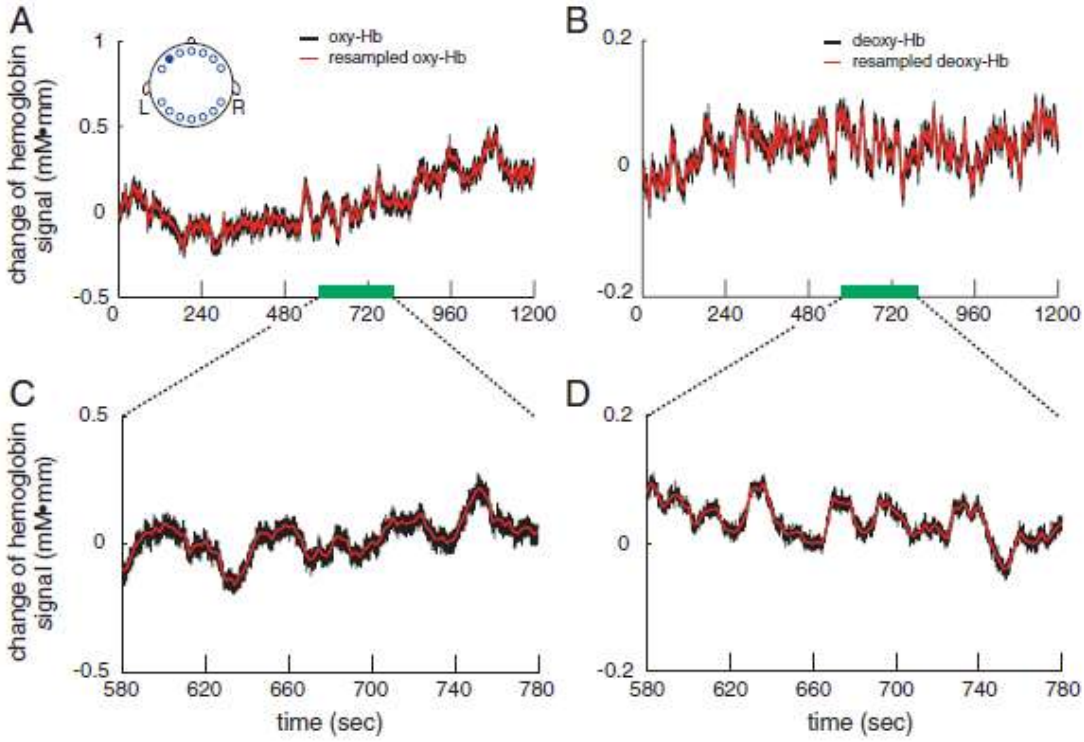

Figure 3.4. Representative examples of continuous data for one participant. The channel of interest is shown in (A). (A) Oxy-Hb time series (black) and resampled data (red). The green bar indicates the enlarged section. (B) Deoxy-Hb time series (black) and resampled data (red). (C) Enlarged section of original oxy-Hb (black) and resampled data (red). (D) Enlarged section of deoxy-Hb (black) and resampled data (red).

projection point) were sorted by the tissue type. Most of the HCVs with both Hb signals were located within the brain tissue, whereas the HCVs in two brain regions (Frontal_Inf_Tri_R, Frontal_Inf_Orb_L) were located equally in brain and non-brain tissues (Table 3.5). By picking up more than 100 voxels as HCVs and sorting by tissue types, the robustness of the results shown in Table 3.5 was confirmed (Table 3.S1). These results show that NIRS signals obtained with all but two channels mainly reflect changes in the Hb concentration that occur in the brain regions adjacent to the channels during the resting state.

Table 3.4. Descriptive statistics of LBCV

ch	anatomical location of channel	oxy-Hb averaged distance	SD	averaged r value	deoxy-Hb averaged distance	SD	averaged r value
1	Frontal_Sup_Medial_L	4.6	1.8	0.39	5.4	1.7	-0.37
2	Frontal_Sup_R	5.2	1.7	0.49	5.4	1.7	-0.46
3	Frontal_Sup_L	5.8	2.3	0.48	5.1	2.0	-0.49
4	Frontal_Mid_R	4.9	1.9	0.42	6.0	2.4	-0.43
5	Frontal_Mid_Orb_L	5.2	1.5	0.33	5.7	1.9	-0.39
6	Frontal_Inf_Tri_R	5.4	1.8	0.29	5.8	1.5	-0.29
7	Frontal_Inf_Orb_L	5.0	1.4	0.26	5.6	1.7	-0.28
8	Temporal_Mid_R	4.9	2.3	0.47	5.4	2.0	-0.41
9	Temporal_Mid_L	5.2	1.8	0.43	5.2	2.1	-0.38
10	Occipital_Mid_R	5.3	1.8	0.52	5.3	1.6	-0.46
11	Occipital_Mid_Ant_L	6.6	2.0	0.45	5.4	1.8	-0.38
12	Occipital_Sup_R	6.3	1.6	0.55	6.4	1.7	-0.52
13	Occipital_Mid_Post_L	5.4	1.9	0.55	6.0	2.3	-0.50
14	Calcarine_L	5.0	1.7	0.51	5.4	1.5	-0.38

Anatomical labels were determined by using the Automated Anatomical Labeling (AAL) (Tzourio-Mazoyer et al., 2002). Values in the columns indicated as 'averaged distance' and 'SD' are in millimeters, while those in the columns indicated as 'averaged r value' are correlation coefficients. 'averaged distance', 'SD' and 'averaged r value' stands for averaged distance of the LBCV from the projection point across all participants, standard deviation and averaged correlation coefficients of the LBCV across all participants. Abbreviations: L = Left hemisphere, R = Right hemisphere, Sup = Superior, Mid = Middle, Inf = Inferior, Ant = Anterior, Post = posterior, Orb = Orbital part, Tri = Triangular part.

Table 3.5. Distributions of HCVs with NIRS signals

ch	anatomical location of channel	oxy-Hb Brain tissue (%)	Skull	Skin	r value of 100th-ranked voxel	deoxy-Hb Brain tissue	Skull	Skin	r value of 100th-ranked voxel
1	Frontal_Sup_Medial_L	92	6	2	0.33	89	8	3	-0.30
2	Frontal_Sup_R	95	3	2	0.41	93	4	3	-0.37
3	Frontal_Sup_L	93	4	3	0.40	94	4	2	-0.40
4	Frontal_Mid_R	85	5	10	0.32	81	7	12	-0.31
5	Frontal_Mid_Orb_L	70	9	21	0.29	72	8	20	-0.32
6	Frontal_Inf_Tri_R	51	10	39	0.25	55	10	35	-0.24
7	Frontal_Inf_Orb_L	37	9	54	0.25	51	8	41	-0.26
8	Temporal_Mid_R	94	3	3	0.41	90	5	5	-0.34
9	Temporal_Mid_L	91	5	4	0.36	85	7	8	-0.31
10	Occipital_Mid_R	95	2	3	0.49	88	5	7	-0.41
11	Occipital_Mid_Ant_L	94	4	2	0.45	85	8	7	-0.36
12	Occipital_Sup_R	96	2	2	0.54	88	6	6	-0.47
13	Occipital_Mid_Post_L	94	4	2	0.50	89	6	5	-0.44
14	Calcarine_L	92	5	3	0.46	81	10	9	-0.35

Anatomical labels were determined by using the Automated Anatomical Labeling (AAL) (Tzourio-Mazoyer et al., 2002). Values in the columns indicated as 'r value of 100th-ranked voxels' are correlation coefficients. 'r value of 100th-ranked voxels' stands for averaged 100th -ranked correlation coefficients of the HCVs across all participants. Abbreviations: L = Left hemisphere, R = Right hemisphere, Sup = Superior, Mid = Middle, Inf = Inferior, Ant = Anterior, Post = posterior, Orb = Orbital part, Tri = Triangular part.

3.3.3 Whole brain distribution of correlated voxels with NIRS signals obtained during the resting state

To calculate group-averaged statistical maps of cross-correlation, I used oxy-Hb signals, deoxy-Hb signals, and BOLD signals extracted from the ROIs corresponding to the NIRS measurement regions as seed signals (Fig. 3.5). Because of the inconsistency between participants in the tissue type where hemodynamics were reflected in NIRS signals, I did not use signals from Frontal_Inf_Tri_R (channel 6) or Frontal_Inf_Orb_L (channel 7) for calculating the map. For each channel, oxy-maps and cBOLD-maps provided closely resembling spatial distributions, whereas deoxy-maps were clearly similar to the inversed patterns of both oxy-maps and cBOLD-maps. Spatial correlation analyses demonstrated that the oxy-maps and cBOLD-maps had a significant positive correlation for all brain regions (Fig. 3.5, bar graphs). Significant negative correlation was observed between deoxy-maps and cBOLD-maps for all brain regions. These results demonstrate that using NIRS signals measured at various brain regions as seed signals can reproduce the specific distribution patterns of correlation maps generated using BOLD signals extracted from the corresponding seed brain regions.

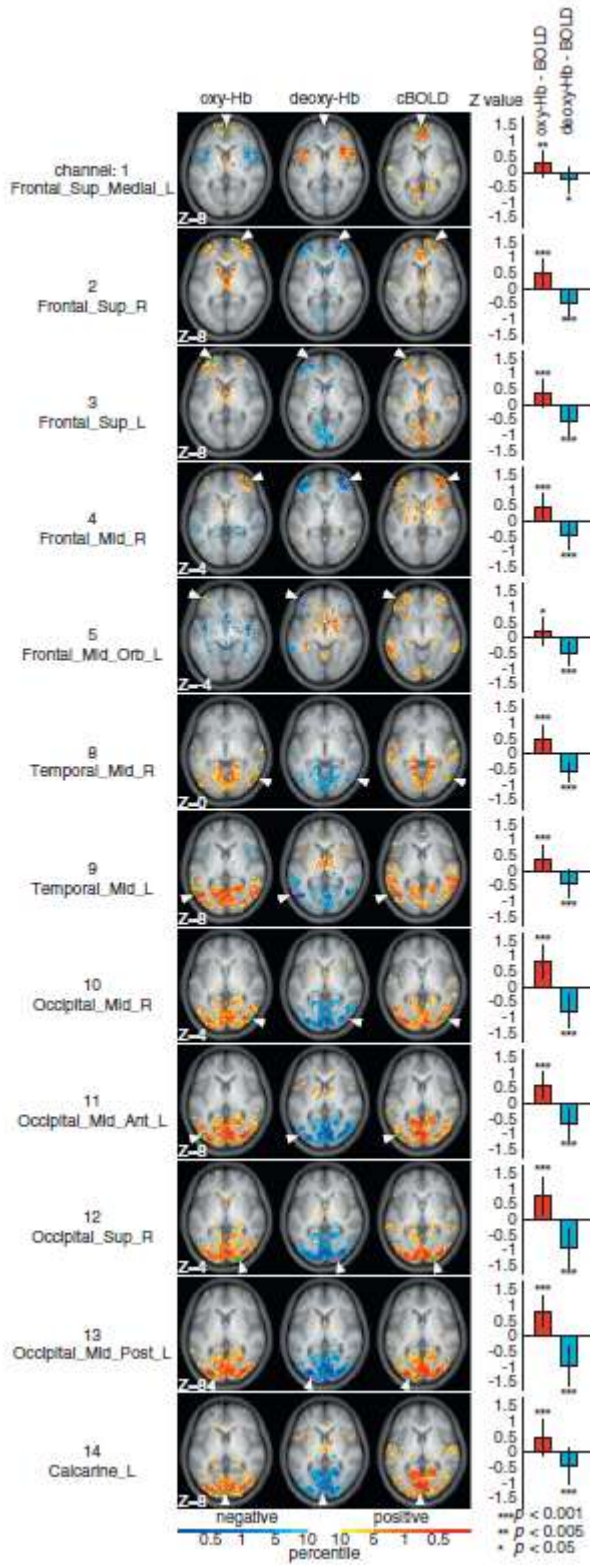

Figure 3.5. Group averaged statistical maps of correlation corresponding to varied seed locations and different seed signals. Each row corresponds to the location of the seed represented by NIRS measurement channels and their projected locations on the cortex. The left, middle, and right maps in each row represent those calculated using different seed signals: oxy-Hb signal, deoxy-Hb signal, and BOLD signal extracted from the ROI around the projection point (Fig. 3.3), respectively. The voxels with the upper 10% of the p-values are colored. The dots indicated by arrowheads (green dots in the left and right maps and pink dots in the middle map) show the cortical projection point of the vitamin tablet representing the NIRS measurement channel. The red and blue bar graphs on the right side of the images represent the spatial correlations between the maps calculated using oxy-Hb signals as seed signals and seed BOLD signals, and those between the maps calculated using deoxy-Hb signals as seed signals and seed BOLD signals, respectively. The error bars indicate standard deviations. Significant spatial correlation coefficients against 0 are shown (*$p < 0.05$, **$p < 0.01$, ***$p < 0.001$).

To identify the non-brain tissue regions that correlated with NIRS signals obtained at Frontal_Inf_Tri_R and Frontal_Inf_Orb_L, I examined the correlation maps using NIRS signals obtained in these regions as seed signals in individual data. I focused examination on two participants whose data showed that over half of all correlating voxels with NIRS signals obtained in these two regions were located within the non-brain tissue regions. The correlation map estimated for each individual's data is shown in Supplemental Figure 3.S1. I found that the correlating voxels mainly localized not within the brain regions but rather within the bilateral temporal muscles and/or in the tissues near the eyes. Furthermore, an overlap was observed between most of the voxels correlating with the NIRS signal obtained at the Frontal_Inf_Tri_R and the Frontal_Inf_Orb_L.

The effect of noise regression in BOLD signals on the correlation between NIRS and BOLD signals was examined (Fig. 3.S2). When no waveform was regressed from the BOLD signals, both the Hb signals correlated not only with the cortical regions but also with cerebral vasculatures, such as the superior sagittal sinus and the transverse sinus. Conversely, when all physiological waveforms (see “Noise signal regression” in the Materials and methods section) were regressed from the BOLD signals, no correlation over threshold was observed in these cerebral vasculature areas.

I also calculated group-averaged statistical maps with BOLD signals extracted from predefined ROIs (DA-map, FPC-map, and DM-map) so that I could determine whether NIRS signals obtained in these areas were correlated with the specific brain regions of these RSNs. The nearest NIRS channels from the predefined ROIs of the dorsal attention and fronto-parietal control networks were located within the same anatomical regions as these ROIs (Occipital_Mid_Ant_L and Frontal_Mid_R), whereas the nearest channel to the ROI of the default mode network was located in the next regions, based on AAL (NIRS channel: Frontal_Sup_Medial_L, ROI: Frontal_Med_Orb_L). The regions

positively correlated with oxy-Hb signals and negatively correlated with deoxy-Hb signals in the Occipital_Mid_Ant_L region were mainly localized within the bilateral inferior temporal gyri, bilateral lingual gyri, right inferior precentral gyrus, and bilateral superior parietal lobule. These brain regions correspond to the regions that have been repeatedly reported as the "dorsal attention network." The DA-map calculated using BOLD signals extracted from the left MT+ region, which corresponds to the Occipital_Mid_L in the AAL, as seed signals also showed positive correlation in these regions (Figs. 3.6A, B). The regions positively correlated with oxy-Hb signals and negatively correlated with deoxy-Hb signals in the Frontal_Mid_R were mainly localized within the bilateral dorsolateral prefrontal cortices, right dorsomedial prefrontal cortex/anterior cingulate, and right anterior inferior parietal lobule. These brain regions correspond to the regions that have been repeatedly reported as the "fronto-parietal control network." The FPC-map calculated using BOLD signals extracted from the right aPFC region, corresponding to the Frontal_Mid_R in the AAL, as seed signals also showed positive correlation in these regions (Figs. 3.6C, D). The regions positively correlated with oxy-Hb signals and negatively correlated with deoxy-Hb signals in the Frontal_Sup_Medial_L were mainly localized within the ventromedial prefrontal cortex, bilateral lateral parietal cortices, bilateral superior frontal cortices, and posterior cingulate. These brain regions correspond to the regions also known as the "default mode network." The DM-map calculated using BOLD signals extracted from right vmPFC, corresponding to the Frontal_Med_Orb_L in the AAL, as seed signals also showed positive correlation in these regions (Figs. 3.6E, F). Spatial correlation analysis revealed that the spatial distributions of correlation coefficients in the oxy-maps and deoxy-maps calculated with signals obtained from the Occipital_Mid_Ant_L, Frontal_Mid_R, and Frontal_Sup_Medial_L were correlated positively and negatively, respectively, with those of the DA-map, FPC-map, and DM-map (Figs. 3.6G–I). These

results demonstrate that NIRS signals obtained at the brain regions of dorsal attention, fronto-parietal control, and default mode networks correlated with spontaneous hemodynamic fluctuation determining the spatial patterns of those RSNs.

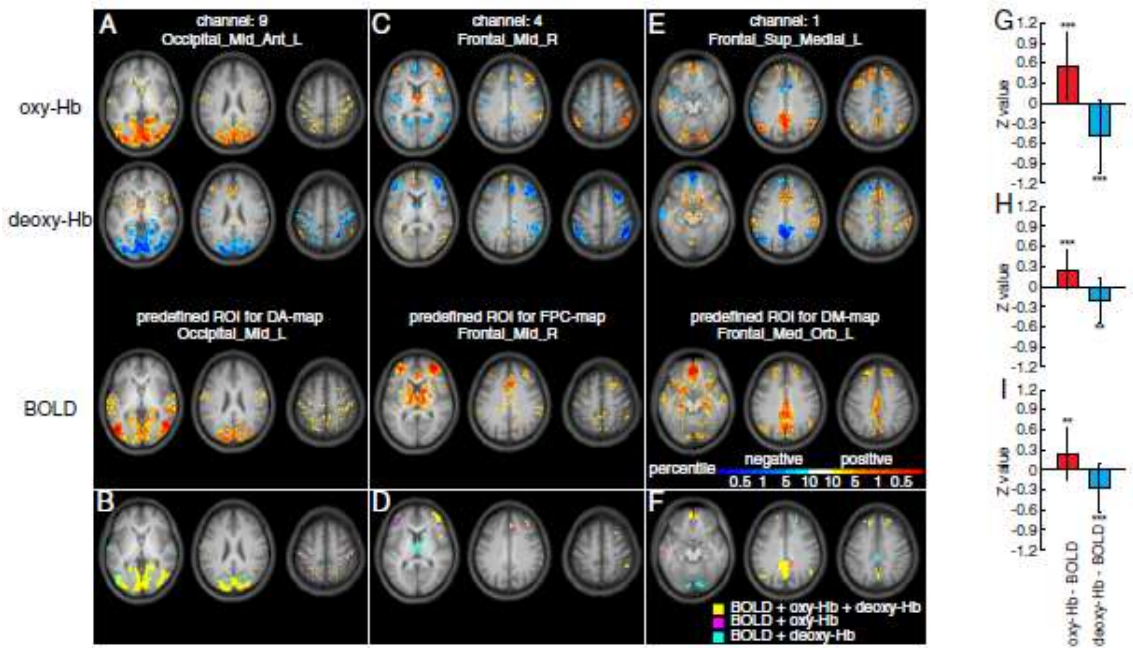

Figure 3.6. RSNs revealed using NIRS signals and BOLD signals as seeds. Group-averaged statistical maps calculated using Hb signals and BOLD signals extracted from predefined ROIs as seed signals. The top and middle rows show oxy-maps and deoxy-maps calculated using Hb signals obtained at (A) Occipital_Mid_Ant_L, (C) Frontal_Mid_R, and (E) Frontal_Sup_Medial_L. The bottom row shows maps calculated using BOLD signals extracted from predefined ROIs (Table 3.1) located within (A) Occipital_Mid_L, (C) Frontal_Mid_R, and (E) Frontal_Med_Orb_L areas. BOLD signals extracted from these areas have been reported to correlate with brain regions of (A) dorsal attention, (C) fronto-parietal control, and (E) default mode networks. (B), (D), and (F) correspond to the conjunction maps of (A), (C), and (E), respectively. Yellow, magenta, and cyan regions were colored as brain regions correlating with BOLD signals and both Hb signals used as seed signals; with BOLD signals and oxy-Hb signals; and with BOLD signals and deoxy-Hb signals, respectively. In (A–F), I applied a threshold to each map at the value of the top 10% of the distribution of p-values of all brain voxels because the distributions of p-values were different between maps calculated with seed signals acquired with different devices. (G–I) Spatial correlation between the map calculated using Hb signals as seed signals and that calculated with BOLD signals. The error bars indicate standard deviations. The significant spatial correlation coefficients against 0 are shown (**$p < 0.01$, ***$p < 0.001$).

A previous study dnstrated that the regions within the fronto-parietal control network are spatially interposed between regions within the dorsal attention and default mode networks, especially within the parietal cortex (Vincent et al., 2008). To determine whether NIRS signals obtained in brain regions near these three RSNs could characterize this spatial relation among the RSNs, I investigated the distributions of the superficial cortical regions correlated with NIRS signals obtained from the Occipital_Mid_Ant_L, Frontal_Mid_R, and Frontal_Sup_Medial_L. I found that there was very little overlap of regions positively correlated with oxy-Hb signals and negatively correlated with deoxy-Hb signals obtained for these three regions (Figs. 3.7A, B). In particular, regions positively correlated with oxy-Hb signals and negatively correlated with deoxy-Hb signals in the Frontal_Mid_R and Frontal_Sup_Medial_L were antero-posteriorly separately localized within the inferior parietal regions (Parietal_Inf_R, SupraMarginal_R, Parietal_Inf_L, and SupraMarginal_L for Frontal_Mid_R; Angular_R and Angular_L for Frontal_Sup_Medial_L), whereas those positively correlated with oxy-Hb signals and negatively correlated with deoxy-Hb signals in the Occipital_Mid_Ant_L were localized in more superior cortical regions (Parietal_Sup_R and Parietal_Sup_L). For each channel, non-overlapping voxels were more than 89% of all voxels positively correlated with oxy-Hb signals of the channel; more than 93% of all voxels negatively correlated with deoxy-Hb signals of the channel. These results demonstrate that NIRS signals obtained within brain regions of these RSNs estimated in previous fMRI studies include adequate information to localize those RSNs within plausibly separate anatomical regions. By comparing the spatial patterns of the DA-map, FPC-map, and DM-map in superficial brain regions, I confirmed this positional relationship between these three networks within the fMRI data set (Fig. 3.7C).

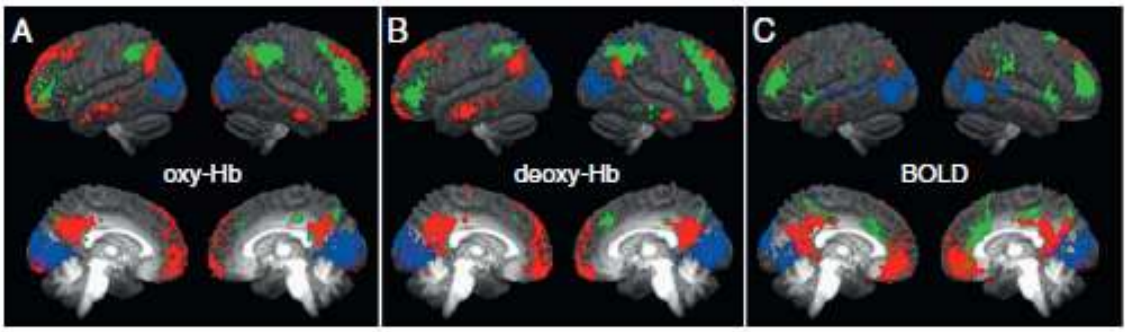

Figure 3.7. Anatomical separation of RSNs. (A) Positively correlated regions with oxy-Hb seed signals. Blue, green, and red represents the voxels with p-values within the upper 5% of all cortical voxels that were positively correlated with oxy-Hb signals obtained at Occipital_Mid_Ant_L, Frontal_Mid_R, and Frontal_Sup_Medial_L, respectively. (B) Negatively correlated regions with deoxy-Hb seed signals. Blue, green, and red represents the voxels with p-values within the upper 5% of all cortical voxels that were negatively correlated with deoxy-Hb signals obtained at Occipital_Mid_Ant_L, Frontal_Mid_R, and Frontal_Sup_Medial_L, respectively. (C) Positively correlated regions with BOLD signals. Blue, green, and red represents the voxels with p-values within the upper 5% of all cortical voxels that were positively correlated with BOLD signals extracted from predefined ROIs (Table 3.1) at Occipital_Mid_L, Frontal_Mid_R, and Frontal_Med_Orb_L, respectively. In this figure, cortical voxels were defined as those classified into cortical regions with AAL.

3.4 Discussion

The purpose of this study was to investigate and establish the relationship between NIRS and fMRI during the resting state to study functional connectivity with special focus on the RSNs. To do so, I conducted simultaneous recordings of NIRS and fMRI and performed subsequent analyses. First, I identified the positions of NIRS channels in the cortical regions using individual data sets and investigated the distribution of these positions across participants in the MNI space. Second, I tried to find the local maximum of the correlation coefficient between NIRS and fMRI signals in the regions close to the NIRS channel. Third, I classified the highly correlated voxels with NIRS signals that resided in the adjacent regions to NIRS channels into brain and non-brain voxels. Finally, I investigated whether NIRS signals correlated with BOLD signals not only within the adjacent brain regions to NIRS channels but also within distant brain regions constituting RSNs. Accordingly, there are four corresponding findings in this study. First, I successfully projected all NIRS measurement channels onto the cortical surface with an average standard deviation of 9 mm (Table 3.2), which is similar to a previously reported value by Okamoto et al. (2004). Second, I found single voxels, which corresponded to the local maxima of correlation coefficients between NIRS and fMRI signals, within a radius of 2 voxels from the projection point independent of the channel location (Table 3.4). Third, I observed that highly correlated voxels with the NIRS signal were mainly localized within brain tissues for all NIRS channels, except for two bilateral inferior frontal channels (Frontal_Inf_Tri_R and Frontal_Inf_Orb_L) (Table 3.5). Finally, I observed cortical regions correlating with the NIRS signals not only within areas adjacent to the channels but also in areas distant from the channels (Fig. 3.5). In particular, I successfully reproduced the correlation maps of three RSNs (dorsal attention, fronto-parietal control, and default mode networks) using NIRS signals as seed signals (Figs. 3.6, 3.7). Collectively, these

findings support the idea that NIRS signals obtained at several cortical regions during the resting state mainly reflect regional spontaneous hemodynamic fluctuations that originate from spontaneous cortical activity and include information characterizing cortico-cortical resting state functional connectivity.

3.4.1 Registration of NIRS channels in the structural MRI

In the current study, I assumed that obtained NIRS signals should mainly reflect hemodynamics of regions along the optical path plane because it has previously been reported that the photon traveling pathways have a “banana shape” between the incident and detection probes (Okada et al., 1997; van der Zee et al., 1990) (see 3.2 Materials and methods). Therefore, I applied a different procedure for registration of NIRS channel positions on the cortical regions, in which the previous study examined cranio-cerebral correlations using MRI, via the guidance of the international 10–20 system for electrode placement (Okamoto et al., 2004). To confirm the reliability of the registration process, I examined whether changes in the projection point of the NIRS channel produced by rotation of the optical path plane affected the resultant correlation between NIRS signals (oxy-Hb and deoxy-Hb) and BOLD signals extracted from spherical ROIs around the projection point (see supplementary materials for a detailed account of the procedure). The best correlation was found between NIRS signals and BOLD signals extracted from the ROI around the projection point without rotation (Fig. 3.S3), indicating that the process can reliably register the channel location on the cortical surface. All channels were projected on the cortical surface with similar accuracy to that previously reported. Cui et al. (2011) projected the channel marker from the scalp to the brain surface by finding the point on the brain surface that was closest to the marker, which is similar to the procedure used by Okamoto et al. (2004). Furthermore, Cui et al. (2011) reported that the mean values of the distances

between the LBCVs and projection points were 18 mm for oxy-Hb signals and 21 mm for deoxy-Hb signals. In the current study, I found that the LBCVs were within a radius of 2 voxels (~6 mm) from the projection point, suggesting that the method of registration applied in our study is also useful in addition to those methods used in the aforementioned previous studies.

3.4.2 Regions where hemodynamic fluctuations were reflected by NIRS signals obtained during the resting state

The fact that LBCVs were found within a radius of 2 voxels from the projection point supports that both oxy-Hb and deoxy-Hb signals reflect hemodynamic fluctuations in regions adjacent to the measurement channels. Furthermore, highly correlated voxels with each of the Hb signals were found within brain tissues regardless of which Hb signal was used to calculate the correlation (Table 3.5). Therefore, correlation between fMRI signals within cortical regions and NIRS signals reported in the current study mainly reflects coherence of hemodynamic changes due to spontaneous cortical activity. On the other hand, NIRS signals obtained at the two frontal regions (Frontal_Inf_Tri_R and Frontal_Inf_Orb_L) showed correlation not only with BOLD signals from brain tissues but also with those from non-brain tissues (Table 3.5). Among these signals, I found a strong correlation between the NIRS signals obtained at the two frontal channels (Frontal_Inf_Tri_R and Frontal_Inf_Orb_L) and the whole head BOLD signals in the soft tissue, such as the bilateral temporal muscles and/or tissues near the eyes (Fig. 3.S1). This finding indicates that NIRS signals obtained at these areas mainly reflect Hb concentration changes in the soft tissue, as shown in the lower proportions of brain tissues in the highly correlated voxels in Table 3.5. Also of note, Cui et al. (2011) demonstrated that the scalp-brain distance affects the NIRS–fMRI correlation. However, the distance between these two channels and brain

surfaces did not have a strong effect on the results of the current study. Although it is unclear why NIRS signals in only two frontal regions showed correlation with those outside of the brain tissue, it is likely that signals in these regions are more strongly affected by global changes of Hb concentrations, such as skin blood flow, as compared to other regions (Gagnon et al., 2012a, 2012b; Kohno et al., 2007; Obrig et al., 2000; Saager and Berger, 2008; Tachtsidis et al., 2008; Takahashi et al., 2011; Toronov et al., 2001; Yamada et al., 2009; Zhang et al., 2007). In particular, Gagnon et al. (2012b) showed that systemic interference occurring in the superficial layers of the human head was inhomogeneous across the surface of the scalp. To clarify the issue, it would be helpful to investigate the effect of the motion of the cephalic muscles and blood stanching on the NIRS signals obtained at these regions. In addition, the effect of participants' posture during measurement of the results must be clarified. Although I measured NIRS signals with individuals in the face-up position, NIRS measurements are generally conducted with participants sitting. Because this positional difference of the participants can affect their blood circulation, it would be useful for future studies to focus on the relevance of participant's posture to functional connectivity. Whatever the case, the present study demonstrated that NIRS can detect regional changes in cortical blood oxygenation during the resting state, though we must be very careful about taking measurements at some restricted head positions, such as the inferior frontal gyrus, where changes in signals are dominated by those originated from non-brain tissues.

3.4.3 Whole brain distribution of correlated voxels with NIRS signals obtained during the resting state

By calculating the cross-correlation, I observed that spatial patterns of correlating brain

regions with NIRS signals were similar to those of correlating regions with BOLD signals extracted from areas close to NIRS channels (Fig. 3.5). RSNs have been reported in many fMRI studies using seed-based correlation analysis (Biswal et al., 1995; Damoiseaux et al., 2006; Fox et al., 2005; Fransson, 2005; Greicius et al., 2003; Vincent et al., 2008) and independent component analysis (Beckmann et al., 2005; Calhoun et al., 2001; De Luca et al., 2006; van de Ven et al., 2004). Despite the different methods used to characterize the RSNs, specific brain regions have been consistently reported as the RSNs across studies (van den Heuvel and Hulshoff, 2010). In the present study, I used NIRS and fMRI simultaneously to successfully reproduce three RSNs (dorsal attention, fronto-parietal control, and default mode networks) using NIRS signals instead of fMRI signals as seed signals (Beckmann et al., 2005; Damoiseaux et al., 2006; De Luca et al., 2006; Fox et al., 2005; Fransson, 2005; Greicius et al., 2003; van den Heuvel et al., 2008b; Vincent et al., 2008) (Fig. 3.6). It should be noted that the voxels that did not satisfy the significance level ($p < 0.05$, corrected) could be included in the correlation maps that had an applied threshold with our method. However, considering that the spatial patterns of previously reported RSNs could be successfully reproduced using both NIRS and BOLD signals, our results strongly support the theory that both oxy-Hb and deoxy-Hb signals can detect the information necessary for determining RSNs included in the fMRI data sets. On the other hand, the BOLD response theoretically results from local concentration changes in paramagnetic deoxy-Hb (Ogawa and Lee, 1990; Ogawa et al., 1990a, 1990b). Previous studies on functional activation revealed a strong temporal and spatial correlation of the BOLD signal with deoxy-Hb, rather than oxy-Hb (Huppert et al., 2006a, 2006b). In contrast, the current study showed that both oxy-Hb and deoxy-Hb produced consistent results in terms of the spatial patterns of the correlation maps. Although the relationships between each of the Hb signals and the BOLD signals are not fully understood (Chen

et al., 2011; Devor et al., 2007; Steinbrink et al., 2006), our results suggest that resting state functional connectivity may arise at least in part from the coupling of spontaneous neural activity that is commonly reflected in cerebral hemodynamic changes in different blood vessels such as arterioles, capillaries, and venules.

Conversely, a previous study indicated that the low-frequency components (0.01–0.10 Hz) of NIRS signals obtained during the resting state were affected by fluctuations in the blood flow and hemoglobin oxygenation at a global circulatory system level (Tong and Frederick, 2010). In this previous study, the authors showed that the spatiotemporal patterns of regions correlating with NIRS signals obtained at the right prefrontal area resembled the spatial patterns of the cerebral venous system. In the current study, when the preprocessing step of the fMRI data similar to the one used in the previous study was adopted, I also observed a correlation over threshold within the cerebral venous regions (Fig. 3.S2). This finding suggests that both NIRS and BOLD signals may include the correlating information of physiological noises originating from non-brain tissue even after being processed with the band-pass filter (0.009–0.10 Hz). However, the correlation within vasculature areas was not found in the correlation maps calculated with the current preprocessing step, which fully regresses out the noises in fMRI data. Furthermore, some RSNs can be successfully reproduced using NIRS instead of fMRI signals as seed signals (Figs. 3.5, 3.6). This result supports the theory that, although NIRS signals obtained during the resting state may be contaminated with physiological noises, they evidently also contain information representing the spontaneous cortical activity that characterizes RSNs.

Recently, another study showed that simultaneously measured NIRS and fMRI signals produce similar resting state functional connectivity between the bilateral primary motor areas (Duan et

al., 2012). In that study, the authors transformed the fMRI data into the NIRS measurement space and estimated the functional connectivity in that space. Generally, NIRS-based functional connectivity is estimated by calculating the cross-correlation of signals obtained from different channels. In our previous NIRS study, the cross-correlation between all pairs of NIRS signals obtained from diverse brain regions was calculated, and the functional connectivity between bilateral homologous brain regions was observed (Sasai et al., 2011). This finding was reproduced using the same analysis with the NIRS signals measured in the current study (data not shown). Thus, accumulating evidence shows that NIRS-based functional connectivity is consistent with fMRI-based functional connectivity.

The dorsal attention and default mode networks have been suggested to have competing functions, that is, information processing from the external world versus internal mentation (Buckner and Vincent, 2007; Buckner et al., 2008; Corbetta and Shulman, 2002; Gusnard et al., 2001; Mason et al., 2007). Recent fMRI studies have focused on switching between these RSNs (depending on the experimental conditions), and they have demonstrated that the interaction of the dorsal attention and default mode networks is causally regulated by the fronto-parietal control network (Gao and Lin, 2012; Sridharan et al., 2008). The fronto-parietal control network is anatomically interposed between the dorsal attention and default mode networks (Vincent et al., 2008). The results of the current study successfully reproduced the same anatomical relationship among these RSNs using NIRS (Fig. 3.6), which supports that use of NIRS can detect cortical activity correlated only within the anatomically specific regions of these RSNs, This suggests that I can evaluate the relationship of these RSNs using NIRS signals obtained at cortical regions of these RSNs. Although I must establish the method to extract only the information determining RSNs from raw NIRS signals, the findings of our study promote the application of NIRS to prove the signal relationship among these RSNs.

Regarding the temporal relationship among the RSNs, many fMRI studies have reported a negative correlation between the dorsal attention and default mode networks (Fox et al., 2005, 2009; Fransson, 2005; Greicius et al., 2003; Kelly et al., 2008). To accurately estimate functional connectivity, a general linear model (GLM) technique has previously been used to remove fluctuations due to scanner instabilities, subject motion, respiration and cardiac effects, and the coherent signal fluctuations across the brain (e.g., global signal) (Fox et al., 2005, 2009). However, the regression of the global signal has also been shown to introduce spurious anti-correlated RSNs (Anderson et al., 2011; Murphy et al., 2009). Thus, it is still unclear whether anti-correlation between RSNs observed in fMRI studies reflects the negatively correlated patterns of spontaneous brain activity. On the other hand, although NIRS measurements were conducted on diverse cortical regions, I could not determine a negative correlation among any pairs of NIRS channels in our previous NIRS study (Sasai et al., 2011) and the current study (data not shown). Although the results of the current study indicated that the signals acquired using both NIRS and fMRI represent the spontaneous neural activity characterizing RSNs, the attributes of noises included in these signals might be different. Considering this difference between fMRI and NIRS and the higher temporal resolution of NIRS, NIRS provides additional information on the temporal relationship between these RSNs. This finding supports the theory that NIRS is a valuable tool that can be used to measure the signals characterizing RSNs and to investigate the intrinsic dynamics of the human brain.

3.4.4 Issues for future studies

Recent studies have demonstrated the relationship between resting state networks and cognitive function and dysfunction. For example, the default mode network is suggested to take the

central role in internally focused cognitive processes, such as mind wandering (Christoff et al., 2009; Mason et al., 2007), self-reference (D'Argembeau et al., 2005; Gusnard et al., 2001), and recollecting one's past or imagining one's personal future (Schacter et al., 2007; Spreng et al., 2009), whereas the increased and decreased connectivity within the default mode network has been demonstrated to be linked to diverse psychiatric brain disorders (Fox and Greicius, 2010). Use of NIRS enables us to obtain the information on focused resting state networks easier than using fMRI because the network information can be measured only by setting NIRS channels onto the regions related to targeting resting state networks. Although several challenges remain before the abnormality of the resting state networks can be used as a diagnostic marker in psychiatric disorders (Fornito and Bullmore, 2010; Fox and Greicius, 2010), the findings of the current study motivate clinical applications of NIRS to study resting state functional connectivity.

In the emerging social cognitive neuroscience literature, it has been suggested that some RSNs have functional roles in social cognition. For example, it has been reported that the activity of the default mode network is associated with the process of social cognition, such as mentalizing or reflecting on the mental states of others (Amodio and Frith, 2006; Buckner and Carroll, 2007; Gallagher and Frith, 2003; Mitchell et al., 2002, 2006; Rilling et al., 2004, 2008) in addition to self-referential processing (D'Argembeau et al., 2005; Gusnard et al., 2001). Furthermore, both an activation in part of the fronto-parietal control network and a deactivation in the default mode network have been observed when participants were imitated as compared to when they imitated others (Guionnet et al., 2012). However, there are only a handful of studies that explore neural mechanisms of social interaction in an interactive context (Guionnet et al., 2012; Redcay et al., 2010; Saito et al., 2010; Schilbach et al., 2010; Tognoli et al., 2007), although social interaction is a coregulated coupling

activity that involves at least two autonomous agents. As Guionnet et al. (2012) highlighted, the major reason for this paucity may be attributed to the methodological and technical difficulties associated with creating a natural social interaction within an MRI environment. Considering that participants can have a direct face-to-face interaction while undergoing NIRS measurement, usage of NIRS enables easier measurement of the activity of the RSNs during social interaction (Cui et al., 2012; Funane et al., 2011). Therefore, our finding should promote investigation of the role of RSNs in social interaction.

In most fMRI and NIRS studies, functional connectivity has been explored by employing methods that assume temporal stationarity, such as cross-correlation. Using fMRI and NIRS independently, it has been previously investigated if resting state functional connectivity estimated using signals obtained from these imaging techniques is test–retest reliable (Zhang et al., 2011 for NIRS; Zuo et al., 2010b for fMRI). On the other hand, recent fMRI studies have demonstrated that resting state functional connectivity exhibits dynamic changes within time scales of seconds to minutes (Chang and Glover, 2010; Kang et al., 2011). Furthermore, one study demonstrated that functional brain networks exhibit task-induced changes in their network topology (Moussa et al., 2011). Moreover, studies using electroencephalography demonstrated that cortical activation induced with transcranial magnetic stimulation during non-rapid eye movement sleep did not propagate to other cortical areas, whereas waves of activation during quiet wakefulness moved to connected cortical areas several centimeters away (Massimini et al., 2005). This suggests that network topology of the RSNs also changes during the sleep state transitions. Because dynamic properties of a network relate to unfolding processes in the network (Butts, 2009), an understanding of the dynamic characteristics of a resting state network is important to reveal the intrinsic information on the processing mechanism of the brain, such as information exchange between different brain regions. Because NIRS places less physical

burden on participants, this device is useful for examining the characteristics of functional connectivity with a relatively long time scale. Indeed, one published NIRS study conducted long-term recordings for over 1 hour at bedside (Roche-Labarbe et al., 2008). Thus, the results of our study should promote investigation of the dynamic characteristics of resting state functional connectivity. NIRS should also be helpful for investigation of some other issues. Some studies have investigated changes in the RSNs along the course of development by measuring spontaneous brain activity of infants with fMRI and NIRS (Doria et al., 2010; Gao et al., 2009; Homae et al., 2010). However, it is often difficult to transport early preterm infants to an fMRI scanner; therefore, there is limited data related to the RSNs in these periods (White et al., 2012). Because NIRS is suitable for use in conditions where participants have difficulty entering an fMRI scanner, application of NIRS should promote gathering of information on the RSNs from these participants. Furthermore, in previous fMRI studies, RSNs have generally been characterized from brain activity recorded with participants lying in the dorsal position inside the scanner. In contrast, NIRS measurement can be conducted without relation to the posture of the involved participant. Therefore, the effect of this postural difference on the RSNs can be investigated using NIRS by running resting state recordings with participants in these two postures.

In this study, I evaluated the NIRS–fMRI signal relationship during the resting state, with particular emphasis on functional connectivity, by concurrently using fMRI and NIRS. Our results showed that NIRS can be used to collect information regarding RSNs as defined in fMRI. This study should encourage development of signal analysis for elucidating the RSNs from measured NIRS signals.

3.5 Supplementary materials

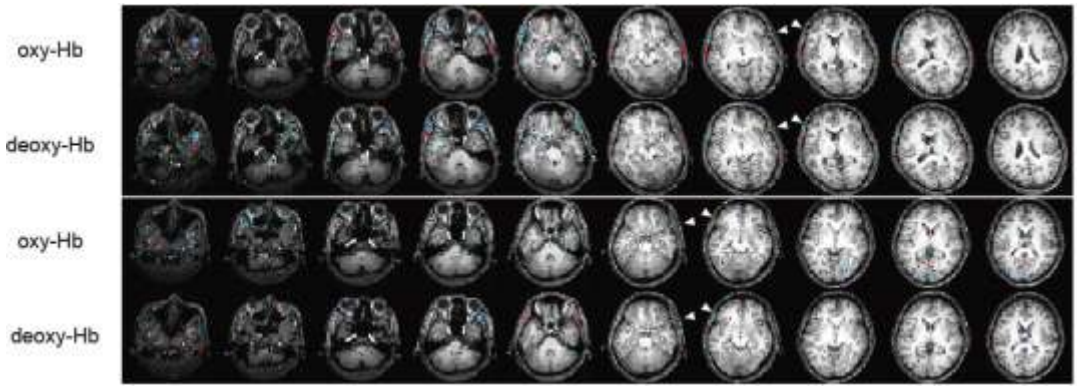

Figure 3.S1. Correlation of NIRS signals obtained at particular frontal regions with localized regions of non-brain tissue. Rows correspond to data for different participants. Red and blue dots represent the correlated voxels with oxy- and deoxy-Hb signals obtained at the Frontal_Inf_Orb_L and Frontal_Inf_Tri_R regions, respectively, in each participant. Cyan dots represent the correlating voxels at both Frontal_Inf_Orb_L and Frontal_Inf_Tri_R regions. Green dots indicated with arrowheads in the maps show the cortical projection point of the vitamin tablet, representing the NIRS measurement channel. Almost all colored voxels were cyan and localized within the temporal muscles and regions near the eyes.

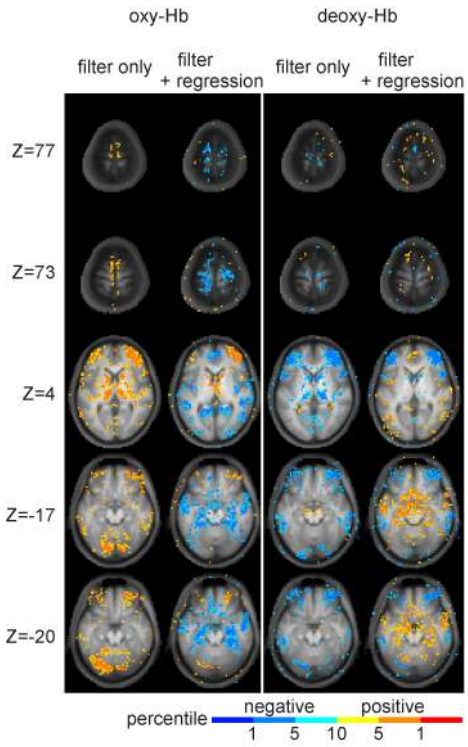

Figure 3.S2. Effect of noise regression in the BOLD signals on the correlation between NIRS and BOLD signals. I chose oxy-Hb and deoxy-Hb signals that had been obtained at Frontal_Mid_R (channel 4, Table 3.2) as seed signals for correlation maps and had been processed with a band-pass filter (0.009–0.10 Hz). Whole-brain BOLD signals were also processed with the same band-pass filter (0.009–0.10 Hz). First, correlation maps were estimated by calculating correlation between whole-brain BOLD signals and the NIRS seed signals. These results are shown in the column indicated as "filter only." Then, I regressed out the physiological waveforms from BOLD signals (see "Noise signal regression" in the Method section) and calculated the correlation between BOLD signals, from which noise had been removed, and the NIRS seed signals. These results are shown in the column indicated as "filter + regression." When no waveform was regressed from BOLD signals (filter only), both Hb signals correlated not only with cortical regions but also with cerebral vasculature areas such as the superior sagittal sinus (Z = 73 and Z = 77 of the "filter only" column) and the transverse sinus (Z = -20 and Z = -17 of the "filter only" column). In contrast, when all the physiological waveforms were regressed from BOLD signals, no correlation over the threshold was observed in these cerebral vasculature areas.

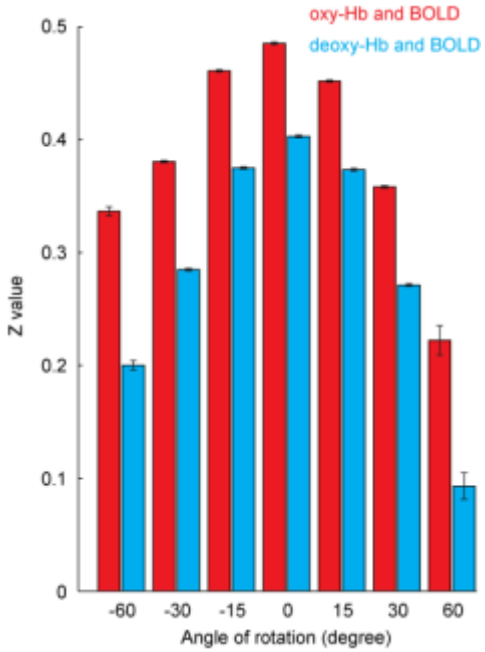

Figure 3.S3. Effect of rotation of the optical path plane on the correlation between NIRS and BOLD signals. To confirm the reliability of the registration process, I examined whether changes that are produced in the projection point of the NIRS channel because of rotation of the optical path plane affect the resultant correlation between the NIRS signals (oxy-Hb and deoxy-Hb) and BOLD signals extracted from spherical ROIs around the projection point. I determined projection points when the optical path plane was rotated around the axis determined by the positions of the emitter and detector as follows: First, I defined the positions of the emitter and detector as the midpoints between the median point of the corresponding tablet and those of the two adjacent tablets on both sides. Second, I rotated the projection line on the optical path plane around the axis determined by the emitter and detector points. Third, I defined the rotated projection points as the intersection of the rotated projection line of each channel and the surface of a gray-matter mask. The rotation angle had a value of −60°, −30°, −15°, 15°, 30°, or 60°. Positive angles correspond to the rotations in the superior directions, while negative angles correspond to those in the inferior directions. Next, I extracted fMRI BOLD signals from spherical ROIs with a 7.5-mm radius around these projection points and calculated the correlation with the oxy-Hb and deoxy-Hb signals for each NIRS channel. The best correlation was found between NIRS signals and BOLD signals extracted from the ROI around the projection point without rotation of the optical path plane, providing evidence that the channel locations were reliably registered on the cortical surface. The error bars show the standard error.

Table 3.S1. Distributions of HCVs with NIRS signals

ch	anatomical location of channel	oxy-Hb Brain tissue (%)	Skull	Skin	r value of 308th-ranked voxel	deoxy-Hb Brain tissue	Skull	Skin	r value of 100th-ranked voxel
1	Frontal_Sup_Medial_L	89	8	3	0.24	84	11	5	-0.21
2	Frontal_Sup_R	91	5	4	0.29	89	6	5	-0.26
3	Frontal_Sup_L	88	7	5	0.28	89	6	5	-0.28
4	Frontal_Mid_R	80	8	13	0.22	76	9	15	-0.21
5	Frontal_Mid_Orb_L	62	12	26	0.20	65	11	24	-0.22
6	Frontal_Inf_Tri_R	48	12	40	0.17	52	11	36	-0.16
7	Frontal_Inf_Orb_L	36	10	54	0.17	47	9	44	-0.18
8	Temporal_Mid_R	92	6	3	0.38	87	8	5	-0.32
9	Temporal_Mid_L	88	6	6	0.26	81	9	10	-0.22
10	Occipital_Mid_R	95	2	3	0.38	88	5	7	-0.30
11	Occipital_Mid_Ant_L	92	5	3	0.33	83	8	9	-0.26
12	Occipital_Sup_R	93	4	3	0.42	86	7	7	-0.36
13	Occipital_Mid_Post_L	92	6	3	0.38	87	8	5	-0.32
14	Calcarine_L	89	7	4	0.37	79	11	10	-0.28

To confirm the result of Table 3.5, I selected the top 308 ranked voxels (representing the top 10% of all voxels included in a 3-cm radius ROI). Although the number of voxels (308) corresponds to that included in the spherical ROI with 4 voxels of radius, which often covers more than one gyrus, the ratio of the tissue types was not changed. Anatomical labels were determined by using the Automated Anatomical Labeling (AAL) (Tzourio-Mazoyer et al., 2002). Values in the columns indicated as 'r value of 100th-ranked voxels' are correlation coefficients. 'r value of 100th-ranked voxels' stands for averaged 100th -ranked correlation coefficients of the HCVs across all participants. Abbreviations: L = Left hemisphere, R = Right hemisphere, Sup = Superior, Mid = Middle, Inf = Inferior, Ant = Anterior, Post = posterior, Orb = Orbital part, Tri = Triangular part.

Chapter 4 Frequency-specific topology of the human functional brain network (Study 3)

4.1 Introduction

The existence of functional connectivity, defined as statistical dependency of brain activities between different brain regions, strongly indicates that brain regions connected by functional connectivity share processed information between each other. Because the similar spatial characteristics of functional connectivity have been demonstrated both within task execution and during rest, the brain may not be regarded as a stimulus-responsive organ but rather is an organ that functions through the intrinsic constraints of activity (Biswal et al., 1995; Fox and Raichle, 2007). Functional magnetic resonance imaging (fMRI) has been used to investigate functional connectivity over whole brain regions; related findings have provided a fundamental view of the brain's spatial organization that simultaneously achieves segregation and integration of processed information (Sporns, 2013). While segregation in the whole brain spatial scale is the idea that information processing is conducted in a specialized module independently of other modules, integration is the concept that processed information in each module is united and shared among all modules of a system. On the other hand, fMRI signals contain multiple timescale components; the coexistence of fMRI signals fluctuating at several time scales has been demonstrated (Baria et al., 2011; He, 2011; Zuo et al., 2010). However, the relevancy of these time scale components to the spatial architecture of functional connectivity is unclear. Thus, the purpose of this research was to investigate the frequency specificity of the brain's functional network organization that contributes to the segregation and integration of information.

Spatial organization of spontaneous brain activity has been studied from the viewpoint of graph theory, in which functional connectivity is regarded as the edge of a graph and the brain region as a node. Network structures that consist of functional connectivity over whole brain regions have a unique organization; some sub-network structures consist of densely interconnected regions called a "module" or a "community" (Dosenbach et al., 2007, 2010; Fornito et al., 2012; Power et al., 2011; Spreng et al., 2013), with a highly connected and central region called a "hub" (Achard et al., 2006; Buckner et al., 2009; Tomasi and Volkow, 2011a,b; van den Heuvel et al., 2008b). The community operates as a single functional system, of which it shows positive or negative increases with attentional demand, and plays a key role in cognitive control (Damoiseaux et al., 2006; De Luca et al., 2006; Dosenbach et al., 2007; Fox and Raichle, 2007; Lowe et al., 1998), while the hub plays an important part in establishing and maintaining efficient global brain communication. Therefore, we can investigate properties of information segregation and integration of the brain network in terms of graph theoretical perspectives by examining presences of the landmark structures characterizing these network properties, that is, the existences of communities and hubs.

It has been demonstrated that time scales of fMRI signals contributing to functional connectivity are "low-frequency fluctuation" within 0.01–0.10 Hz (Cordes et al., 2001). Therefore, most fMRI studies on the network organizations of functional connectivity have focused on synchronized low-frequency fluctuations of fMRI signal changes (0.01–0.10 Hz) in the resting brain (Fox and Raichle, 2007). However, a computational study has demonstrated that topological features of functional connectivity can vary with the time scale of brain activity without changing the underlying connections (Honey et al. 2007). Indeed, frequency-specific characteristics exist in correlation with hemodynamic fluctuations within this low-frequency range and differ depending on the brain region

combination (Chang and Glover 2010; Sasai et al., 2011; Wu et al., 2008). Furthermore, a fMRI study has demonstrated that some brain regions not only show event-related activities occurring at typical time scales for hemodynamic responses to a single event (0.05–0.10 Hz), but they also display signal increases sustained for the duration of a task block (Dosenbach et al., 2006); this suggests that frequency-specific network architecture establishes the implementation of time scale-dependent information processing, thereby generating distinct brain functions. In this study, I conducted resting state fMRI recordings and investigated the frequency-specificity of the FCN implicated in brain communities that serve in cognitive control (Dosenbach et al., 2007; Power et al., 2011). Special emphasis was placed on the network attributes for information segregation and integration.

4.2 Materials and methods

4.2.1 Participants

A total of 28 healthy adults (15 men and 13 women; age range, 22-44 years) participated in this study. All participants were awake with their eyes closed during data acquisition. The protocol was approved by the ethical committee of the National Institute for Physiological Sciences, Okazaki, Japan. Informed consent was obtained from all participants prior to initiation of the experiments.

4.2.2 Data acquisition

In this study, I used the same fMRI and NIRS data sets obtained in Study 2. For detail information about data acquisition, refer to 3.2 Materials and methods.

4.2.3 fMRI preprocessing

Functional MRI volumes were motion-corrected and slice-timing-corrected using the SPM8 package (Wellcome Department of Imaging Neuroscience, London, UK). fMRI data sets were spatially smoothed with 5-mm full width at half maximum Gaussian blur, and they were normalized to the MNI space using DARTEL in SPM8. fMRI data sets are generally contaminated with noise, including fluctuations due to scanner instabilities, subject motion, and respiration and cardiac effects, resulting in coherent signal fluctuations across the brain (e.g., global signal). In many studies, these contaminating signals are estimated by utilizing fMRI data-inherent information and removed using a general linear model (GLM) technique (Fox et al., 2005). However, the regression of global signals has been shown to introduce spurious anti-correlation (Anderson et al., 2011; Murphy et al., 2009). Anderson et al. (2011) have proposed an alternate method to avoid this bias of correlation estimation; this method uses an optimally phase-shifted waveform extracted from soft tissues of the face and calvarium, as well as regressors obtained from subject motion parameters, white matter, ventricles, and physiological waveforms, a method termed phase-shifted soft tissue correction [PSTCor]. Based on the method proposed by Anderson et al. (2011), I previously used a modified version of PSTCor that only used fMRI inherent information and I observed no anti-correlation (Sasai et al., 2012). In this study, I applied this modified method of PSTCor to eliminate noise.

4.2.4 ROI selection

It has been suggested that spontaneous brain activity is organized into two widespread brain regions in terms of activity profiles recruited by cognitively demanding tasks: “task-positive systems” and “task-negative systems”. While several studies have consistently reported activation of

the dorsal anterior cingulate cortex, frontal insula, lateral prefrontal cortex, and lateral parietal cortex in tasks of attention and working memory (Menon et al., 2001; Curtis and D'Esposito, 2003; Fox et al., 2005; Kerns et al., 2004; Ridderinkhof et al., 2004), decreases in the medial prefrontal cortex, angular gyrus, and posterior cingulate cortex have been observed during such tasks (Fox et al.,, 2005; Gusnard et al., 2001; Raichle et al., 2001). Recently, it has been shown that the task-positive system consists of at least two different sets of brain regions in terms of its functions: central executive and saliency systems (Menon and Uddin, 2010; Seeley et al., 2007b). Furthermore, Dosenbach et al. (2006) also demonstrated that the task-positive system is composed of multiple sub-systems, including the fronto-parietal task control system overlapping with central executive systems and the cingulo-opercular task control system overlapping with the saliency system, whereas the task-negative system is composed of a single system (the default mode system). In order to investigate the existence of frequency-specific topology in a large-scale functional brain network, I selected the following three systems, which included hub regions from both task-positive and task-negative systems: the default mode system (DMS), the fronto-parietal task control system (FPS), and the cingulo-opercular task control system (COS) (names quoted from Power et al., 2011). Coordinates corresponding to these functional systems are available in published literature where coordinates were identified by conducting meta-analysis of a series of task-activation studies and were used to extract the time series corresponding to the functional systems (Dosenbach et al., 2010). These ROIs were located in areas of the cerebral cortex and sub-cortical regions. The total number of ROIs was 87. Table 4.1 summarizes the MNI coordinates, original labels, and names of automated anatomical labeling (AAL) of ROIs (Tzourio-Mazoyer et al., 2002).

Table 4.1. List of coordinates of ROIs

No	MNI			Network	AAL
	x	y	z		
1	6	64	3	default	Frontal_Sup_Medial_R
2	0	51	32	default	Frontal_Sup_Medial_L
3	-25	51	27	default	Frontal_Mid_L
4	9	51	16	default	Cingulum_Ant_R
5	-6	50	-1	default	Cingulum_Ant_L
6	-11	45	17	default	Frontal_Sup_Medial_L
7	8	42	-5	default	Cingulum_Ant_R
8	9	39	20	default	Cingulum_Ant_R
9	46	39	-15	default	Frontal_Inf_Orb_R
10	23	33	47	default	Frontal_Sup_R
11	-16	29	54	default	Frontal_Sup_L
12	52	-15	-13	default	Temporal_Mid_R
13	-59	-25	-15	default	Temporal_Mid_L
14	1	-26	31	default	Cingulum_Mid_R
15	28	-37	-15	default	Fusiform_R
16	-3	-38	45	default	Cingulum_Mid_L
17	-8	-41	3	default	Calcarine_L
18	-61	-41	-2	default	Temporal_Mid_L
19	-28	-42	-11	default	Lingual_L
20	-5	-43	25	default	Cingulum_Post_L
21	9	-43	25	default	Cingulum_Post_R
22	5	-50	33	default	Precuneus_R
23	-5	-52	17	default	Precuneus_L
24	10	-55	17	default	Precuneus_R
25	-6	-56	29	default	Precuneus_L
26	-11	-58	17	default	Cuneus_L
27	51	-59	34	default	Angular_R
28	-48	-63	35	default	Angular_L
29	11	-68	42	default	Precuneus_R
30	-36	-69	40	default	Parietal_Inf_L
31	-9	-72	41	default	Precuneus_L
32	45	-72	29	default	Occipital_Mid_R
33	-2	-75	32	default	Cuneus_L
34	-42	-76	26	default	Occipital_Mid_L
35	29	57	18	fronto-parietal	Frontal_Mid_R
36	-29	57	10	fronto-parietal	Frontal_Mid_L
37	42	48	-3	fronto-parietal	Frontal_Inf_Tri_R
38	-43	47	2	fronto-parietal	Frontal_Inf_Tri_L
39	39	42	16	fronto-parietal	Frontal_Mid_R
40	40	36	29	fronto-parietal	Frontal_Mid_R
41	-1	28	40	fronto-parietal	Frontal_Sup_Medial_L
42	46	28	31	fronto-parietal	Frontal_Mid_R
43	-52	28	17	fronto-parietal	Frontal_Inf_Tri_L
44	-44	27	33	fronto-parietal	Frontal_Mid_L
45	40	17	40	fronto-parietal	Frontal_Mid_R
46	44	8	34	fronto-parietal	Precentral_R
47	-42	7	36	fronto-parietal	Precentral_L
48	-41	-40	42	fronto-parietal	Parietal_Inf_L
49	54	-44	43	fronto-parietal	Parietal_Inf_R
50	-35	-46	48	fronto-parietal	Parietal_Inf_L
51	-48	-47	49	fronto-parietal	Parietal_Inf_L
52	-53	-50	39	fronto-parietal	Parietal_Inf_L
53	44	-52	47	fronto-parietal	Parietal_Inf_R
54	-32	-58	46	fronto-parietal	Parietal_Inf_L
55	32	-59	41	fronto-parietal	Angular_R
56	27	49	26	cingulo-opercular	Frontal_Mid_R
57	34	32	7	cingulo-opercular	Frontal_Inf_Tri_R
58	-2	30	27	cingulo-opercular	Cingulum_Mid_L
59	51	23	8	cingulo-opercular	Frontal_Inf_Tri_R
60	38	21	-1	cingulo-opercular	Insula_R
61	9	20	34	cingulo-opercular	Cingulum_Mid_R
62	-36	18	2	cingulo-opercular	Insula_L
63	-6	17	34	cingulo-opercular	Cingulum_Mid_L
64	0	15	45	cingulo-opercular	Supp_Motor_Area_L
65	-46	10	14	cingulo-opercular	Rolandic_Oper_L
66	-20	6	7	cingulo-opercular	Putamen_L
67	14	6	7	cingulo-opercular	Caudate_R
68	-48	6	1	cingulo-opercular	Insula_L
69	37	-2	-3	cingulo-opercular	Putamen_R
70	-12	-3	13	cingulo-opercular	Caudate_L
71	-12	-12	6	cingulo-opercular	Thalamus_L
72	11	-12	6	cingulo-opercular	Thalamus_R
73	32	-12	2	cingulo-opercular	Putamen_R
74	-30	-14	1	cingulo-opercular	Putamen_L
75	11	-24	2	cingulo-opercular	Thalamus_R
76	-30	-28	9	cingulo-opercular	Heschl_L
77	51	-30	5	cingulo-opercular	Temporal_Sup_R
78	-4	-31	-4	cingulo-opercular	Thalamus_L
79	54	-31	-18	cingulo-opercular	Temporal_Mid_R
80	8	-40	50	cingulo-opercular	Precuneus_R
81	58	-41	20	cingulo-opercular	Temporal_Sup_R
82	43	-43	8	cingulo-opercular	Temporal_Mid_R
83	-55	-44	30	cingulo-opercular	SupraMarginal_L
84	42	-46	21	cingulo-opercular	Angular_R
85	-41	-47	29	cingulo-opercular	Angular_L
86	-59	-47	11	cingulo-opercular	Temporal_Mid_L
87	-52	-63	15	cingulo-opercular	Temporal_Mid_L

In a column named "network," network assignments of ROIs in the Dosenbach et al., 2010 are shown. In a column named "AAL," labels of ROIs determined by Automated Anatomical Labeling (AAL) (Tzourio-mazoyer et al., 2002) are listed.

4.2.5 Detection of frequency-specificity of functional connectivity

For each individual data set, I calculated the coherence between all pairs of signals extracted from the above-mentioned 87 ROIs whose radii are 6mm. Coherence measures the linear and time-invariant relationship between two signals at frequency λ. It is defined as follows:

$$C_{xy}(\lambda) = \frac{\left|P_{xy}(\lambda)\right|^2}{P_{xx}(\lambda)P_{yy}(\lambda)} \quad (1)$$

where $C_{xy}(\lambda)$ refers to the coherence between signals x and y, while $P_{xy}(\lambda)$ is the cross-spectrum of x and y, $P_{xx}(\lambda)$ is the power spectrum of signal x, and $P_{yy}(\lambda)$ is the power spectrum of signal y. For each pair of signals, I obtained coherence matrices by averaging coherence values within 23 narrow, 50% overlapping frequency bands, with band widths of 0.02 Hz (Fig. 4.1A). Chang and Glover (2010) showed that the frequency-dependency of coherence among the ROIs organizing the DMS is different from that estimated from the ROIs of two distinct functional systems (DMS and dorsal attention systems). Taking this into consideration, I further averaged these band-averaged coherence values within two categories of ROI pairs in order to identify frequency-dependency of functional connectivity: 1) both ROIs in the pair were labeled in the same functional system (intra-system), and 2) both ROIs were assigned to two different functional systems (inter-system) by Dosenbach et al. (2010) (Fig. 4.1B). I then identified and conducted analyses on the frequency bands showing higher coherence values than other bands in both spectrums obtained from the averaged coherence in the two categories.

In order to confirm that the high coherence in the VLF and LF was not generated by aliasing of physiological confounds contained in hemodynamic signals, or that it was not attributed to measurement modality (e.g., fMRI), I investigated coherence spectrums with NIRS signals. By projecting vitamin tablets onto cortical surfaces in structural MR images, I identified ROIs where NIRS

signals were obtained. While two ROIs were identified within brain regions constituting the fronto-parietal system, one ROI were located within the brain region forming the default mode system. Then, I calculated coherence between two ROIs in the fronto-parietal system and among ROIs between fronto-parietal and default mode systems as counterparts of coherence for intra- and inter-system.

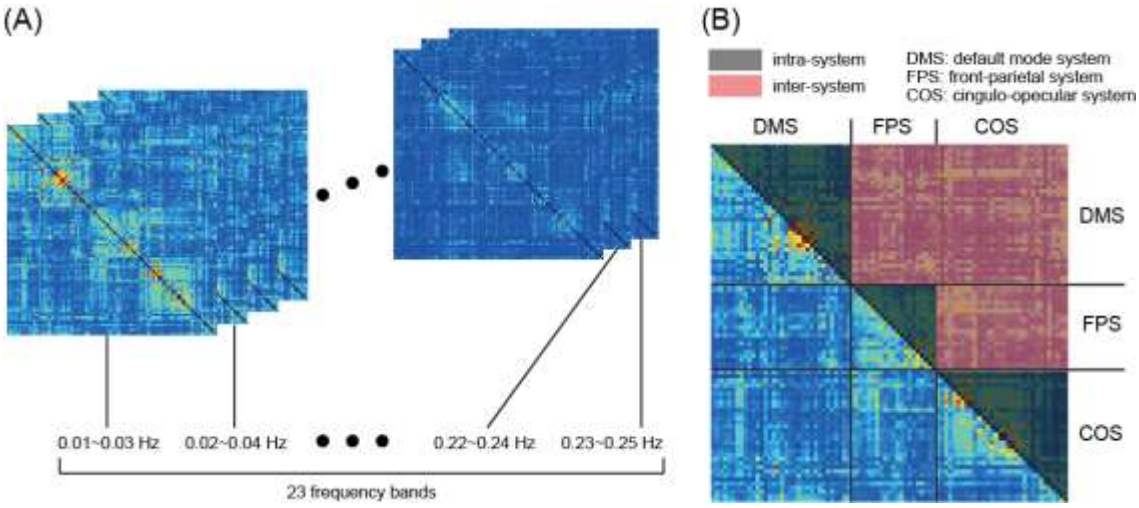

Figure 4.1. Procedure for detecting frequency-specificity of functional connectivity. Coherence was estimated in all pairs of ROIs between 0.01 and 0.25 Hz and averaged within narrow, 50% overlapping frequency bands that had a band width of 0.02 Hz. As a result, I obtained 23 coherence matrices in each frequency band (A). (B) Considering that frequency-specificity is different between ROIs in the same functional system and ROIs of two distinct functional systems, coherence values were divided into two categories: (1) coherence values within the same functional system (intra-system); and, (2) coherence values between different functional systems (inter-system). Coherence values were further averaged within each category.

4.2.6 Network analysis

4.2.6.1 Frequency-specific network construction in individual data set

To define frequency-specific networks, I obtained adjacency matrices, ***A,*** by applying the

sparsity thresholds, *S*, ranging from 0.05 to 0.25 in 0.05 increments, to the coherence matrices corresponding to the frequency bands showing higher coherence values than other bands (see above). Sparsity, *S*, was defined as the number of edges in a graph divided by the maximum possible number of edges, and this was used to measure threshold (Latora and Marchiori, 2001; Achard and Bullmore, 2007).

$$S = \frac{1}{n(n-1)} \sum_{i \in N} d_i \qquad (2)$$

where n is the number of all nodes in graph N, i is a node in graph N, and d_i is the number of edges connected to the node, i. The greater the sparsity threshold, the greater the number of edges in a graph with applied thresholds (i.e., bigger sparsity results in a weaker threshold). Unlike thresholds using values quantifying the strength of functional connectivity, *S* can control the number of edges in the network between different conditions. Because many network metrics are affected by the number of edges in a graph, usage of *S* enables us to attribute the different results of graph measure to differences of patterns of network connections. When one *S* is selected, corresponding threshold values of the strength of functional connectivity is determined. Therefore, the range of *S* should be determined so that corresponding threshold values of the measure of functional connectivity is significantly higher than 0. To choose the lower bound of *S*, I calculated null-distributions of 10,000 coherence values by repeating calculations of shuffled signals obtained by the bootstrap method for each ROI pair. By ensuring the statistical significance ($p < 0.05$) of the coherence values corresponding to the sparsity thresholds for all participants' data sets, I selected the lower bound of the sparsity thresholds as $S = 0.25$.

4.2.6.2 Graph metrics

I calculated graph theoretical metrics characterizing information segregation and integration in adjacency matrices. I calculated the mean clustering coefficient, mean local efficiency, and modularity as measures of functional segregation and global efficiency as a measure of functional integration.

The mean clustering coefficient, *ClusterCoef* (Latora and Marchiori, 2001), represents the prevalence of clustered connectivity around individual nodes and is defined as follows:

$$ClusterCoef = \frac{1}{n}\sum_{i \in N} \frac{2t_i}{k_i(k_i - 1)} \quad (3)$$

where k_i is the degree of node i, and t_i is the number of triangles around i, defined as:

$$t_i = \frac{1}{2}\sum_{i,j,h \in N} a_{ij}a_{ih}a_{jh} \quad (4)$$

where i, j, and h are nodes in the graph, and a_{ij} is the connection status between nodes i and j; if i and j are connected, then $a_{ij} = 1$, otherwise $a_{ij} = 0$.

The mean local efficiency, E_{loc} (Latora and Marchiori, 2001), indicates a network mean of local efficiency of information transfer within the immediate neighborhood of each node and is defined as:

$$E_{loc} = \frac{1}{n}\sum_{i \in N} \frac{\sum_{j,h \in N, j \neq i} a_{ij}a_{ih}\left[d_{jh}(N_i)\right]^{-1}}{k_i(k_i - 1)} \quad (5)$$

where $d_{jh}(N_i)$ is the length of the shortest path between node j and node h in the "local network" that consists of only nodes linking to node i.

Modularity, Q (Newman, 2004, 2006), indicates the degree to which the network may be subdivided into non-overlapping communities. For a set of non-overlapping communities, M and Q are

defined as:

$$Q = \sum_{u \in M} \left[e_{uu} - \left(\sum_{v \in M} e_{uv} \right)^2 \right] \quad (6)$$

where u and v are communities and e_{uv} is the fraction of all links that connect nodes in u with nodes in v.

Global efficiency, E (Latora and Marchiori, 2001), is an indicator of global efficiency of parallel information transfer in the network and is defined as follows:

$$E = \frac{1}{n} \sum_{i \in N} \frac{\sum_{j \in N, j \neq i} d_{ij}^{-1}}{n-1} \quad (7)$$

In this case, n is the number of nodes in the network, N is the set of all nodes, and d_{ij} is the shortest path length between nodes i and j.

All of these metrics were computed for each sparsity threshold in each individual data set by using the Brain Connectivity Toolbox (Rubinov and Sporns 2010).

4.2.6.3 Statistical comparison

For each threshold level, I conducted a two-tailed *t*-test with subjects (random effects analysis) against the null hypothesis, defined as no significant group-level difference between graph metrics calculated in the frequency bands that showed higher coherence values as compared to other bands. The false discovery rate (FDR) method was used to correct for multiple comparisons, and significant differences were detected at $p < 0.05$ after FDR correction (Benjamini and Yekutieli, 2001).

4.2.7 Graph structures of segregation and integration in group-level networks

While brain networks possess characteristic structures that play key roles in information

integration and segregation, it remains unclear if these structures can be consistently found in frequency-specific networks. I tackled this issue by estimating group-level network structures and identifying hub regions and community structures for each group-level frequency-specific network.

4.2.7.1 Group-level network construction

Network connection patterns have inter-individual variability. In order to investigate consistent structure in the group level, I constructed a network-level adjacency matrix, $\boldsymbol{A^g}$, from individual-level adjacency matrices, $\boldsymbol{A}$, of all individual data sets. $\boldsymbol{A}$ is a binary matrix, defined as $\boldsymbol{A}_{ij}$ = 1 when there was functional connectivity between nodes *i* and *j*, otherwise it is defined as $\boldsymbol{A}_{ij}$ = 0. I generated a matrix representing the consistency of functional connectivity across all participants by averaging $\boldsymbol{A}$. I refer to this matrix as a consistent edge matrix, $\boldsymbol{Ce}$ ($0 \leqq \boldsymbol{Ce}_{ij} \leqq 1$). Then, by applying sparsity thresholds on $\boldsymbol{Ce}$, I obtained $\boldsymbol{A^g}$ in frequency bands where the coherence showed higher values than other frequency bands in both spectrums obtained from the averaged coherence in the two categories. Although the same sparsity thresholds, *S*, between 0.05 and 0.25 for the 0.05 increments were used in producing $\boldsymbol{A}$ and $\boldsymbol{A^g}$, I finally selected *S*s that generated connected $\boldsymbol{A^g}$s, which are graphs with at least one direct or indirect pathway among all nodes, for all frequency bands showing high coherence values than other ones.

4.2.7.2 Force-directed layout using a spring embedding algorithm

I aimed to investigate frequency dependency of network structures contributing to information segregation. I applied a Fruchterman-Reingold graph drawing algorithm (Fruchterman and Reingold, 1991) for force-directed placement in order to visually compare the degree of segregation in

the group-level networks. Basically, this algorithm assigns forces, as if the edges were springs and the nodes were electrically charged particles, and it simulates the graph as a physical system. With iterative application of forces on the graph until it comes to an equilibrium state, the algorithm can determine the location of nodes in a two-dimensional space. These calculations were conducted using the Matlab BGL toolbox (http://www.mathworks.com/matlabcentral/fileexchange/10922-matlabbgl).

4.2.7.3 Community detection

I then examined group-level community structures in group-level networks obtained in different frequency bands. Since community structures have between-participant variability, group-level community structures were not identified with the consistent edge matrix, ***Ce***, but were detected with the consistent assignment matrix, ***Ca*** (Fornito et al., 2012; van den Heuvel et al., 2008a). This matrix was constructed as follows: First, community detection was conducted on the adjacency matrix, ***A***, of each participant. Individual-level consistency of community assignment was expressed in a matrix, ***ICa***, in which element $\boldsymbol{ICa}_{ij} = 1$ if ROIs i and j are assigned in the same community. Then, ***ICa***s were averaged across participants to produce ***Ca***s, in which element $\boldsymbol{Ca}_{ij}$ represents the incidence of two ROIs being assigned to an identical community within the group ($0 \leqq \boldsymbol{Ca}_{ij} \leqq 1$). Finally, by applying community detection algorithm on ***Ca***s, I estimated group-level community structures in all frequency bands with higher coherence values than other ones. These were performed using the Brain Connectivity Toolbox.

4.2.7.4 Hub detection

I also detected the hub regions in all group-level networks obtained in different frequency

bands in order to assess if topological difference was reflected in different hub alignments between these networks. In order to identify hub regions, I measured two graph theoretical metrics for each node: 1) nodal degree and 2) eigenvector centrality (Lohmann et al., 2010). While nodal degree was calculated in group-level adjacency matrices, $\boldsymbol{A^g}$s, eigenvector centrality was computed in consistent edge matrices, ***Ce***s, without applying a threshold. In the current study, I defined hubs as nodes, in which nodal degree and eigenvector centrality were at least one standard deviation above the network mean (Sporns et al., 2007).

4.2.7.5 Rich-club detection

A study of human anatomical connectivity has demonstrated that structural brain hubs are not independent of each other but form a *rich-club*, characterized by a tendency for high-degree nodes to be more densely anatomically connected among themselves compared to nodes of a lower degree (van den Heuvel and Sporns, 2011). The appearance of a rich-club in human anatomical networks suggests that these regions identified as structural brain hubs perform some collaborative function, like information integration. This raises a question of whether hubs identified in FCNs also organize the rich-club.

By denoting the number of nodes with a higher degree than k as N_k and designating the edges within the sub-network that consist of these nodes as E_k, *k-density* $\Phi(k)$ is defined as follows:

$$\phi(k) = \frac{2E_k}{N_k(N_k - 1)} \quad (8)$$

The denominator represents the maximal number of edges within the sub-network. Several graphs including a random network, in which nodes are interconnected by chance, show that $\Phi(k)$ grows with

k. Therefore, if there is a tendency for hubs to be more inter-connected as compared to nodes of a lower degree, $\Phi(k)$ increases with k at a higher rate than that expected from random networks (i.e., $\Phi(k)$ is informative when this coefficient is normalized by the expected one) (Colizza et al., 2006; McAuley et al., 2007). Therefore, I identified a range of k expressing this characteristic as follows, and I subsequently refer to such phenomenon as a rich-club regime (van den Heuvel and Sporns, 2011). First, $\Phi(k)$ for all $\boldsymbol{A}^{\boldsymbol{g}}$s was calculated. Then, I constructed 1,000 randomized networks for each of the $\boldsymbol{A}^{\boldsymbol{g}}$s using the Brain Connectivity Toolbox and computed 1,000 coefficients in these networks, $\Phi_{randomized}(k)$. I defined the range of k where $\Phi(k)$ was significantly higher than the values calculated in the randomized networks. To evaluate the statistical significance, I compared $\Phi(k)$ with the distribution consisting of 1,000 of $\Phi_{randomized}(k)$ and identified the range where $\Phi(k)$ values were consistently included within the upper 1% of the distribution. When I detected more than two ranges satisfying this condition, I defined a rich-club regime as the highest range. Finally, normalized rich-club coefficients, $\Phi_{normalized}(k)$, were calculated by dividing $\Phi(k)$ with $\Phi_{meanrand}(k)$, which represents the mean of 1,000 of $\Phi_{randomized}(k)$.

4.2.8 Power spectral analysis

A consistent spatial structure of power spectral density distribution for signal oscillations in the whole brain in resting-state fMRI has been reported in previous studies (Baria et al., 2011; Zuo et al., 2010a). The highest power is found below 0.05 Hz and is localized mainly to the prefrontal, parietal, and occipital cortices. On the other hand, frequency components greater than 0.05 Hz localize more within subcortical structures. To confirm this regional variability of power spectrums, frequency powers of the BOLD signal of hub regions were calculated using Welch's periodogram method and

normalized by dividing by the total power. For each hub region, I obtained a power spectrum by averaging squared powers within 50 narrow frequency bands that had band widths of 0.005 Hz.

4.3 Results

4.3.1 Frequency-dependency of functional connectivity

Group-averaged coherence values were calculated and averaged within the following two categories of ROI pairs: 1) both ROIs in the pair were labeled in the same functional system (intra-system), and 2) the 2 ROIs were assigned to two different functional systems (inter-system) according to Dosenbach et al., 2010 (Fig. 4.1B). The highest value of the averaged coherence in the intra-system was observed in the lowest frequency band (VLF: very low frequency, [0.01–0.03 Hz]). There was one more frequency band (LF: low frequency, [0.07–0.09 Hz]), where the coherence values were higher than others (Fig. 4.2). In these two frequency bands, I found that the averaged coherence values obtained in the inter-system were also higher than other frequency bands. In order to ensure that observed frequency characteristics were reproducible in data sets obtained in other institutions, I estimated the above-mentioned coherence spectrum in public resting state fMRI data sets, where n = 96 participants from the 1,000 Functional Connectome Project (http://fcon_1000.projects.nitrc.org/index.html). As a result, I confirmed that coherence values in the VLF and LF were larger than those in other frequency bands (Fig. 4.S1). Furthermore, to confirm that this frequency-specificity was not due to aliasing of physiological noises contained in higher frequency regions, I investigated coherence spectrum of simultaneously obtained NIRS data sets. NIRS signals were measured with a sufficiently higher sampling rate (10 Hz) to characterize hemoglobin signals, including respiratory and cardiac pulsations, which were observed as separate peaks in the power

spectrum. I confirmed that while there were peaks corresponding to typical respiratory and cardiac pulsations around 0.3 and 1 Hz in the coherence spectrum, VLF and LF were still signature frequency bands where coherence values were higher than other frequency bands within 0.01–0.10 Hz (Fig. 4.3). Collectively, these results demonstrate that there are two frequency components that strongly contribute to resting state functional connectivity within the frequency band (0.01–0.10 Hz), where functional connectivity has been estimated in many studies. Thus, I focused and conducted analyses on these two frequency bands.

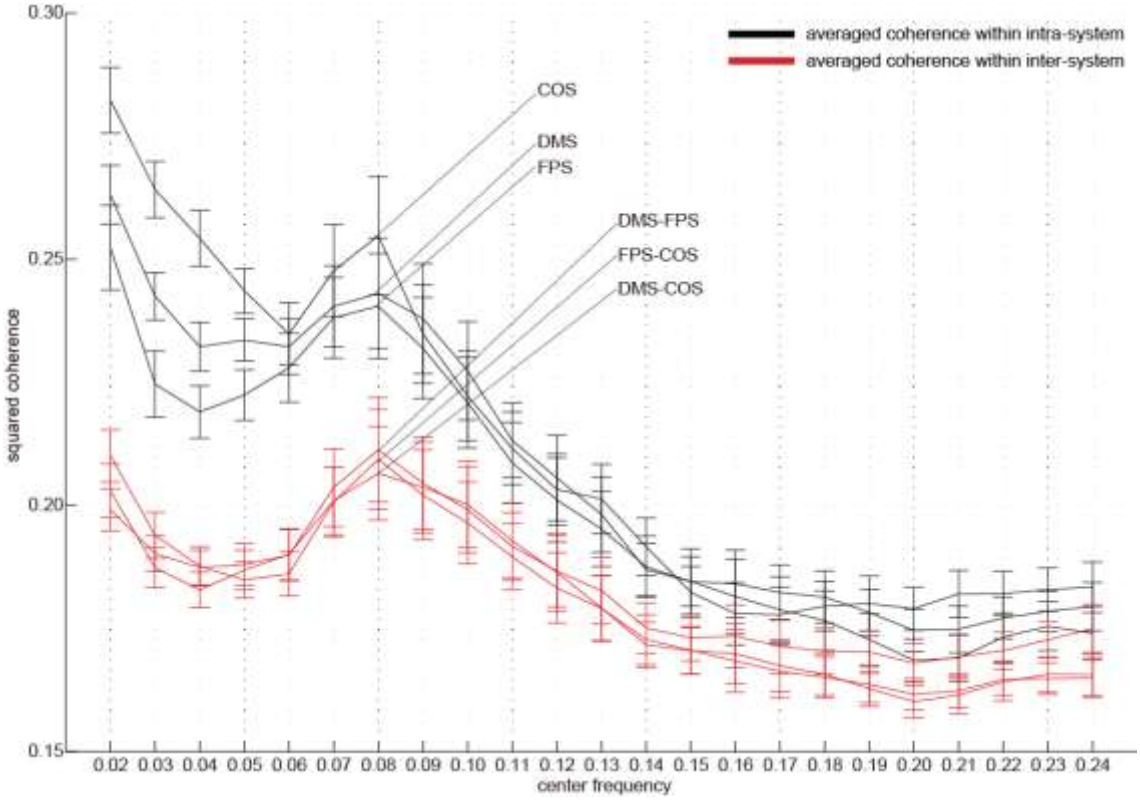

Figure 4.2. Frequency-specificity of functional connectivity. Averaged coherence values in two categories are shown. Black curves represent coherence values averaged within three functional systems, and red curves indicate values calculated in the inter-system groups (see Fig. 4.1). Error bars show the standard errors. The x-axis represents the center frequencies of the frequency bands, where coherence values were averaged. For all curves, coherence within 0.01–0.03 Hz (very low frequency, [VLF]) and 0.07–0.09 Hz (low frequency, [LF]) were higher than other frequency bands.

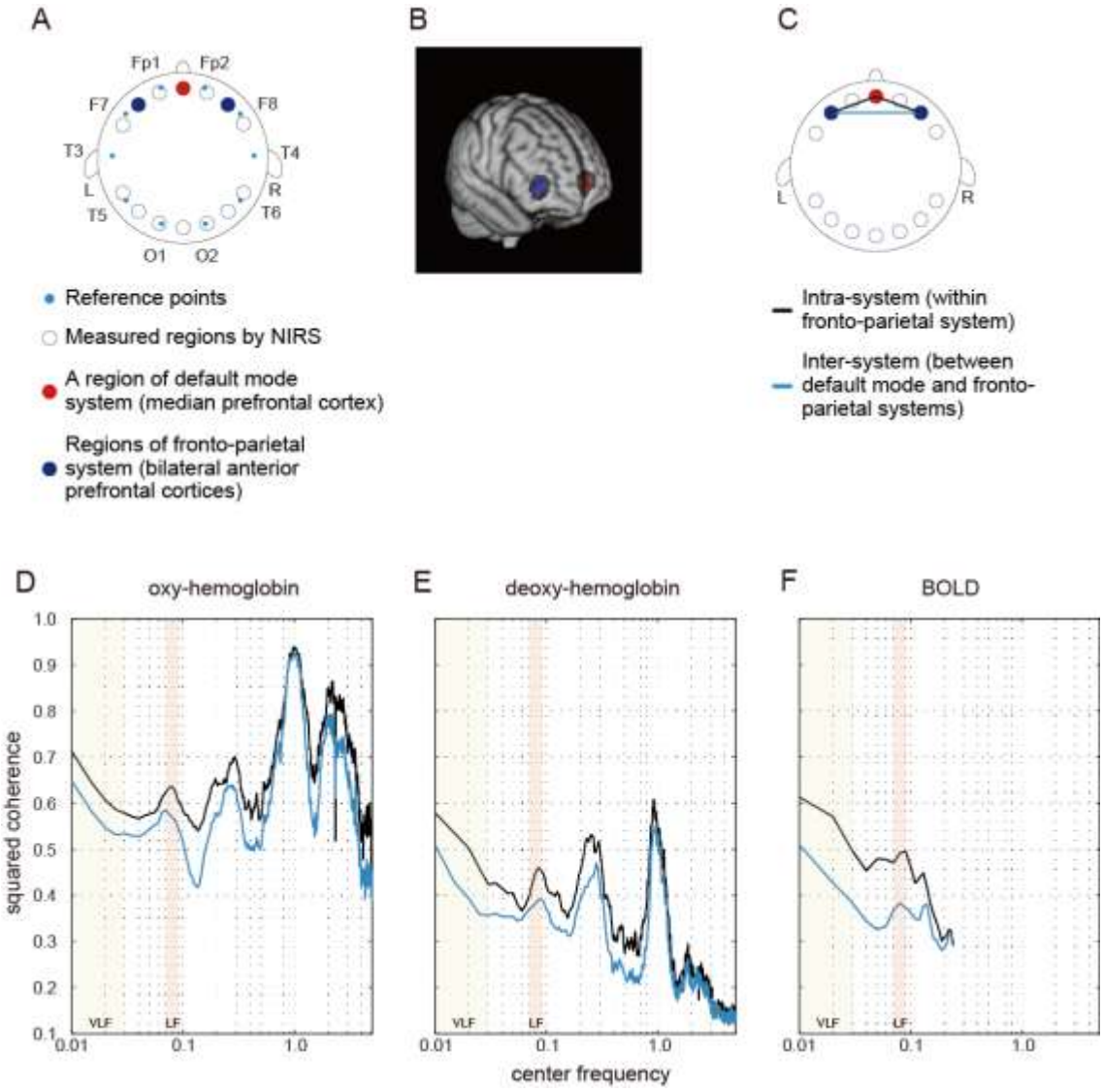

Figure 4.3. Coherence spectra estimated by using a simultaneously obtained NIRS data set. (A) I obtained NIRS signals at 14 cortical regions that are indicated as blue rings. Cyan dots represent standard reference points that are used in locating channels of electroencephalography on the scalp. In the previous study, I identified 14 cortical regions where NIRS signals were obtained in MNI spaces to determine ROI corresponding to each NIRS measurement region of each individual. For detailed methods of the identification and MNI coordinates, refer to Sasai et al., 2012. As a result, I found one cortical region (medial prefrontal cortex [mPFC]) included in the default mode system (red filled circle) and two bilateral cortical regions (left and right anterior prefrontal cortices [laPFC and raPFC]) contained in the fronto-parietal system (blue filled circles). (B) Voxels corresponding to measured regions by NIRS are shown. Colors are the same as those defined in (A). (C) While I calculated

coherence between laPFC and raPFC to investigate intra-system coherence spectrum (fronto-parietal system), I also estimated coherence between mPFC and laPFC and between mPFC and raPFC to examine inter-system coherence spectra (default-mode and fronto-parietal systems): Cyan line indicates intra-system pairs of ROI, while black lines represent inter-system pairs. (D, E) Coherence spectra of two NIRS signals (oxygenated [oxy-] hemoglobin and deoxygenated [deoxy-] hemoglobin) clearly had two peaks corresponding to typical frequency bands of respiratory fluctuations around 0.3 Hz and cardiac pulsations around 1 Hz. High coherences in VLF and LF could still be observed in the spectrum, supporting that higher coherences in these bands are not due to aliasing. (F) Coherence spectrum obtained by using fMRI signals extracted from ROIs corresponding to NIRS measurement regions (same as regions shown in B). I could confirm the high coherence values in VLF and LF in this spectrum, supporting that the characteristics of coherence spectrum could not be attributed to the difference in ROI locations between our current and previous studies.

4.3.2 Graph metrics of frequency-specific networks

To construct frequency-specific networks identified in VLF and LF in each individual data set ($\boldsymbol{I}_{\mathrm{VLF}}$ and $\boldsymbol{I}_{\mathrm{LF}}$), I applied five sparsity thresholds to two band-averaged coherence matrices, and I calculated graph theoretical metrics on the adjacency matrices, $\boldsymbol{A}$. I then conducted two-tailed *t*-tests against the null-hypothesis, which was defined as no group-level difference between $\boldsymbol{I}_{\mathrm{VLF}}$ and $\boldsymbol{I}_{\mathrm{LF}}$ in the calculated graph metrics. For all sparsity levels, graph metrics of segregation, including the mean normalized clustering coefficient, the mean local efficiency, and modularity obtained in $\boldsymbol{I}_{\mathrm{VLF}}$, were significantly higher as compared to values obtained in $\boldsymbol{I}_{\mathrm{LF}}$ ($p < 0.05$, FDR corrected; Fig. 4.4A–C), thus demonstrating that $\boldsymbol{I}_{\mathrm{VLF}}$ had a significantly higher capacity for information segregation than $\boldsymbol{I}_{\mathrm{LF}}$. On the other hand, no significant differences were found for global efficiency (measure of information integration) (Fig. 4.4D).

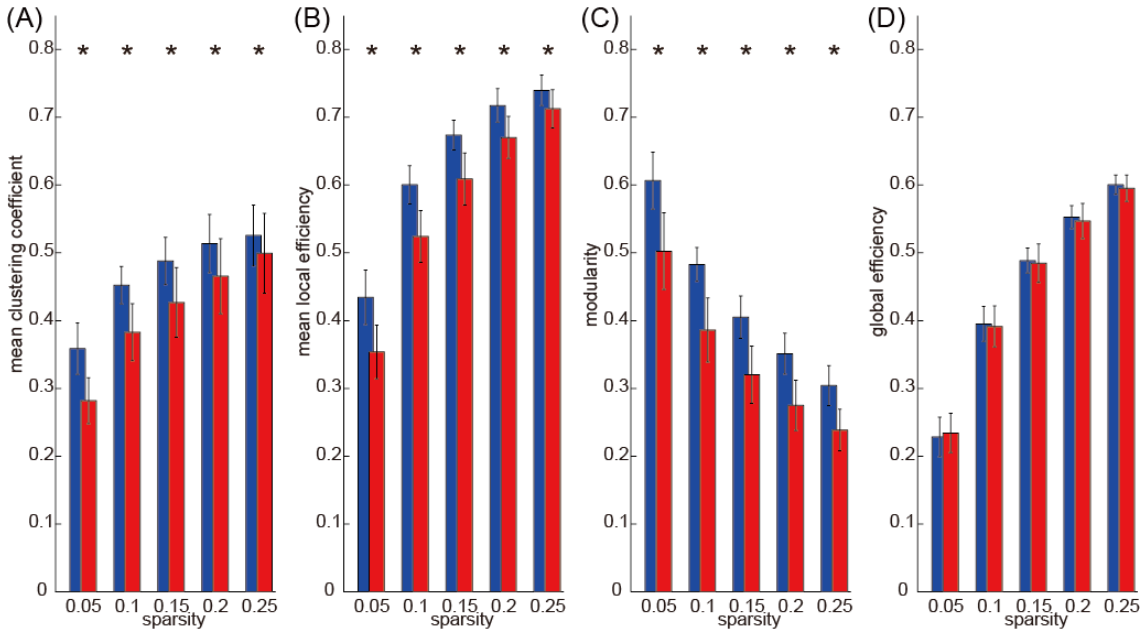

Figure 4.4. Graph metrics. I calculated the following four graph metrics in two frequency-specific networks (VLF and LF) estimated in each individual data set: (A) mean clustering coefficient, (B) mean local efficiency, (C) modularity, and (D) global efficiency. Blue bars represent the mean of each graph metric obtained, which was computed in networks estimated in the VLF, and red bars indicate the mean graph metric in the LF. In this study, I selected the sparsity of the brain networks (number of existing edges over the maximum possible number of edges) as threshold measurements. Because different threshold values may affect these graph metrics, I examined the between-group differences in these parameters over a wide range of threshold levels, 0.05–0.25. Asterisks indicate statistically significant differences between the metrics obtained in the VLFN and the LFN as tested by two-sampled *t*-tests ($p < 0.05$, FDR corrected).

4.3.3 Structure of segregation in frequency-specific networks

I applied a threshold to the consistent edge matrix, ***Ce***, by applying the sparsity thresholds, *S*, ranging from 0.05 to 0.25 in 0.05 increments in order to obtain group-level frequency-specific networks, $\boldsymbol{A^g}$, in both the VLF and LF range ($\boldsymbol{A^g}_{\mathrm{VLF}}$ and $\boldsymbol{A^g}_{\mathrm{LF}}$). It was only when I applied $S = 0.25$ as a threshold that both $\boldsymbol{A^g}_{\mathrm{VLF}}$ and $\boldsymbol{A^g}_{\mathrm{LF}}$ became a connected graph. Therefore, I conducted the following analyses using this sparsity threshold.

$\boldsymbol{A^g}_{\mathrm{VLF}}$ and $\boldsymbol{A^g}_{\mathrm{LF}}$ were visualized using a force-directed layout (Fig. 4.5 A, B). While the layout of $\boldsymbol{A^g}_{\mathrm{VLF}}$ showed three relatively segregated communities, $\boldsymbol{A^g}_{\mathrm{LF}}$ formed a centrally-condensed structure, supporting the result that $\boldsymbol{A^g}_{\mathrm{VLF}}$ has higher potentiality for information segregation than $\boldsymbol{A^g}_{\mathrm{LF}}$ (see Fig. 4.4). On the other hand, by detecting consistent community structures across participants for both networks (Fig. 4.5C, D), I found that both $\boldsymbol{A^g}_{\mathrm{VLF}}$ and $\boldsymbol{A^g}_{\mathrm{LF}}$ contained three highly similar communities. I found three specific pairs of communities that shared over 80% ROIs between $\boldsymbol{A^g}_{\mathrm{VLF}}$ and $\boldsymbol{A^g}_{\mathrm{LF}}$. Furthermore, ROIs in the three communities mainly included DMS, FPS, and COS, respectively. These findings suggest that while both $\boldsymbol{A^g}_{\mathrm{VLF}}$ and $\boldsymbol{A^g}_{\mathrm{LF}}$ consisted of three communities corresponding to functional systems, these communities were more strongly segregated in $\boldsymbol{A^g}_{\mathrm{VLF}}$ compared to $\boldsymbol{A^g}_{\mathrm{LF}}$.

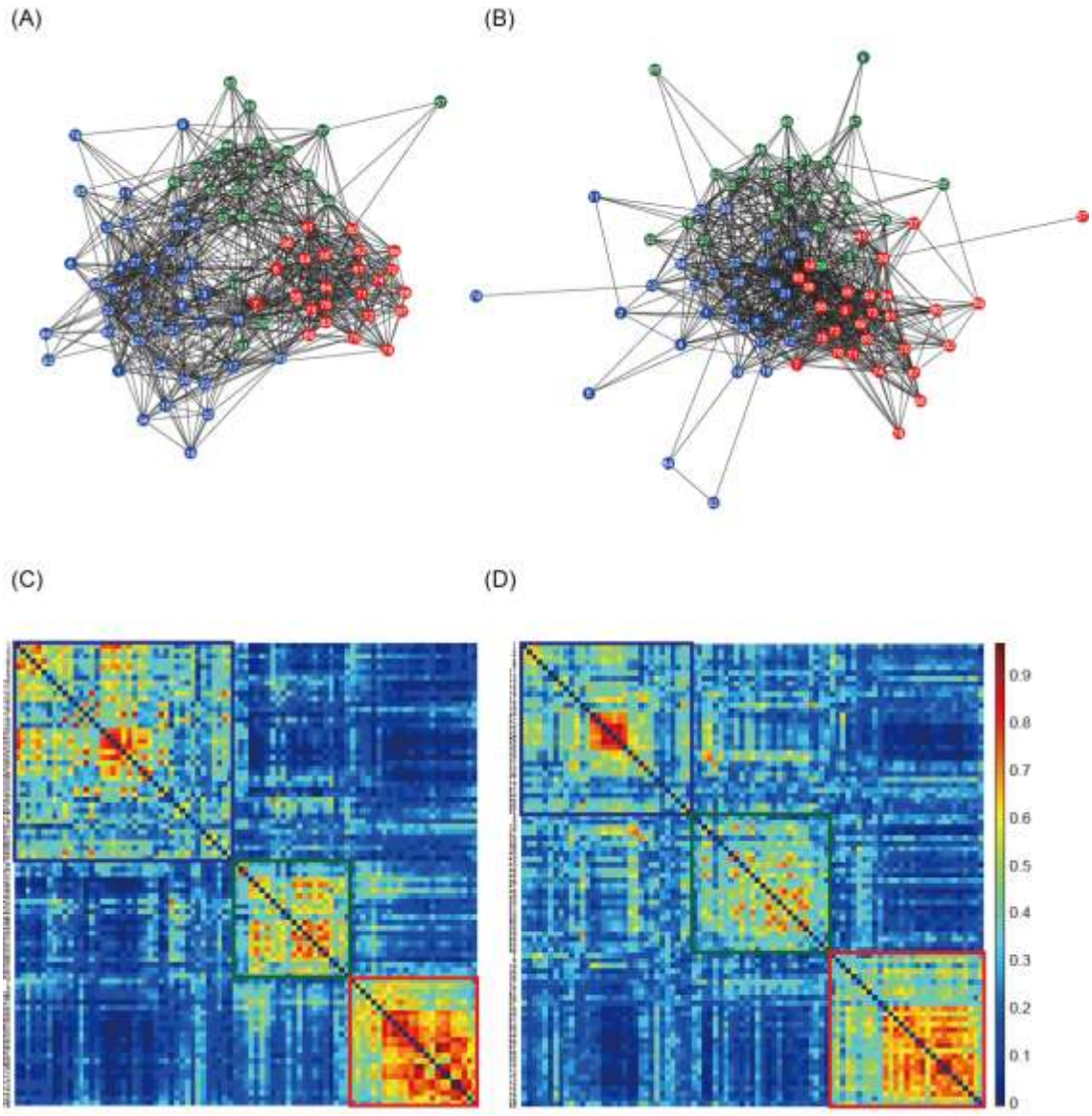

Figure 4.5. Force-directed layouts and consistent communities. (A, B) Fruchterman–Reingold force-directed projections showing frequency-specific connectivity in networks identified in the VLF and LF. Strongly interconnected nodes are demoted by their closer proximity to each other. The color of each node represents the assigned community detected from the consistent assignment matrix, ***Ca***. Three highly similar communities were detected in both networks of VLF and LF. ROIs in the three communities mainly included DMS (blue), FPS (green), and COS (red), respectively. While three segregated communities, which were densely interconnected to each other, appeared in (A), no such community was found in (B). (C, D) shows the consistent assignment matrices, ***Ca***, which were obtained in the VLF and LF. To emphasize the modular structures, both ***Ca*** were reordered by putting

the ROIs in the same module next to each other. By detecting communities in both matrices, three communities were found in the VLF and LF and surrounded by squares. The color of each square corresponds to the assigned community of each node in (A, B). Each of the three communities identified in a frequency band had a corresponding community detected in the other band. These correspondences are expressed by the color of the squares. Numbers described within nodes in force-directed layouts and along the matrices correspond to those in Table 4.1.

4.3.4 Structure of integration in frequency-specific networks

In order to identify hub regions in frequency-specific networks, nodal degrees and eigenvectors for $\boldsymbol{A}^{\boldsymbol{g}}{}_{\mathrm{VLF}}$ and $\boldsymbol{A}^{\boldsymbol{g}}{}_{\mathrm{LF}}$ were calculated (Fig. 4.6). In both metrics, I identified high degree and high centrality nodes with metrics greater than the network mean, plus one standard deviation (yellow bars in Fig. 4.6A–D). Hub regions were then defined as ROIs detected as both high degree and high centrality nodes (Table 4.2). While seven ROIs were identified as hubs for both $\boldsymbol{A}^{\boldsymbol{g}}{}_{\mathrm{VLF}}$ and $\boldsymbol{A}^{\boldsymbol{g}}{}_{\mathrm{LF}}$, all hubs except the one for the left dorsal anterior precuneus cortex (ldaPrCC, [AAL: Cingulum_Mid_L]) were different between $\boldsymbol{A}^{\boldsymbol{g}}{}_{\mathrm{VLF}}$ and $\boldsymbol{A}^{\boldsymbol{g}}{}_{\mathrm{LF}}$. While frequency-specific hubs in $\boldsymbol{A}^{\boldsymbol{g}}{}_{\mathrm{VLF}}$ were detected in the left superior medial frontal cortex, left supplementary motor area, left middle, and right anterior cingulate cortices, those in $\boldsymbol{A}^{\boldsymbol{g}}{}_{\mathrm{LF}}$ were identified in the left cuneus cortex, right precuneus cortex, and right thalamus.

Figures 4.6E and 4.6F show the rich-club coefficient curves obtained in both $\boldsymbol{A}^{\boldsymbol{g}}{}_{\mathrm{VLF}}$ and $\boldsymbol{A}^{\boldsymbol{g}}{}_{\mathrm{LF}}$. I found a range of k values showing significantly higher rich-club coefficients compared to those calculated in randomized topologies in both $\boldsymbol{A}^{\boldsymbol{g}}{}_{\mathrm{VLF}}$ and $\boldsymbol{A}^{\boldsymbol{g}}{}_{\mathrm{LF}}$. While the rich-club regime in $\boldsymbol{A}^{\boldsymbol{g}}{}_{\mathrm{VLF}}$ was $29 \leqq k \leqq 31$, it was $10 \leqq k \leqq 39$ in $\boldsymbol{A}^{\boldsymbol{g}}{}_{\mathrm{LF}}$. In the rich-club regime observed in each frequency band, I found a value of k whereby the rich-club organization in each frequency-specific network was formed by a detected hub region ($\underline{k} = 30$ for $\boldsymbol{A}^{\boldsymbol{g}}{}_{\mathrm{VLF}}$ and $k = 36$ for $\boldsymbol{A}^{\boldsymbol{g}}{}_{\mathrm{LF}}$), demonstrating that significantly dense

interconnections exist among hubs in each frequency-specific network.

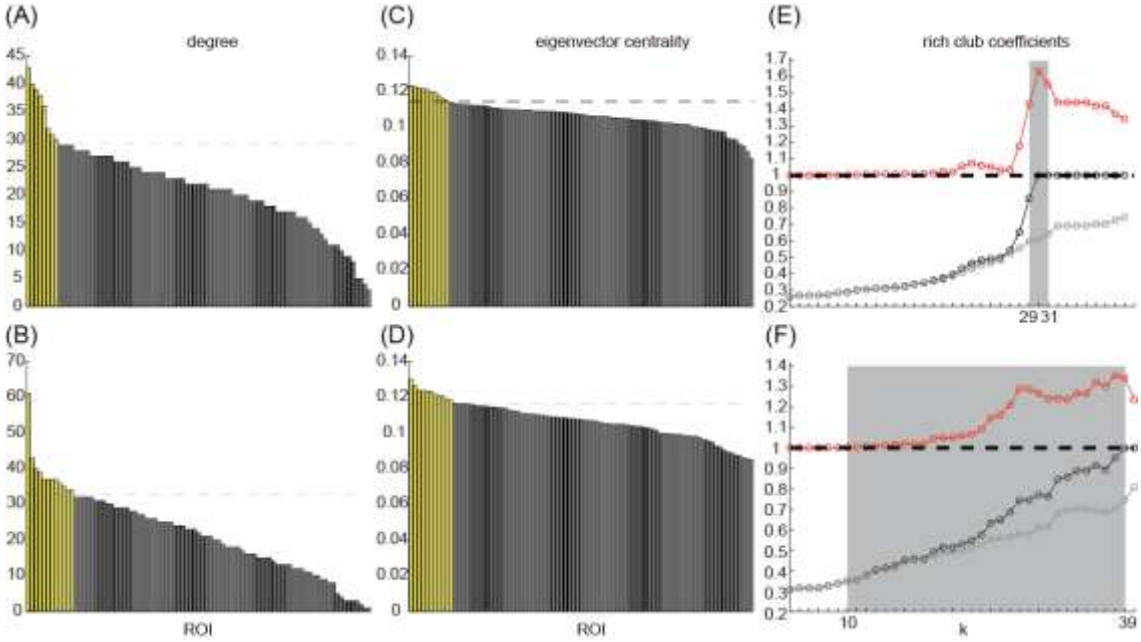

Figure 4.6. Degree, eigenvector centrality, and rich-club coefficients. Degrees and eigenvector centralities of all nodes were calculated in the group-level network estimated in the VLF and LF. (A) shows the distribution of degrees estimated in the VLF, and (B) shows the distribution of degrees estimated in the LF. (C) corresponds to the distribution of eigenvector centrality estimated in the VLF, and (D) corresponds to the distribution of eigenvector centrality estimated in the LF. Dashed lines express the mean plus one standard deviation. Also, rich-club coefficients in group-level frequency-specific networks were calculated (see 'Rich-club detection'). Black curves correspond to $\Phi(k)$, gray curves corresponds to $\Phi_{meanrand}(k)$, and red curves corresponds to $\Phi_{normalized}(k)$. In both (E) and (F), there was a tendency for $\Phi(k)$ to increase with k at a higher rate than $\Phi_{meanrand}(k)$. Ranges of k, where $\Phi(k)$ became significantly higher than $\Phi_{meanrand}(k)$, are highlighted by a gray background.

Table 4.2 List of hubs identified in 2 frequency-specific networks

VLF				LF			
No	k	eigenvector	AAL	No	k	eigenvector	AAL
41	1	6	Frontal_Sup_Medial_L	**16**	1	1	Cingulum_Mid_L
16	2	4	Cingulum_Mid_L	**80**	2	4	Precuneus_R
7	3	10	Cingulum_Ant_R	**33**	3	3	Cuneus_L
58	4	1	Cingulum_Mid_L	**72**	4	4	Thalamus_R
8	5	9	Cingulum_Ant_R	**24**	5	2	Precuneus_R
64	6	4	Supp_Motor_Area_L	**75**	5	7	Thalamus_R
63	7	2	Cingulum_Mid_L	**29**	5	9	Precuneus_R
45	8		Frontal_Mid_R	69	5		Putamen_R
24		3	Precuneus_R	22	9		Precuneus_R
61		7	Cingulum_Mid_R	36	10		Frontal_Mid_L
23		8	Precuneus_L	5	11		Cingulum_Ant_L
				14	12		Cingulum_Mid_R
				71		6	Thalamus_L
				26		8	Cuneus_L
				63		10	Cingulum_Mid_L
				23		11	Precuneus_L

The hubs identified in each network are shown. To identify hub regions, we calculated the group means of the coherence values and the estimated group-averaged VLFN and LFN. We selected a sparsity of 0.25 as the threshold value because all networks become connected in graphs only using this value. Then, a hub was defined as a node satisfying the following 2 conditions: 1) its nodal degree was higher than the mean plus the standard deviation of the degree distribution; and 2) its eigenvector centrality that was measured in a weighted nonthresholded network was higher than the mean plus the standard deviation of the distribution of the centrality. In column No, identified hubs are listed in boldface. The numbers in column k and the eigenvector indicate the ranks of the nodes for the above 2 conditions, respectively. Anatomical labels obtained from AAL are listed in column AAL.

Anatomical perspectives of hub regions in both networks are shown in Figures 4.7A and 4.7B. While many ROIs have functional connectivity with hub regions in each network, among the hubs there were dense interconnections, referred to as 'rich-club connections' in the figure. This finding demonstrates that while there is no significant difference regarding global efficiency between the two frequency-specific networks, their structures contributing to information integration consisted of distinct sets of functional brain hubs that formed different rich-club organizations.

While hub regions in the VLF mainly contained areas of the anterior cingulate and superior medial frontal cortices, those in the LF consisted of the precuneus cortex and thalamus. In order to investigate if this difference was specific to the relationship between VLF and LF, I identified hub regions within typical frequency bands used for the studies of functional connectivity (0.01–0.10 Hz) and within three frequency bands (bandwidth: 0.02 Hz) that were located within 0.01–0.11 Hz without overlapping with VLF and LF (0.03–0.05, 0.05–0.07, and 0.09–0.11 Hz) (Fig. 4.7C). Within 0.01–0.10 Hz, I observed hub regions located in the anterior and posterior cingulate cortices and thalamus,

providing support to the fact that network characteristics of integration in VLF and LF coexist in the network obtained in the wide frequency band. I found that hub regions identified in the frequency bands higher than 0.05 Hz mainly, and consistently, included ROIs in the precuneus cortex and thalamus, thus supporting the notion that hub regions in the LF reflect the representative integration architecture at this frequency range. On the other hand, the VLF was the only frequency band where hubs mainly consisted of medial frontal regions. In the frequency band between 0.03 Hz and 0.05 Hz, which was located between VLF and frequency ranges over 0.05 Hz, hub regions were identified in both the medial frontal and parietal regions. The network topology of this frequency band may reflect characteristics of information processing of both networks estimated in the VLF and LF (Fig. 4.7C).

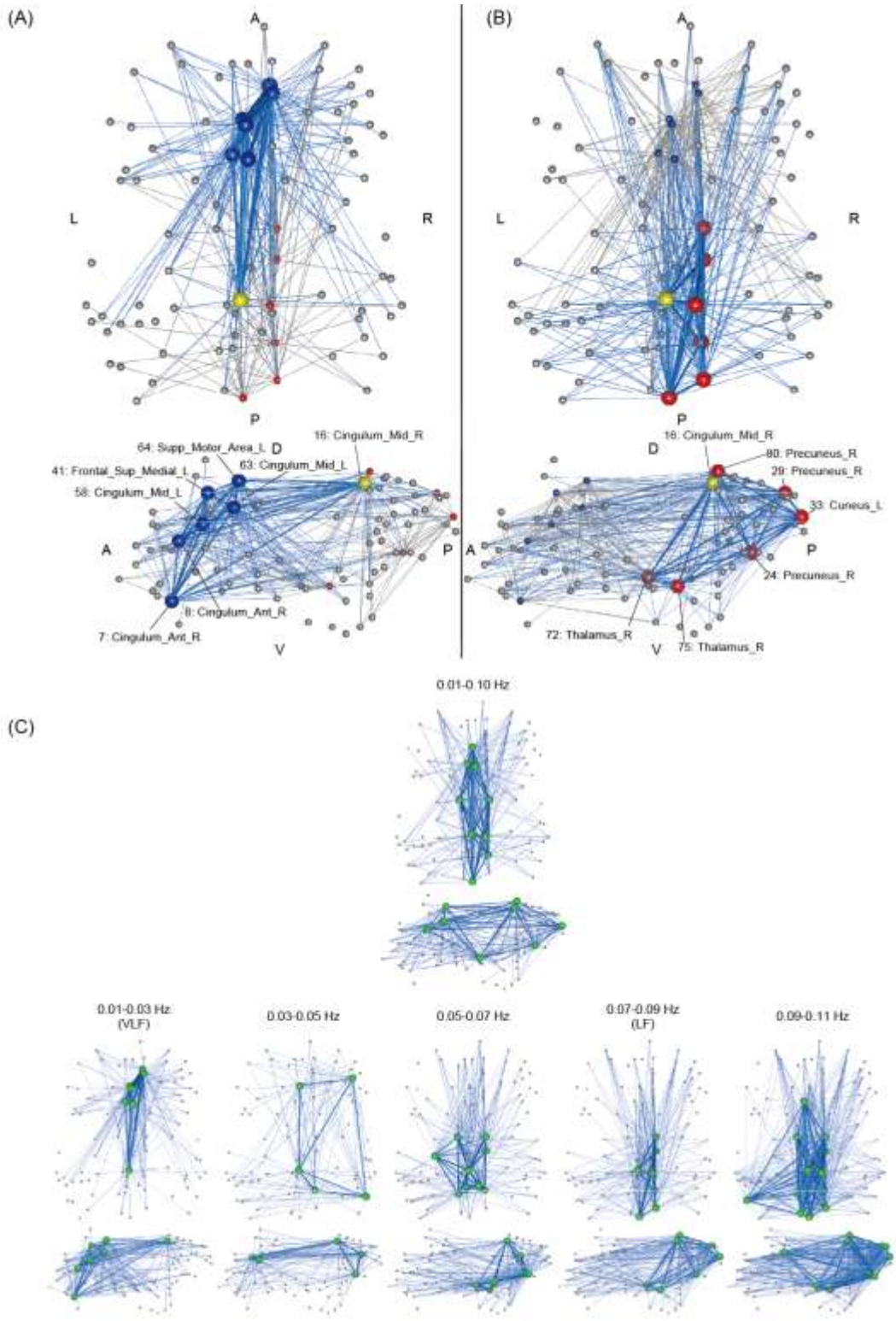

Figure 4.7. Anatomical perspective of hub regions. Hub regions in frequency-specific networks were the seven highest degree nodes in each frequency band (A, B). The yellow node is a hub that is

consistently identified in both the VLF and LF. The blue nodes are hubs identified only in the VLF, and the red nodes are those identified only in the LF. Hubs are represented by big spheres. While blue lines indicate functional connectivity with hubs within the frequency band, gray lines represent functional connectivity with hubs within the other band. When k = 30 for $\boldsymbol{G}_{\mathrm{VLF}}$ and k = 30 for $\boldsymbol{G}_{\mathrm{LF}}$ are selected, rich-club organizations are formed with hub regions. Bold lines indicate connections among rich-club nodes, showing dense interconnection. The numbers correspond to those in Table 4.1. Anatomical labels were selected using AAL. The abbreviations represent the direction in the brain: A, anterior; P, posterior; L, left; R, right; D, dorsal; V, ventral. (C) Hub regions identified within the three narrow frequency bands located within 0.01–0.11 Hz and without overlapping with the VLF and LF (0.03–0.05, 0.05–0.07, and 0.09–0.11 Hz). All hub nodes are represented with green-colored, big spheres. The attributes of the lines are the same as described above.

4.3.5 Regional variability of power spectra

The amount of VLF and LF components for all hub ROIs was calculated. Figure 4.8A shows the average power spectrum among all participants' data sets. As a result, one thalamic hub (No. 72 in Table 4.1) had a relatively higher amount of LF components compared to all other hub regions. This is consistent with the previously reported regional variability of power spectrum of the whole brain fMRI signals obtained during rest (Baria et al., 2011; Zuo et al., 2010a). I then investigated if there was a significant difference between the average powers of cortical hubs and those of subcortical hubs within the LF. I obtained group-means of powers in the LF for both cortical and subcortical hubs. By conducting two-tailed *t*-tests over subjects against the null hypothesis, which was defined as no difference of powers between cortical and subcortical hubs, I confirmed that subcortical hubs had significantly higher amounts of LF components compared to cortical hubs (Fig. 4.8B).

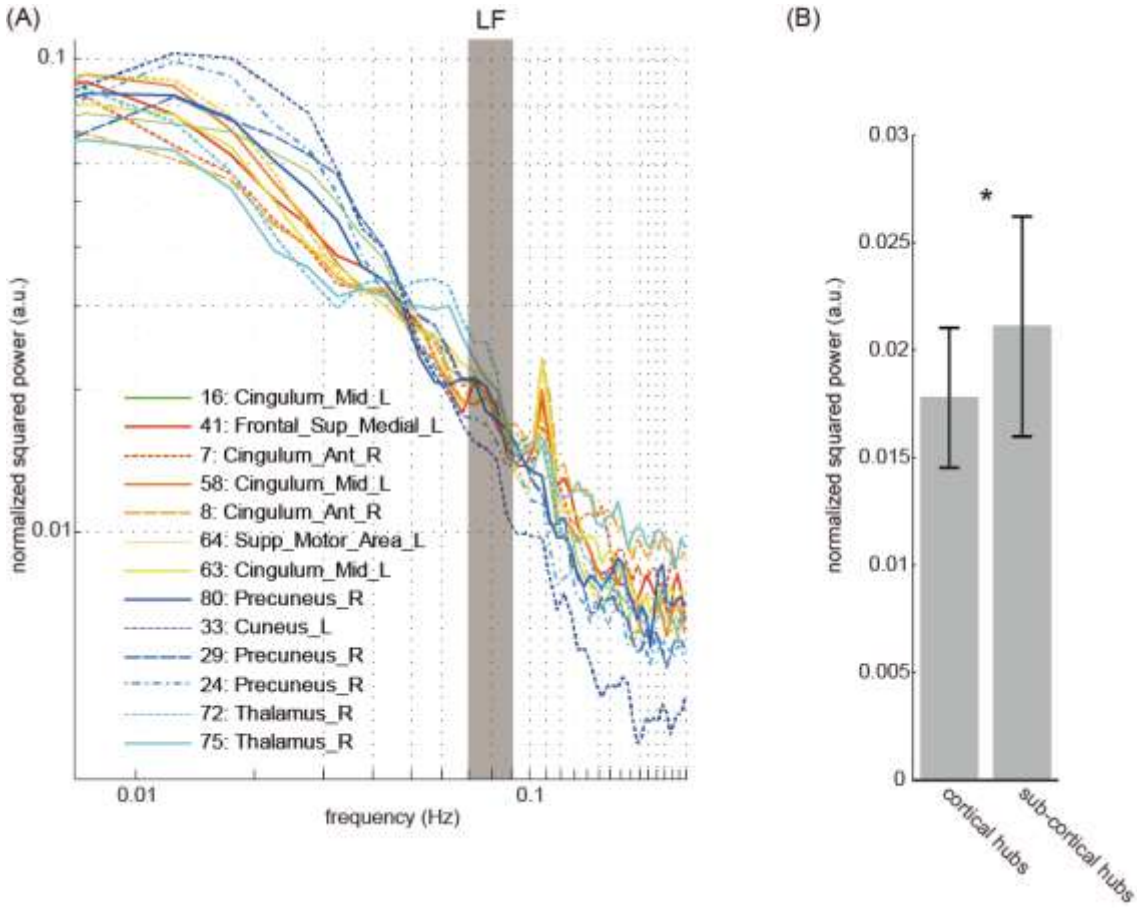

Figure 4.8. Power spectra of hub regions. (A) Normalized power spectra (i.e., power spectral density) of spontaneous fMRI signals extracted from 13 hub regions. The color of curves indicate the categories of the hubs: green, a hub detected in both the VLF and LF band; red to yellow, hubs only in the VLF band; blue to cyan, hubs only in the LF band. The numbers correspond to those in Table 4.1. Anatomical labels were selected using AAL. One thalamic hub showed the highest amount of power density within the LF band (a shaded region). (B) Differences between the cortical and subcortical hubs in averaged powers within the LF band. In each individual data set, I averaged the power spectrum within the LF band for each hub. These mean powers of the LF were further averaged within two groups of hubs: (1) cortical hubs consisting of 11 ROIs (No. 7, 8, 16, 24, 29, 33, 41, 58, 63, 64, and 80 in Table 4.1), and (2) subcortical (thalamic) hubs consisting of 2 ROIs (No. 72 and 75 in Table 4.1). By conducting two-tailed *t*-tests over subjects against the null hypothesis, which was defined as no difference of powers between cortical and subcortical hubs, I found that subcortical hubs had significantly higher amounts of LF components compared to cortical hubs. Gray bars correspond to the population averages of LF powers of these two hub groups. Error bars express standard deviations. The asterisk indicates a statistically significant difference ($p = 0.0014$).

4.4 Discussion

In this study, I investigated frequency-specificity of functional network architecture contributing to information segregation and integration. By calculating coherence among all pairs of ROIs, I found two frequency bands within 0.01–0.10 Hz, VLF and LF, where coherence was higher than other frequency bands (Fig. 4.2). While graph theoretical metrics showed that the network estimated in the VLF had a higher degree of segregation than that in the LF (Fig. 4.4A-C), no difference was found regarding measurement for integration (Fig. 4.4D). While force-directed layout of frequency-specific network estimated in the VLF showed more segregated community structures than that in the LF, both frequency-specific networks could be decomposed into the highly similar set of communities corresponding to three functional brain systems (DMS, FPS, and COS) (Fig. 4.5). This indicates that while networks in the VLF and LF consisted of the same community sets, these communities were more functionally segregated in the VLF compared to the LF. Furthermore, by identifying hub regions in each frequency-specific network, I observed that hub regions were different between all frequency bands except for one region, the left dorsal anterior precuneus cortex (Table 4.2), thus supporting the notion that there are at least two distinct sets of functional hubs depending on the time scale of brain activities. Collectively, our findings demonstrate spontaneous fMRI signal fluctuations in two different frequency bands organized into large-scale networks with distinct topologies for information segregation and integration.

Spontaneous hemodynamic signals include not only fluctuations by spontaneous neural activity but also those generated by physiological signals like respiratory and cardiac pulsations. By using NIRS, it has been demonstrated that respiratory and cardiac pulsations have typical frequencies (0.3 Hz and 1 Hz) and dominate in these frequency bands in the power spectrum (Obrig et al., 2000).

Importantly, it has also been shown that there are two other frequency bands corresponding to VLF and LF (0.01–0.03 Hz and 0.06–0.08 Hz), where coherence values estimated by signal fluctuations of oxygenated hemoglobin concentration are higher than those values in other frequency regions within 0.01–0.10 Hz (Sasai et al., 2011). This result was reconstructed by using both signals of oxygenated and deoxygenated hemoglobin concentration changes from simultaneously obtained fMRI data analyzed in the current study (Fig. 4.3). These results demonstrate the following two facts: (1) high coherence in VLF and LF is not due to aliasing of physiological signals in higher frequency regions; (2) high coherence in the VLF and LF can be consistently observed by different measurement modalities of hemodynamic signals, that is, fMRI and NIRS. Moreover, I conducted additional spectrum analysis on public resting state fMRI data sets and ensured that these characteristics of coherence spectrum represent a universal nature of resting state fMRI signals (Fig. 4.S1). These results support that high coherences in the VLF and LF of fMRI signals reflect coherent spontaneous neural activities.

In analyzing the brain from the view of graph theory, the minimal node is defined as each voxel in the MRI data set. Although there are some studies constructing voxel-based networks of the brain (Buckner et al., 2009; Cecchi et al., 2007; Eguíluz et al., 2005; Hayasaka et al., 2010; van den Heuvel et al., 2008b), this method is computationally demanding. To reduce the volume of MRI data sets, nodes are determined in larger spatial scales as ROIs. ROIs are generally determined by referring to the boundary of brain regions that are activated by a specific category of tasks (Deshpande et al., 2011; Dosenbach et al., 2007, 2010; Power et al., 2011; Spreng et al., 2013) or defined as anatomically separate regions (Achard et al., 2006; Bassett et al., 2008; Hagmann et al., 2008; Salvador et al., 2005a, 2005b, 2007, 2008). However, to obtain an accurate description of FCN, the ROIs should be selected to

represent underlying functional areas of the brain (Butts, 2009; Dosenbach et al., 2010). Therefore, I selected nodes as ROIs defined by meta-analysis on several task-activation studies in order to ensure the reliability on the functional uniformity of voxels within ROIs (Dosenbach et al., 2010). The variability of selections of ROIs can cause inconsistency in the results of the network topology. However, hubs and rich-clubs identified in the present study (0.01–0.10 Hz; see Fig. 4.7C) are located in similar brain regions that have been repeatedly reported by previous studies using different ROI definitions (see Achard et al., 2006; Buckner et al., 2009; Spreng et al., 2013; Tomasi and Volkow, 2011a,b; van den Heuvel et al., 2008b for hub; see van den Heuvel and Sporns, 2011 for rich-club). I observed the consistent community assignment with those reported in other studies using distinct ROI sets (Dosenbach et al., 2007; Power et al., 2011; Spreng et al., 2013) as well as the study using the same ROIs (Dosenbach et al., 2010). Collectively, it is likely that all of our findings did not depend on our selection of ROI.

All hubs observed in this study were part of the structural hubs forming rich-club organizations (van den Heuvel and Sporns, 2011). While I observed the similar hub regions to those reported in van den Heuvel and Sporns (2011) within FCN constructed from fMRI signals fluctuating in 0.01–0.10 Hz (Fig. 4.7C), hubs in FCNs differed in a frequency-dependent manner within FCNs of VLF and LF (Fig. 4.7A, B). This is consistent with the result of a computational study demonstrating that while the topology of a FCN is shaped by the underlying anatomical structure, it contains rich temporal structures at multiple time scales (Honey et al., 2007). Cortico-cortical functional connectivity can be mediated by both cortico-cortical connections and cortico-thalamo-cortical loops. Wu et al. (2008) showed that while correlations among cortical ROIs that form these functional systems are concentrated around the VLF (0.01–0.06 Hz), connections within the subcortical networks are

distributed over a wider frequency range (0.01–0.14 Hz). Furthermore, using diffusion tensor imaging (DTI), cortico-cortical structural connections have been observed among the brain regions constituting each functional system focused in this study (Greicius et al., 2009; van den Heuvel et al., 2009). Although it has been shown by DTI that distinct subregions of the thalamus have distinct cortical projections (Behrens et al. 2003; Zhang et al., 2010a), there is no direct evidence of cortico-thalamo-cortical loops that specifically exist within each functional system. Therefore, it is likely that the existence of a community is reflective of the fact that the network topology is more strongly shaped by cortico-cortical connections than cortico-thalamo-cortical loops. Considering that the network architecture in the VLF had clearly segregated communities corresponding to three functional systems, DMS, FPS, and COS, the network topology in the VLF is strongly constrained by cortico-cortical connections.

Segregation in the LF was significantly lower compared to the VLF, suggesting that network topology in this frequency range was less constrained by cortico-cortical connections. Hubs in the LF included the thalamus, which has direct structural connections with various regions of the cerebral cortex, and may mediate cortico-cortical communications through thalamic relays (Guillery and Sherman, 2002). Because some neurons in the thalamus act in the faster frequency band than those in the cerebral cortex (Jones et al., 2002), these neurons can provide a coherent oscillatory bias that may facilitate long-range cortico-cortical interactions (Alkire et al., 2008). This electrophysiological observation is consistent with our result that one thalamic hub included a higher amount of squared power within the LF compared to other cortical hubs, suggesting that network topology in the LF reflects coherence mediated by cortico-thalamo-cortical loops. In the current study, ROIs were determined by referring to coordinates published by Dosenbach et al. (2010) and were constructed as

12 mm diameter spheres centered at the coordinates. However, different thalamic regions have functional connectivity connecting to different cerebral cortices (Zhang et al., 2010a). Therefore, further investigation of hub location within the thalamus will determine the thalamic nuclei playing a role in the hub of FCN.

Several studies have demonstrated that three functional systems, corresponding to segregated communities within the VLF band, do not function independently but establish context-dependent interaction in order to operate multiple cognitive functions. For example, the task-positive systems, including FPS and COS, and the task-negative system, corresponding to DMS, show anti-correlation during externally focused goal-directed tasks and resting state (Fox et al., 2005; Fransson, 2005; Gao and Lin, 2012). In contrast, positive correlation between task-positive and task-negative systems has also been found during specific tasks (Bluhm et al., 2011; Christoff et al., 2009; Leech et al., 2011; Sadaghiani et al., 2009; Simons et al., 2008; Spreng et al., 2010). Because frontal insula and anterior cingulate cortices showed not only rapid activations related to the onset of the task but also activations sustained for the duration of a task block (minimum task period length is 85 s), these regions may contribute to the establishment and maintenance of context-dependent relationships (Dosenbach et al., 2006). Meanwhile, the anterior cingulate cortex reacts to stimuli more slowly than the frontal insula cortex, but more rapidly than regions within the DMS and FPS, and is causally influenced by the frontal insula cortex independent of context (Sridharan et al., 2008). From this result, Sridharan et al. (2008) hypothesized that the frontal insula cortex initiates appropriate control signals to engage the anterior cingulate cortex and the fronto-parietal system in task-related information processing. Interestingly, the present study revealed that several regions in the anterior cingulate cortices, but not the frontal insula cortex, were hubs in the VLF. Thus, we consider that this

network topology in the VLF can subserve information propagation to maintain the relationship among task-positive and task-negative systems. Clarifying this mechanism is open to future studies.

Experimental investigations of neural correlates of consciousness (NCC) can be categorized into two different approaches: 1) studying contents of consciousness and 2) studying levels of consciousness (Hohwy, 2009). In studies regarding contents of consciousness, NCC is defined as the minimally sufficient condition to generate a conscious perception, such as a color or a face. On the other hand, NCC is identified as the correlation between changes of conscious states and those of neural phenomena in the second approach (i.e. studying NCC by focusing on levels of consciousness). NCC is also thought to be a single dynamic entity endowed with a large number of discriminable states (Alkire et al., 2008). Some studies have shown evidences that the level of consciousness has correlates with the network properties of functional connectivity. For example, impaired consciousness during non rapid eye movement (NREM) sleep is associated with a higher degree of segregation among different functional systems (Boly et al. 2012). Furthermore, the functional connectivity of thalamus, posterior cingulate cortex, and precuneus is reduced during impaired consciousness due to vegetative state, anesthesia, and deep sleep (Boveroux et al. 2010; Horovitz et al., 2009; Laureys et al., 2000; Vanhaudenhuyse et al., 2010). Considering that LF, but not VLF, includes typical hemodynamic timescales to a single event (10–20 s), functional connectivity in the LF may reflect transient coherence that is well suited to generate dynamic integration among different brain regions. Therefore, the investigation of topological property of the frequency-specific network in the LF may provide a clue to understand the issue of consciousness.

There are two limitations in the method used in our study. First, non-neural fluctuations included in hemodynamic signals may affect the current results. It has been demonstrated that

hemodynamic signals included signal fluctuations due to non-neural physiological origins such as respiratory and cardiac pulsations (Bhattacharyya and Lowe, 2004; Lowe et al., 1998), changes of respiratory and cardiac rates (Birn et al., 2006; Shmueli et al., 2007; Wise et al., 2004), blood pressure (Katura et al., 2006), changing of vascular tone for cerebral autoregulation (Lagopoulos et al., 2006), and vasomotion (Aalkjaer et al., 2011). The coherence due to the respiratory and cardiac pulsations had peaks out of 0.01–0.10 Hz ([respiratory: ~0.3 Hz] and [cardiac: ~1Hz]) (Fig. 4.3D, E). Because the sampling rate of fMRI is not sufficiently high, the functional connectivity can be biased by aliasing of these confounds with higher frequency. On the other hand, usage of NIRS, whose sampling rate is 10 Hz, revealed that frequency characteristics of functional connectivity is not due to aliasing of the noises. However, the frequency ranges of some of these non-neural fluctuations, such as changes of respiratory and cardiac rates, blood pressure, and vasomotion are included in hemodynamic signals fluctuating within 0.01–0.10 Hz. Moreover, it is possible that signal fluctuations by these non-neural tissues are contained uniformly in the gray matter voxels (Desjardins et al., 2001; Greicius et al., 2003; Macey et al., 2004). To avoid the bias in the estimation of functional connectivity due to the physiological confounds, there are many methods to remove these confounds by using simultaneously recorded physiological data with fMRI signals (Glover et al., 2000) and/or by exploiting inherent information in the resting state fMRI data (Anderson et al., 2011; Chai et al., 2012; Chang and Glover, 2009; Fox et al., 2005). In this study, I used one method called PSTCor, which uses only resting state fMRI data sets for correction, in order to factor out non-neural fluctuations for increasing confidence in the results of functional connectivity (Anderson et al., 2011). However, although using the method for physiological correction can suppress the over-estimation of functional connectivity, it may cause under-estimation in turn because variations in physiological regulations may be correlated with neural activities (Murphy et

al., 2013). For example, emotional arousal and activity levels of the autonomic nervous system are indicated by the variability of heart rate (Macefield, 2009). Furthermore, it has been still unclear if there are regionally specific physiological confounds or not. Because the above-mentioned corrections cannot treat such signals, other correction methods will be required. Moreover, with comparison to other physiological confounds, the contribution of vasomotion on hemodynamic signals is still poorly understood (Murphy et al., 2013). For example, it is still contested as to whether or not vasomotion has an effect on hemodynamics independently of other physiological origins (Morita-Tsuzuki et al., 1992; Biswal and Kannurpatti, 2009; Hudetz et al., 1998). Further studies of the relationship between physiology and hemodynamic signals are of importance to ensure certainty of the results of functional connectivity.

Second, I should also be careful to the stationarity of the functional connectivity. Although most of the studies in functional connectivity collect 5–11 min of resting state fMRI data, some studies have reported that there are non-stationary characteristics in functional connectivity used by the similar length of resting state data sets (Chang and Glover, 2010; Hutchison et al., in press). To characterize the length of time that is required to acquire reproducible functional connectivity measurements, much effort has been focused on test-retest reproducibility of the functional connectivity map. Earlier studies showed that the strength of functional connectivity becomes stable by using data sets longer than 7 min (Braun et al., 2012; Li et al., 2012; Shehzad et al., 2009; Thomason et al., 2011; Van Dijk et al., 2010). However, recent investigation into this issue with longer scan length (27 min), as compared to previous studies, demonstrated that improvements of the test-retest reliability plateaued around 12–16 min for intra-session comparisons and 8–12 min for inter-session comparisons (Birn et al., in press). Therefore, to estimate reliable results by averaging the non-stationarity of functional connectivity, I need to

acquire resting state data longer than 16 min. Because 20 min resting state data was used to calculate functional connectivity in the current study, I could derive our results without being disturbed by non-stationarity. However, it should be noted that although the highest test-retest reliabilities can be provided by scan length, the degree of reliability of inter-session variability is lower than that of intra-session variability (Birn et al., in press). Considering the fact that the brain has a dynamic, condition-dependent nature (Hutchison et al., 2013; Rabinovich et al., 2012; von der Malsburg et al., 2010), this result seems rather natural. Further investigation into the state-dependency of functional connectivity will provide more insight in handling the variability of functional connectivity.

To determine functional connectivity from correlation and coherence matrices, I must threshold these matrices. While I applied thresholds to correlation and coherence matrices by using a correlation and coherence value (> 0.6) in Study 1, where functional connectivity was studied by using NIRS (see Chapter 2), I also applied thresholds to coherence matrices by using several sparsity thresholds, *S*s, which ensured that coherence values corresponding to functional connectivity detected by all different *S*s were significantly higher than 0 in the current study. In this study, I found that, while consistent differences on graph metrics between frequency-specific networks constructed from VLF and LF of fMRI signals were provided by all *S*s, hubs were also detected in consistent regions by using different *S*s values (data not shown). On the other hand, only one threshold value was used in Study 1. Considering the results from the current study, the selection of the threshold value may not affect the relative difference of network topology for segregation and integration between frequency-specific networks obtained from VLF and LF of NIRS signals, although applying thresholds can change the network structure itself (see Fig. 2.2).

Theoretical views on the anatomical wiring of the brain portray the basic idea that the brain

has fundamental characteristics of reconciling apparently opposing demands of local segregation and global integration of information in order to generate brain function (Felleman and Van Essen, 1991; Tononi et al., 1994). Until now, this attribute has also been demonstrated to exist in the network structure of functional brain organization (Sporns, 2013). Meanwhile, our results suggest that the spatial order of the brain can vary by measuring it with different time scales. Indeed, I demonstrated the co-existence of two functional brain organizations in a frequency-dependent manner. Because different network topologies may contribute to different brain functions, the present study promotes further investigation into the relationship between frequency-specific network topologies and the time scales of human behavior.

4.5 Supplementary material

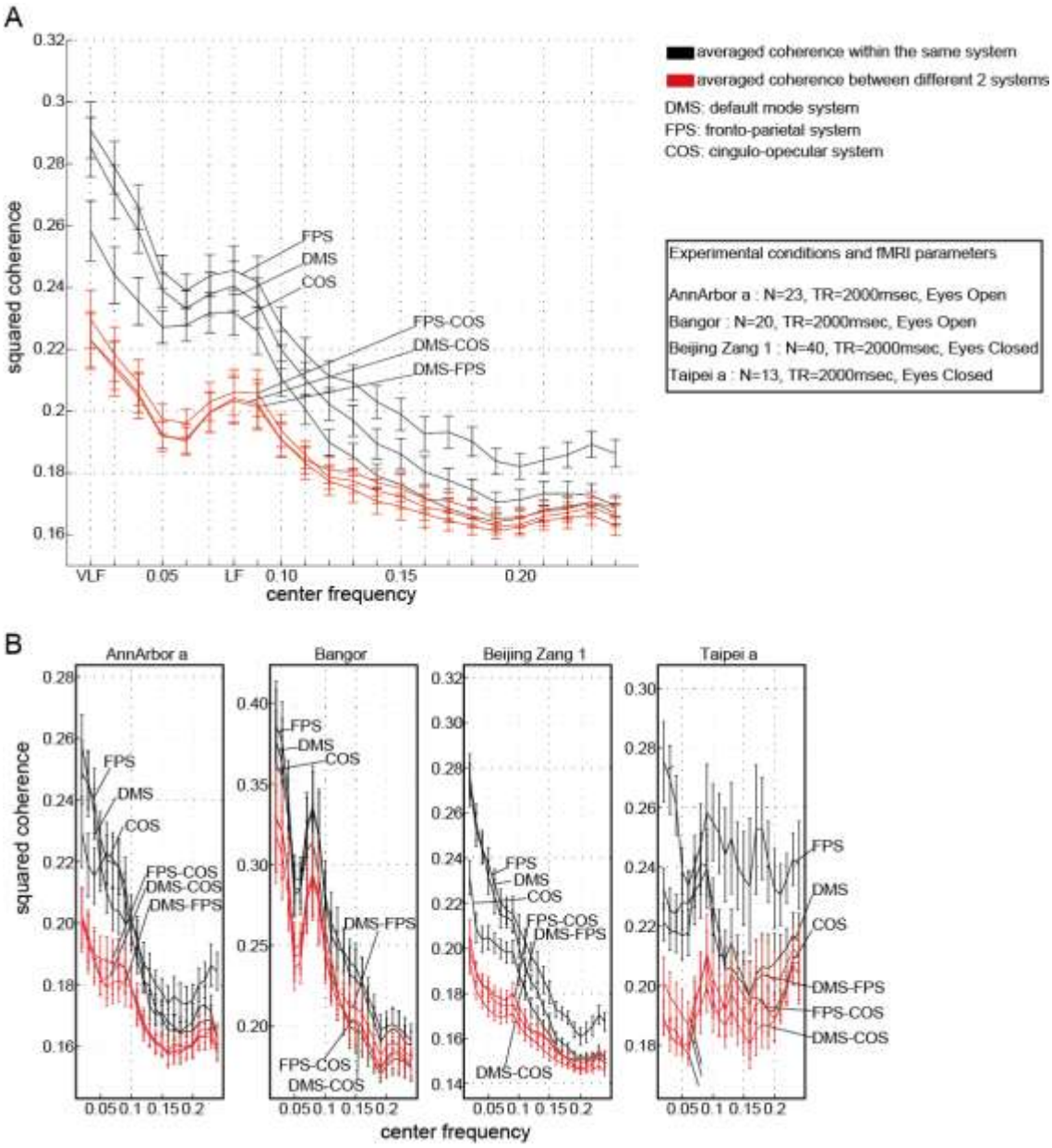

Figure 4.S1. Coherence spectra estimated by using public data sets provided by the 1,000 Functional Connectome Project. From the pool of resting state fMRI data, I selected four data sets that were obtained under similar conditions to our data set. The names of the data sets are AnnArbor_a, Bangor, Beijing_Zang, and Taipei_a. Experimental conditions and a part of fMRI parameters that may be influential on the estimation of coherence spectra are summarized in a box in the figure. Because only

Beijing_Zang had a large number of subjects compared to the other three data sets and was separated into five files in the data pool, I used the first file of Beijing_Zang, where the number of subjects was 40, and referred to it as Beijing_Zang_1. For these four data sets, I conducted the same preprocessing and signal extraction with the same ROI sets and ROI-by-ROI coherence analysis in order to investigate if characteristics of coherence spectra observed in our data set could be consistently found in other data sets. (A) By averaging coherence spectra obtained in the four data sets, I confirmed that the coherence values in VLF and LF were higher than those values in other frequency ranges. (B) Coherence spectra in each data set.

Chapter 5 General discussion

5. 1 Scientific breakthrough

5.1.1 Topology of the functional connectivity network varies with the time scale of brain activity

In Study 1 and Study 3, the relationship between the time scales of brain activity and spatial characteristics of functional connectivity was investigated by measuring hemodynamic fluctuations by using NIRS and fMRI. First, in Study 1, by taking advantage of higher temporal resolution of NIRS as compared to fMRI, frequency-specific characteristics were examined on the functional connectivity among bilateral frontal, temporal, and occipital cortical regions. As a result, functional connectivity between bilateral homologous cortical regions was found within 0.01–0.10 Hz, which is a typical frequency band where functional connectivity is generally estimated. On the other hand, within 0.04–0.10 Hz of NIRS signals, frequency-specific functional connectivity was observed between prefrontal and occipital cortical regions. This suggests that frequency-specific information integration can be performed between specific brain regions.

Then, in Study 3, frequency-specific topologies of functional connectivity networks (FCNs) were observed (Fig. 5.1). By using fMRI signals obtained during the resting state, the coherence among 87 brain regions distributed over the whole brain was estimated. As a result, there were two frequency bands where coherence was higher than other bands: 0.01–0.03 Hz and 0.07–0.09 Hz. By investigating the topological architecture bearing information segregation and integration in the FCN, communities and hubs were identified in frequency-specific FCNs constructed from band-averaged coherence within 0.01–0.03 Hz and 0.07–0.09 Hz. While clearly segregated

communities were found in the FCN estimated in 0.01–0.03 Hz, FCN estimated in 0.07–0.09 Hz had no segregated community. On the other hand, hubs were located in different brain regions in each frequency-specific network (ACC [anterior cingulate cortex] in 0.01–0.03 Hz, and PCC [posterior cingulate cortex], precuneus, and thalamus in 0.07–0.09 Hz). These results suggest that the spatial order contributing information on segregation and integration in the brain has frequency-specificity.

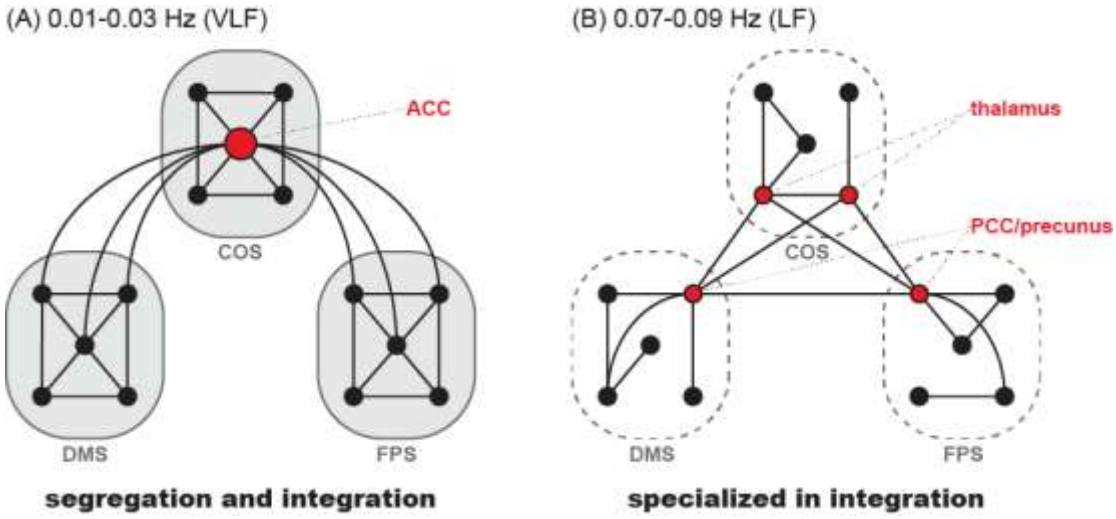

Figure 5.1. Schematic figure of findings. (A) Frequency-specific FCN constructed from fMRI time series fluctuating within 0.01–0.03 Hz (VLF). Observations in Study 3 demonstrated that FCN constructed within VLF has clearly separated three communities (default mode system [DMS], fronto-parietal system [FPS], and cingulo-opecular system [COS]) and six frequency-specific hub regions (a big red node) within anterior cingulate cortices (ACC) that were brain regions consisting of COS. The structure of FCN suggests that, while functional segregation is achieved by three separate communities, functional integration among communities is also established by hubs locating in ACC. Black nodes indicate brain regions, black lines indicate functional connectivity, and gray regions surrounded by gray lines indicate the sets of brain regions forming community. (B) Frequency-specific FCN constructed from fMRI time series fluctuating within 0.07–0.09 Hz (LF). The results of Study 3 showed that, while there was no separation among three communities, hub regions (red nodes) exist in posterior cingulate cortex (PCC), precuneus, and thalamus. Loss of separation among communities are represented by broken lines surrounding brain regions consisting of DMS, FPS, and COS. This suggests that, because functional segregation with mesoscopic functional systems such as DMS, FPS, and COS is difficult to be achieved, direct functional integration among different brain regions may be facilitated by coherent brain activities reflected by functional connectivity of hemodynamic fluctuations within LF. Black nodes indicate brain regions, black lines indicate functional connectivity.

5.1.2 Time scales of functional connectivity may reflect anatomical constraints mediating long-range interactions

There are remarkable consistencies between the results of NIRS and fMRI studies. In the 0.01–0.04 Hz, functional connectivity estimated by NIRS was found between different brain regions directly connected by cortico-cortical white matter pathways, that is, the corpus callosum, between bilateral homologous cortical regions. Results given by fMRI study suggest that topology of the network estimated in the 0.01–0.03 Hz range reflects coherence via cortico-corital pathways. On the other hand, so far, there have been no reports of the existence of direct cortico-cortical pathways between brain regions linked by functional connectivity observed only within 0.04–0.10 Hz of NIRS signal fluctuations. Considering that the thalamus was consistently identified as a hub of frequency-specific FCN calculated within 0.05–0.10 Hz of fMRI signals, functional connectivity observed in 0.04–0.10 Hz of NIRS signals may reflect coherence through poly-synaptic pathways via the thalamic hub.

5.1.3 Impact on the study of functional connectivity

About 20 years have passed since functional connectivity during the resting state was first reported by Biswal et al. (1995). Now, this technique is widely accepted as the standard analysis in the field of neuroimaging. However, almost all studies focused only on the space structure of the interaction between brain regions and disregarded its relevancy to the time scale of brain activity. The above findings demonstrated the dependency between the time scales of brain activity and the spatial structure of the FCN contributing to information processing in the brain. This means that we must consider this dependency in order to investigate network structure in charge of information processing

in the brain. In other words, the concept of an information processing mechanism of the brain, as advocated in the studies only investigating the spatial order of functional connectivity, has to be re-interpreted by taking the time scale of brain activity into consideration.

5.2 Methodological breakthrough

NIRS has several practical merits compared to fMRI: NIRS requires lower physical constraints to participants during measurement, and it is an easily-handled method. However, although it is assumed that both NIRS and fMRI measure hemodynamic fluctuations in relation to neural activities theoretically, it has not been clarified if NIRS and fMRI signals share information on functional connectivity. Furthermore, because signals of NIRS are obtained external to participants' craniums and are contaminated by skin blood flow (Takahashi et al., 2011), the reliability of the NIRS signal has always been the target of argument. In Study 3, the consistency of estimation of functional connectivity between NIRS and fMRI was investigated by conducting concurrent recording of hemodynamic fluctuations with these two methods during the resting state in order to clarify whether time series measured by NIRS reflect spontaneous hemodynamic fluctuations contributing to functional connectivity that is observed among several brain regions, including deep brain regions where NIRS measurement cannot be conducted. As shown in Chapter 3, NIRS signals showed significant correlation with fMRI signals not only within cortical regions close to NIRS channels, but also within a number of distant regions consisting of functional systems such as default mode, dorsal attention, and fronto-parietal systems.

Furthermore, fMRI has a potential limitation to estimate functional connectivity as compared to NIRS: low sampling rate of fMRI may affect the estimation of functional connectivity

especially within high frequency ranges such as 0.07–0.09 Hz (LF). However, in Study 3, I confirmed that signals obtained by NIRS and fMRI could consistently produce the result that coherence values within 0.01–0.03 (VLF) and LF are higher than those within other frequency bands (see Figs. 4.2, 4.3). Collectively, these results obtained in Studies 2 and 3 support that these different modalities produce consistent results in estimation of functional connectivity.

These findings suggest that the usage of NIRS can estimate resting state functional connectivity that has been reported by using fMRI. This discovery is very influential for the following reasons. The reduced physiological demands of NIRS enables us to collect neuroimaging data in unique populations, such as infants, and in situations unsuitable to fMRI recordings, such as data acquisition in patients with neurological movement disorders and in experimental conditions with normal body motion. Furthermore, considering that humans are social animals, investigation of neural correlates of social behavior is very important to understand human nature. However, since fMRI measurements need to completely cover the head with the device, it is not suitable for acquisition of brain activity during direct face-to-face communication, which reflects fundamental social behavior. In contrast, usage of NIRS does not disturb such communication and has already succeeded in investigating inter-individual interactions (Suda et al., 2010). However, it should be noted that, because NIRS can measure hemodynamic fluctuations only within the superficial regions of the cerebral cortex, usage of NIRS can investigate functional connectivity only between superficial cortical regions. Therefore, the invention of a methodology by which we can estimate brain activity of the deep brain regions from a NIRS time series obtained within superficial brain regions is a necessary condition to study functional connectivity among whole brain regions by using NIRS alone. Historically, technical innovation has always brought novel discovery of scientific truth. For example, until the invention of

fMRI, there was no technique of non-invasive whole brain functional imaging that provided information on the profound nature of the brain such as FCN. The consistency of the NIRS-fMRI data shown in this research adds a new option to the methodology of the acquisition of brain activity, and it may promote development of technology in the field of neuroimaging.

5.3 Related topics and future issues

5.3.1 What are the functions of frequency-specific networks?

Human cognitive behavior requires the brain to process information over several time scales. Considering this, studying a cerebral operation mechanism that focuses attention on the time scale of brain activity is reasonable. In the previous chapter, the relationship between frequency-specific topology of FCN and the level of consciousness was discussed. As mentioned above, most of the studies on neural correlation of consciousness can be divided into two categories by the focus of the study: while some studies focus on the levels of consciousness, others focus on the contents of consciousness. However, because it is very difficult for us to imagine both the conscious state without contents and coma with rich contents of consciousness, the level and content may not be independent, but, rather, mutually-dependent aspects of consciousness. Therefore, the topology of FCN within 0.07–0.09 Hz takes a role on both the level and content of consciousness. On the other hand, as we cannot have visual experiences of an external object without orientation of attention to it, the maintenance of the cognitive state may be a prerequisite of the conscious experience. This means that the time scale of information processing required to maintain a cognitive state should be longer than that required to produce content of consciousness that is constrained by the cognitive state. These speculations obtained from the observation of human behavior are consistent with findings introduced

in Study 3: while FCNs may contribute to the maintenance of the cognitive state as found within 0.01–0.03 Hz, the network that may take charge of consciousness was observed within 0.07–0.09 Hz. However, the result was obtained by analyzing the brain activity measured during the resting state. Therefore, future work needs to test the above-mentioned hypothesis by investigating frequency-specific network topology in several cognitive and conscious states.

5.3.2 Do frequency-specific networks work independently or coordinately?

Although various typical time scales exist in our behavior, do behaviors with different time scales take place independently? Or, do they interact with each other? Considering the example of speech comprehension introduced in Chapter 1, discrimination of each word in a sentence is necessary to understand a sentence as a clump of words. In contrast, when we do not need to understand speech or a sentence consisting of a lot of words, we also do not need to identify each of the syllables spoken per second as a word. So, speech comprehension is a consequence of the interaction of information processing occurring in different time scales in the brain. This view is consistent with the above-mentioned relationship between cognitive state and consciousness. Therefore, interaction of information processing in different time scales may be essential to generate normal brain functions. There are some EEG studies investigating the interaction of neural oscillations fluctuating in different frequency ranges. This interaction called cross-frequency coupling is suggested to relate cognitive functions like top-down attention and working memory (Axmancher et al., 2010; Buzsáki and Wang, 2012; Canolty and Knight, 2010; Jensen and Colgin, 2007). Our results promote study focusing on cross-frequency coupling by using fMRI with the special emphasis on network topology.

5.3.3 How do frequency-specific networks work in real time?

Stationarity has been assumed in the study of functional connectivity. However, in keeping with the information processing in charge of the dynamic nature of human behavior, the brain can vary its spatiotemporal order of activity. Recently, some studies reported findings supporting that functional connectivity changes during the fMRI measurement (Chang and Glover, 2010; Hutchison et al., 2012). While it has been shown that some of the fluctuations of functional connectivity are periodic (Handwerker et al., 2012), network topology like community also varies with the time series (Jones et al., 2012). There are supportive evidences of the idea that non-stationarity of functional connectivity estimated by fMRI has something to do with information processing in the brain (Bassett et al., 2011; Ekman et al., 2012; Fornito et al., 2012; Kinnison et al., 2012; Kitzbichler et al., 2011). For example, it has been shown that dynamic reconfiguration among fronto-parietal and default mode systems occurs with the changes of cognitive states (Fornito et al., 2012). Furthermore, it has been shown that the flexibility of reconfiguration of the topology of FCN predicts the amount of learning (Bassett et al., 2011). Moreover, it has been observed that functional connectivity and the topology of FCN dramatically changes in the course of development (Homae et al., 2010, 2011; Fair et al., 2008). These evidences indicate that the information processing mechanism in the brain has a dynamic property in nature. However, because current studies assumed stationarity of functional connectivity, the non-stationary aspects of frequency-specific FCN should be investigated in future studies.

In the current study, NIRS had a 20-times higher sampling rate than fMRI. Recently, a high-speed data acquisition method (~2 Hz) was invented for fMRI (Boyacioglu and Barth, 2012; Feinberg and Yacoub, 2012), and it has been successfully applied to identify temporally independent components of FCN (Smith et al. 2012). Application of the high-speed imaging method will provide

accurate information on functional connectivity with emphasis on temporal information and time-frequency relationships.

5.3.4 Is there any relevance of the results to frequency-specific interactions observed in electrophysiological data?

Because only hemodynamic fluctuations were acquired and analyzed in the current thesis, the relevance of the current findings to electrophysiological evidence cannot be investigated. However, because some groups have already reported the relationship, the alternative ideas are introduced in this section.

Since hemodynamic signals do not represent neural activity in itself, the neurophysiological substance of such signals has been a focus of attention. It has been demonstrated that fMRI signals increase and the relative signals from tissue oxygenation are generated not by spiking activity but by synaptic activity (Lauritzen et al., 2003; Logothetis et al., 2001, 2002; Niessing et al., 2005; Viswanathan and Freeman, 2007), indicating that functional connectivity observed by fMRI signals reflects coherence of synaptic inputs between different brain regions. Subsequently, some groups investigated the relationship between spontaneous neural fluctuation and functional connectivity and observed the results indicating that slow spontaneous fluctuation (< 0.10 Hz) of gamma-power (40–100 Hz) is a basis of inter-hemispheric functional connectivity (Nir et al., 2008). Some reports demonstrated that long-range functional connectivity within this frequency range contributes to cognitive function, supporting this idea. On the other hand, there are evidences supporting that “slow cortical potential,” which is generally observed as fluctuation under 4 Hz (He and Raichle, 2009), has direct relationship with hemodynamic signals and functional connectivity (He

et al., 2008). For example, He et al. (2008) demonstrated that, by conducting simultaneous recording of electrocorticogram (ECoG) and fMRI, a functional connectivity map calculated with slow cortical potential of ECoG signals is the most consistent correspondence to that estimated by fMRI signals. Because task-related modulation occurs in slow cortical potential of both electrophysiological and fMRI signals, this frequency band also relates to fMRI-based functional connectivity (He et al., 2010; Palva and Palva, 2012). This diversity of findings can be marshaled by the idea that each frequency-specific interaction takes charge of specific computation in the brain (Siegel et al., 2012). In the future, this idea should be examined with thorough investigation of the relationship between frequency-specific interaction and multiple behavioral states.

5.4 Final comments

In this thesis, three experimental studies were conducted: Study 1, which assessed the frequency-specificity of functional connectivity by recording spontaneous hemodynamic fluctuations with NIRS; Study 2, which examined the consistency between NIRS and fMRI on resting state functional connectivity; and, Study 3, which investigated frequency-specific topology of FCN by using resting state fMRI data. The corresponding findings are as follows: From Study 1, the frequency-dependency of functional connectivity varies depending on the combination of cortical regions. From Study 2, the usage of NIRS signals obtained during the resting state can reconstruct fMRI-based FCN. And, from Study 3, the topology in charge of information processing in the FCN varies in a frequency-dependent manner.

Human behaviors take place with several time scales. Therefore, it is indispensable to investigate cerebral information processing structure in various time scales in order to understand human nature. Unlike the previous studies of functional connectivity, I investigated the relationship between the structure of FCN and the time scales of the brain activities. The findings introduced in this thesis suggest that the brain has an information processing mechanism depending on the time scales of brain activities. This suggests that investigations of the relationship between spatial structures and time scales of brain activities provide more comprehensive understanding about an operational principle on the brain governing human behavior.

The evidences supporting that the mind is produced by various activities of the brain are overwhelming. However, it is still unclear as to how the brain obtains the activity that produces the faculty of the mind in the process of development. In other words, we have no idea as to how our brains arise from clumps of neurons to become the "seat of mind." It is very important to further

explore and elucidate this concept for better understanding of how the mind emerges from matter. Therefore, we must put much effort into examining how the brain changes in the course of development to obtain cerebral function. The paradigm introduced in this thesis is combinable with various psychological and clinical approaches, and it may promote the elucidation of development mechanisms involved in the cerebral functions in charge of human behavior.

References list

Aalkjaer, C., Boedtkjer, D., Matchkov, V., 2011. Vasomotion — what is currently thought? Acta Physiol 202, 253–269.

Achard, S., Bullmore, E., 2007. Efficiency and cost of economical brain functional networks. PLoS Comput Biol 3, e17.

Achard, S., Salvador, R., Whitcher, B., Suckling, J., Bullmore, E., 2006. A resilient, low frequency, small-world human brain functional network with highly connected association cortical hubs. J. Neurosci. 26, 63–72.

Aertsen, A.M., Gerstein, G.L., Habib, M.K., Palm, G., 1989. Dynamics of neuronal firing correlation: modulation of "effective connectivity". J Neurophysiol 61, 900–917.

Aeschbach, D., Matthews, J.R., Postolache, T.T., Jackson, M.A., Giesen, H.A., Wehr, T.A., 1999. Two circadian rhythms in the human electroencephalogram during wakefulness. Am J Physiol 277, R1771–1779.

Alkire, M.T., Hudetz, A.G., Tononi, G., 2008. Consciousness and anesthesia. Science 322, 876–880.

Allen, G., Barnard, H., McColl, R., Hester, A.L., Fields, J.A., Weiner, M.F., Ringe, W.K., Lipton, A.M., Brooker, M., McDonald, E., Rubin, C.D., Cullum, C.M., 2007. Reduced hippocampal functional connectivity in Alzheimer disease. Arch. Neurol. 64, 1482–1487.

Ames, A.I. 2000. CNS energy metabolism as related to function. Brain Res. Rev. 34, 42–68.

Amodio, D.M., Frith, C.D., 2006. Meeting of minds: the medial frontal cortex and social cognition. Nat. Rev., Neurosci. 7, 268–277.

Anand, A., Li, Y., Wang, Y., Lowe, M.J., and Dzemidzic, M., 2009. Resting state corticolimbic

connectivity abnormalities in unmedicated bipo¬lar disorder and unipolar depression. Psychiatry Res. 171, 189–198.

Anand, A., Li, Y., Wang, Y., Wu, J., Gao, S., Bukhari, L., Mathews, V.P., Kalnin, A., Lowe, M.J., 2005a. Activity and connectivity of brain mood regulating circuit in depression: a functional magnetic resonance study. Biol. Psychiatry 57, 1079–1088.

Anand, A., Li, Y., Wang, Y., Wu, J., Gao, S., Bukhari, L., Mathews, V.P., Kalnin, A., Lowe, M.J., 2005b. Antidepressant effect on connectivity of the mood-regulating circuit: an fMRI study. Neuropsychopharmacology 30, 1334–1344.

Anderson, J.S., Druzgal, T.J., Lopez-Larson, M., Jeoung, E., Desai, K., Yurgelun-Todd, D., 2011. Network anticorrelations, global regression, and phase-shifted soft tissue correction. Hum. Brain Mapp. 32, 9–934.

Andrews-Hanna, J.R., Snyder, A.Z., Vincent, J.L., Lustig, C., Head, D., Raichle, M.E., Buckner, R.L. 2007. Disruption of large-scale brain systems in advanced aging. Neuron 56, 924–935.,

Ashburner, J., 2007. A fast diffeomorphic image registration algorithm. Neuroimage, 38, 95–113.

Astafiev, S.V., Shulman, G.L., Stanley, C.M., Snyder, A.Z., Van Essen, D.C., Corbetta, M., 2003. Functional organization of human intraparietal and frontal cortex for attending, looking, and pointing. J Neurosci 23, 4689–4699.

Astafiev, S.V., Stanley, C.M., Shulman, G.L., Corbetta, M., 2004. Extrastriate body area in human occipital cortex responds to the performance of motor actions. Nat Neurosci 7, 542–548.

Attwell, D. & Laughlin, S. B. 2001. An energy budget for signalling in the grey matter of the brain. J. Cereb. Blood Flow Metab. 21, 1133–1145.

Axmacher, N., Henseler, M.M., Jensen, O., Weinreich, I., Elger, C.E., Fell, J., 2010. Cross-frequency

coupling supports multi-item working memory in the human hippocampus. Proc. Natl. Acad. Sci. U.S.A. 107, 3228–3233.

Baria, A.T., Baliki, M.N., Parrish, T., Apkarian, A.V., 2011. Anatomical and functional assemblies of brain BOLD oscillations. J Neurosci 31, 7910–7919.

Bassett, D.S., Bullmore, E., Verchinski, B.A., Mattay, V.S., Weinberger, D.R., Meyer-Lindenberg, A., 2008. Hierarchical organization of human cortical networks in health and schizophrenia. J. Neurosci. 28, 9239–9248.

Bassett, D.S., Wymbs, N.F., Porter, M.A., Mucha, P.J., Carlson, J.M., Grafton, S.T., 2011 Dynamic reconfiguration of human brain networks during learning. Proc. Natl. Acad. Sci. U.S.A., 108, 7641–7646.

Beckmann, C.F., DeLuca, M., Devlin, J.T., Smith, S.M., 2005. Investigations into resting-state connectivity using independent component analysis. Philos. Trans. R. Soc. Lond. B. Biol. Sci. 360, 1001–1013.

Behrens, T.E., Johansen-Berg, H., Woolrich, M.W., Smith, S.M., Wheeler-Kingshott, C.A., Boulby, P.A., Barker, G.J., Sillery, E.L., Sheehan, K., Ciccarelli, O., Thompson, A.J., Brady, J.M., Matthews, P.M., 2003. Non-invasive mapping of connections between human thalamus and cortex using diffusion imaging. Nat. Neurosci. 6, 750-757.

Benjamini, Y., Yekutieli, D., 2001. The control of the false discovery rate in multiple testing under dependency. Annals of Statistics 29, 1165–1188.

Bettus, G., Guedj, E., Joyeux, F., Confort-Gouny, S., Soulier, E., Laguitton, V., Cozzone, P.J., Chauvel, P., Ranjeva, J.P., Bartolomei, F., Guye, M., 2009. Decreased basal fMRI functional con¬nectivity in epileptogenic networks and contralateral compensatory mechanisms. Hum. Brain Mapp. 30,

1580–1591.

Bhattacharyya, P.K., Lowe, M.J., 2004. Cardiac-induced physiologic noise in tissue is a direct observation of cardiac-induced fluctuations. Magn Reson Imaging 22, 9–13.

Birn, R.M., Diamond, J.B., Smith, M.A., Bandettini, P.A., 2006. Separating respiratory-variation-related fluctuations from neuronal-activity-related fluctuations in fMRI. Neuroimage 31, 1536–1548.

Birn, R.M., Molloy, E.K., Patriat, R., Parker, T., Meier, T.B., Kirk, G.R., Nair, V.A., Meyerand, M.E., Prabhakaran, V., 2013. The effect of scan length on the reliability of resting-state fMRI connectivity estimates. Neuroimage.. http://dx.doi.org/10.1016/j.neuroimage.2013.05.099 (in press).

Biswal, B., Yetkin, F.Z., Haughton, V.M., Hyde, J.S., 1995. Functional connectivity in the motor cortex of resting human brain using echo-planar MRI. Magn. Reson. Med. 34, 537–541.

Biswal, B.B., Kannurpatti, S.S., 2009. Resting-state functional connectivity in animal models: modulations by exsanguination. Methods Mol. Biol. 489, 255–274.

Bluhm, R.L., Miller, J., Lanius, R.A., Osuch, E.A., Boksman, K., Neufeld, R., Theberge, J., Schaefer, B., and Williamson, P., 2007. Spontaneous low-frequency fluctuations in the BOLD signal in schizophrenic patients: anomalies in the default network. Schizophr. Bull. 33, 1004–1012.

Bluhm, R.L., Clark, C.R., McFarlane, A.C., Moores, K.A., Shaw, M.E., Lanius, R.A., 2011. Default network connectivity during a working memory task. Hum. Brain Mapp. 32, 1029–1035.

Bluhm, R.L., Miller, J., Lanius, R.A., Osuch, E.A., Boksman, K., Neufeld, R.W., Theberge, J., Schaefer, B., and Williamson, P. C., 2009a. Retrosplenial cortex connectivity in schizophrenia. Psychiatry Res. 174, 17–23.

Bluhm, R., Williamson, P., Lanius, R., Theberge, J., Densmore, M., Bartha, R., Neufeld, R., and Osuch, E., 2009b. Resting state default-mode network connectivity in early depression using a seed region-of-interest analysis: decreased connectivity with caudate nucleus. Psychiatry Clin. Neurosci. 63, 754–761.

Bluhm, R.L., Williamson, P.C., Osuch, E.A., Frewen, P.A., Stevens, T.K., Boksman, K., Neufeld, R.W., Theberge, J., and Lanius, R.A., 2009c. Alterations in default network connectivity in posttraumatic stress disorder related to early-life trauma. J. Psychiatry Neurosci. 34, 187–194.

Boccaletti, S., Latora, V., Moreno, Y., Chavez, M., Hwang, D.U., 2006. Complex networks: Structure and dynamics. Phys. Rep. 424, 175–308.

Boly, M., Balteau, E., Schnakers, C., Degueldre, C., Moonen, G., Luxen, A., Phillips, C., Peigneux, P., Maquet, P., Laureys, S., 2007. Baseline brain activity fluctuations predict somatosensory perception in humans. Proc. Natl. Acad. Sci. U.S.A. 104, 12187–12192.

Boly, M., Perlbarg, V., Marrelec, G., Schabus, M., Laureys, S., Doyon, J., Pélégrini-Issac, M., Maquet, P., Benali, H., 2012. Hierarchical clustering of brain activity during human nonrapid eye movement sleep. Proc. Natl. Acad. Sci. U.S.A. 109, 5856–5861.

Boly, M., Phillips, C., Balteau, E., Schnakers, C., Degueldre, C., Moonen, G., Luxen, A., Peigneux, P., Faymonville, M.E., Maquet, P., Laureys, S., 2008. Consciousness and cerebral baseline activity fluctuations. Hum Brain Mapp 29, 868–874.

Boly, M., Tshibanda, L., Vanhaudenhuyse, A., Noirhomme, Q., Schnakers, C., Ledoux, D., Boveroux, P., Garweg, C., Lambermont, B., Phillips, C., Luxen, A., Moonen, G., Bassetti, C., Maquet, P., and Laureys, S., 2009. Functional con¬nectivity in the default network during resting state is preserved in a vegetative but not in a brain dead patient. Hum. Brain Mapp. 30, 2393–2400.

Boveroux, P., Vanhaudenhuyse, A., Bruno, M.A., Noirhomme, Q., Lauwick, S., Luxen, A., Degueldre, C., Plenevaux, A., Schnakers, C., Phillips, C., Brichant, J.F., Bonhomme, V., Maquet, P., Greicius, M.D., Laureys, S., Boly, M., 2010. Breakdown of within- and between-network resting state functional magnetic resonance imaging connectivity during propofol-induced loss of consciousness. Anesthesiology 113, 1038–1053.

Boyacioğlu, R., Barth, M., 2012. Generalized iNverse imaging (GIN): Ultrafast fMRI with physiological noise correction. Magn Reson Med.

Braun, U., Plichta, M.M., Esslinger, C., Sauer, C., Haddad, L., Grimm, O., Mier, D., Mohnke, S., Heinz, A., Erk, S., Walter, H., Seiferth, N., Kirsch, P., Meyer-Lindenberg, A., 2012. Test-retest reliability of resting-state connectivity network characteristics using fMRI and graph theoretical measures. Neuroimage 59, 1404–1412.

Broca, P., 1861. Remarks on the Seat of the Faculty of Articulated Language, Following an Observation of Aphemia (Loss of Speech)". Bulletin de la Société Anatomique, 6, 330–357.

Buckner R.L, Andrews-Hanna J., Schacter D., 2008. The brain's default network: anatomy, function, and relevance to disease. Ann. N.Y. Acad. Sci. 1124, 1–38.

Buckner, R.L., Carroll, D.C., 2007. Self-projection and the brain. Trends Cogn. Sci. 11, 49–57.

Buckner, R.L., Sepulcre, J., Talukdar, T., Krienen, F.M., Liu, H., Hedden, T., Andrews-Hanna, J.R., Sperling, R.A., Johnson, K.A., 2009. Cortical hubs revealed by intrinsic functional connectivity: mapping, assessment of stability, and relation to Alzheimer's disease. J. Neurosci. 29, 1860–1873.

Buckner, R.L., Vincent, J.L., 2007. Unrest at rest: Default activity and spontaneous network correlations. Neuroimage 37, 1091–1096; discussion 1097–1099.

Bullmore, E., Sporns, O., 2009. Complex brain networks: graph theoretical analysis of structural and

functional systems. Nat. Rev. Neurosci. 10, 186–198.

Butts, C., 2009. Revisiting the foundations of network analysis. Science 325, 414–416.

Buzsáki, G., Draguhn, A., 2004. Neuronal oscillations in cortical networks. Science 304, 1926–1929.

Buzsáki, G., Wang, X.J., 2012. Mechanisms of gamma oscillations. Annu. Rev. Neurosci. 35, 203–225.

Cajochen, C., Wyatt, J.K., Czeisler, C.A., Dijk, D.J., 2002. Separation of circadian and wake duration-dependent modulation of EEG activation during wakefulness. Neuroscience 114, 1047–1060.

Calhoun, V.D., Adali, T., Pearlson, G.D., Pekar, J.J., 2001. A method for making group inferences from functional MRI data using independent component analysis. Hum. Brain Mapp. 14, 140–151.

Canolty, R.T., Knight, R.T., 2010. The functional role of cross-frequency coupling. Trends. Cogn. Sci. 14, 506–515.

Cao, Q., Zang, Y., Sun, L., Sui, M., Long, X., Zou, Q., and Wang, Y., 2006. Abnormal neural activity in children with attention deficit hyperactivity disorder: a resting-state functional magnetic resonance imaging study. Neuroreport 17, 1033–1036.

Castellanos, F.X., Margulies, D.S., Kelly, C., Uddin, L.Q., Ghaffari, M., Kirsch, A., Shaw, D., Shehzad, Z., Di Martino, A., Biswal, B., Sonuga-Barke, E.J., Rotrosen, J., Adler, L.A., Milham, M.P., 2008. Cingulate-precuneus interactions: a new locus of dysfunc¬tion in adult attention-deficit/hyper¬activity disorder. Biol. Psychiatry 63, 332–337.

Cauda, F., D'Agata, F., Sacco, K., Duca, S., Cocito, D., Paolasso, I., Isoardo, G., Geminiani, G., 2010. Altered resting state attentional networks in diabetic neuropathic pain. J Neurol Neurosurg Psychiatry 81, 806–811.

Cauda, F., Micon, B. M., Sacco, K., Duca, S., D'Agata, F., Geminiani, G., and Canavero, S., 2009a.

Disrupted intrinsic functional connectivity in the vegetative state. J. Neurol. Neurosurg. Psychiatr. 80, 429–431.

Cauda, F., Sacco, K., D'Agata, F., Duca, S., Cocito, D., Geminiani, G., Migliorati, F., and Isoardo, G., 2009b. Low-frequency BOLD fluctuations demonstrate altered thalamocortical connectivity in diabetic neuropathic pain. BMC Neurosci. 10, 138.

Cauda, F., Sacco, K., Duca, S., Cocito, D., D'Agata, F., Geminiani, G.C., Canavero, S., 2009c. Altered resting state in diabetic neuropathic pain. PLoS ONE 4, e4542. doi: 10.1371/journal.pone.0004542.

Cecchi, G.A., Rao, A.R., Centeno, M.V., Baliki, M., Apkarian, A.V., Chialvo, D.R., 2007. Identifying directed links in large scale functional networks: application to brain fMRI. BMC. Cell. Biol. 8 (Suppl. 1), S5.

Chance, B., Zhuang, Z., Unah, C., Alter, C., Lipton, L., 1993. Cognition-activated lowfrequency modulation of light absorption in human brain. Proc. Natl. Acad. Sci. U.S.A. 90, 3770–3774.

Chang, C., Glover, G.H., 2009. Relationship between respiration, end-tidal CO2, and BOLD signals in resting-state fMRI. Neuroimage 47, 1381–1393.

Chang, C., Glover, G.H., 2010. Time–frequency dynamics of resting-state brain connectivity measured with fMRI. Neuroimage 50, 81–98.

Chai, X.J., Castanon, A.N., Ongur, D., Whitfield-Gabrieli, S., 2012. Anticorrelations in resting state networks without global signal regression. Neuroimage 59, 1420–1428.

Chen, B., Bouchard, M., McCaslin, F., Burgess, S., Hillman, E., 2011. High-speed vascular dynamics of the hemodynamic response. Neuroimage 54, 1021–1030.

Cherkassky, V.L., Kana, R.K., Keller, T.A., and Just, M.A., 2006. Functional connectivity in a baseline

resting-state network in autism. Neuroreport 17, 1687–1690.

Christoff, K., Gordon, A.M., Smallwood, J., Smith, R., Schooler, J.W., 2009. Experience sampling during fMRI reveals default network and executive system contributions to mind wandering. Proc. Natl. Acad. Sci. U. S. A. 106, 8719–8724.

Church, J.A., Fair, D.A., Dosenbach, N.U., Cohen, A.L., Miezin, F.M., Petersen, S.E., Schlaggar, B.L., 2009. Control networks in paediat¬ric Tourette syndrome show immature and anomalous patterns of functional connectivity. Brain 132, 225–238.

Cole, M.W., Yarkoni, T., Repovs, G., Anticevic, A., Braver, T.S., 2012. Global connectivity of prefrontal cortex predicts cognitive control and intelligence. J. Neurosci. 32, 8988–8999.

Colizza, V., Flammini, A., Serrano, M.A., Vespignani A., 2006. Detecting rich- club ordering in complex networks. Nat. Phys. 2, 110 –115.

Corbetta M., Shulman G.L., 2002. Control of goal-directed and stimulus-driven attention in the brain. Nat. Rev. Neurosci. 3, 201–215.

Corbetta, M., Shulman, G.L., Miezin, F.M., Petersen, S.E., 1995. Superior parietal cortex activation during spatial attention shifts and visual feature conjunction. Science 270, 802–805.

Cordes, D., Haughton, V.M., Arfanakis, K., Carew, J.D., Turski, P.A., Moritz, C.H., Quigley, M.A., Meyerand, M.E., 2001. Frequencies contributing to functional connectivity in the cerebral cortex in “resting-state” data. Am. J. Neuroradiol. 22, 1326–1333.

Cordes, D., Haughton, V.M., Arfanakis, K., Wendt, G.J., Turski, P.A., Moritz, C.H., Quigley, M.A., Meyerand, M.E., 2000. Mapping functionally related regions of brain with functional connectivity MR imaging. AJNR Am. J. Neuroradiol. 21, 1636–1644.

Cordes, D., Haughton, V., Carew, J.D., Arfanakis, K., Maravilla, K., 2002. Hierarchical clustering to

measure connectivity in fMRI resting-state data. Magn. Reson. Imaging 20, 305–317.

Cottingham, J., Stoothoff, R., Murdoch, D. (Eds.), 1985. The philosophical writings of Rene Descartes. Cambridge University Press.

Cui, X., Bray, S., Bryant, D.M., Glover, G.H., Reiss, A.L., 2011. A quantitative comparison of NIRS and fMRI across multiple cognitive tasks. Neuroimage 54, 2808–2821.

Cui, X., Bryant, D.M., Reiss, A.L., 2012. NIRS-based hyperscanning reveals increased interpersonal coherence in superior frontal cortex during cooperation, Neuroimage 59, 2430–2437.

Curtis, C.E., D'Esposito, M., 2003. Persistent activity in the prefrontal cortex during working memory. Trends. Cogn. Sci. 7, 415– 423.

Dagli, M.S., Ingeholm, J.E., Haxby, J.V., 1999. Localization of cardiac-induced signal change in fMRI. Neuroimage 9, 407–415.

Damasio, A. 1990. Synchronous activation in multiple cortical areas: a mechanism for recall. Sem. Neurosci. 2, 287–296 .

Damoiseaux, J.S., Beckmann, C.F., Arigita, E.J., Barkhof, F., Scheltens, P., Stam, C.J., Smith, S.M., Rombouts, S.A., 2008. Reduced resting-state brain activity in the "default network" in normal aging. Cereb. Cortex. 18, 1856–1864.

Damoiseaux, J.S., Rombouts, S.A., Barkhof, F., Scheltens, P., Stam, C.J., Smith, S.M., Beckmann, C.F., 2006. Consistent resting-state networks across healthy subjects. Proc. Natl Acad. Sci. U. S. A. 103, 13848–13853.

D'Argembeau, A., Collette, F., Van der Linden, M., Laureys, S., Del Fiore, G., Degueldre, C., Luxen, A., and Salmon, E., 2005. Self-referential reflective activity and its relationship with rest: a PET study. Neuroimage 25, 616–624.

De Luca, M., Beckmann, C.F., De, S.N., Matthews, P.M., Smith, S.M., 2006. fMRI resting state networks define distinct modes of long-distance interactions in the human brain. Neuroimage 29, 1359–1367.

De Luca, M., Smith, S. M., De Stefano, N., Federico, A., and Matthews, P. M., 2005. Blood oxygenation level dependent contrast resting state net¬works are relevant to functional activ¬ity in the neocortical sensorimotor system. Exp. Brain Res. 167, 587–594.

Deshpande, G., Santhanam, P., Hu, X., 2011. Instantaneous and causal connectivity in resting state brain networks derived from functional MRI data. Neuroimage 54, 1043–1052.

Desjardins, A.E., Kiehl, K.A., Liddle, P.F., 2001. Removal of confounding effects of global signal in functional MRI analyses. Neuroimage 13, 751–758.

D'Esposito, M., Deouell, L.Y., Gazzaley, A., 2003. Alterations in the BOLD fMRI signal with ageing and disease: a challenge for neuroimaging. Nat. Rev. Neurosci. 4, 863–872.

Devor A., Tian P., Nishimura N., Teng I., Hillman E., Narayanan S., Ulbert I., Boas D., Kleinfeld D., Dale A., 2007. Suppressed neuronal activity and concurrent arteriolar vasoconstriction may explain negative blood oxygenation level-dependent signal. J. Neurosci. 27, 4452–4459.

Dijk, D.J., Brunner, D.P., Beersma, D.G., Borbély, A.A., 1990. Electroencephalogram power density and slow wave sleep as a function of prior waking and circadian phase. Sleep 13, 430–440.

Dijk, D.J., Shanahan, T.L., Duffy, J.F., Ronda, J.M., Czeisler, C.A., 1997. Variation of electroencephalographic activity during non-rapid eye movement and rapid eye movement sleep with phase of circadian melatonin rhythm in humans. J. Physiol. 505 (Pt 3), 851–858.

Doria, V., Beckmann, C.F., Arichi, T., Merchant, N., Groppo, M., Turkheimer, F.E., Counsell, S.J., Murgasova, M., Aljabar, P., Nunes, R.G., Larkman, D.J., Rees, G., Edwards, A.D., 2010.

Emergence of resting state networks in the preterm human brain. Proc. Natl Acad. Sci. U. S. A. 107, 20015–20020.

Dosenbach, N.U., Visscher, K.M., Palmer, E.D., Miezin, F.M., Wenger, K.K., Kang, H.C., Burgund, E.D., Grimes, A.L., Schlaggar, B.L., Petersen, S.E., 2006. A core system for the implementation of task sets. Neuron 50, 799–812.

Dosenbach, N.U., Fair, D.A., Miezin, F.M., Cohen, A.L., Wenger, K.K., Dosenbach, R.A., Fox, M.D., Snyder, A.Z., Vincent, J.L., Raichle, M.E., Schlaggar, B.L., Petersen, S.E., 2007. Distinct brain networks for adaptive and stable task control in humans. Proc. Natl. Acad. Sci. U.S.A. 104, 11073–11078.

Dosenbach, N.U., Nardos, B., Cohen, A.L., Fair, D.A., Power, J.D., Church, J.A., Nelson, S.M., Wig, G.S., Vogel, A.C., Lessov-Schlaggar, C.N., Barnes, K.A., Dubis, J.W., Feczko, E., Coalson, R.S., Pruett, J.R., Barch, D.M., Petersen, S.E., Schlaggar, B.L., 2010. Prediction of individual brain maturity using fMRI. Science 329, 1358–1361.

Douglas, R.J., Koch, C., Mahowald, M., Martin, K.A., Suarez, H.H., 1995. Recurrent excitation in neocortical circuits. Science 269, 981–985.

Duan, L., Zhang, Y., Zhu, C., 2012. Quantitative comparison of resting-state functional connectivity derived from fNIRS and fMRI: A simultaneous recording study. Neuroimage, 60, 2008–2018.

Eguíluz, V.M., Chialvo, D.R., Cecchi, G.A., Baliki, M., Apkarian, A.V., 2005. Scale-free brain functional networks. Phys. Rev. Lett. 94, 018102.

Ekman, M., Derfuss, J., Tittgemeyer, M., Fiebach, C.J., 2012. Predicting errors from reconfiguration patterns in human brain networks. Proc. Natl. Acad. Sci. U.S.A. 109, 16714–16719.

Elwell, C.E., Springett, R., Hillman, E., Delpy, D.T., 1999. Oscillations in cerebral haemodynamics.

Implications for functional activation studies. Adv. Exp. Med. Biol. 471, 57–65.

Etkin, A., Prater, K.E., Schatzberg, A.F., Menon, V., and Greicius, M.D., 2009. Disrupted amygdalar subregion func¬tional connectivity and evidence of a compensatory network in generalized anxiety disorder. Arch. Gen. Psychiatry 66, 1361–1372.

Fair, D.A., Dosenbach, N.U., Church, J.A., Cohen, A.L., Brahmbhatt, S., Miezin, F.M., Barch, D.M., Raichle, M.E., Petersen, S.E., Schlaggar, B.L., 2007. Development of distinct control networks through segregation and integration. Proc. Natl. Acad. Sci. U.S.A. 104, 13507–13512.

Fair, D.A., Cohen, A.L., Dosenbach, N.U., Church, J.A., Miezin, F.M., Barch, D.M., Raichle, M.E., Petersen, S.E., Schlaggar, B.L., 2008. The maturing architecture of the brain's default network. Proc. Natl. Acad. Sci. U.S.A. 105, 4028–4032.

Fair, D.A., Cohen, A.L., Power, J.D., Dosenbach, N.U., Church, J.A., Miezin, F.M., Schlaggar, B.L., Petersen, S.E., 2009. Functional brain networks develop from a "local to distributed" organization. PLoS Comput. Biol. 5, e1000381.

Feinberg, D.A., Yacoub, E., 2012. The rapid development of high speed, resolution and precision in fMRI. Neuroimage 62, 720–725.

Felleman, D.J., Van Essen, D.C., 1991. Distributed hierarchical processing in the primate cerebral cortex. Cereb Cortex 1, 1–47.

Fellous, J.M., Tiesinga, P.H., Thomas, P.J., Sejnowski, T.J., 2004. Discovering spike patterns in neuronal responses. J Neurosci 24, 2989–3001.

Fornito, A., Bullmore, E.T., 2010. What can spontaneous fluctuations of the blood oxygenation-level-dependent signal tell us about psychiatric disorders? Curr. Opin. Psychiatry 23, 239–249.

Fornito, A., Harrison, B.J., Zalesky, A., Simons, J.S., 2012. Competitive and cooperative dynamics of large-scale brain functional networks supporting recollection. Proc. Natl. Acad. Sci. U.S.A. 109, 12788–12793.

Fox, M.D., Corbetta, M., Snyder, A.Z., Vincent, J.L., Raichle, M.E., 2006. Spontaneous neuronal activity distinguishes human dorsal and ventral attention systems. Proc. Natl. Acad. Sci. U. S. A. 103, 10046–10051.

Fox, M.D. Greicius, M.D., 2010. Clinical applications of resting state functional connectivity. Front. Syst. Neurosci. 4. 1–13.

Fox, M.D., Raichle, M.E., 2007. Spontaneous fluctuations in brain activity observed with functional magnetic resonance imaging. Nat. Rev. Neurosci. 8, 700–711.

Fox, M.D., Snyder, A.Z., Vincent, J.L., Corbetta, M., Van Essen, D.C., Raichle, M.E., 2005. The human brain is intrinsically organized into dynamic, anticorrelated functional networks. Proc. Natl. Acad. Sci. U. S. A. 102, 9673–9678.

Fox, M.D., Zhang, D., Snyder, A.Z., Raichle, M.E., 2009. The global signal and observed anticorrelated resting state brain networks. J. Neurophysiol. 101, 3270–3283.

Franceschini, M.A., Fantini, S., Thompson, J.H., Culver, J.P., Boas, D.A., 2003. Hemodynamic evoked response of the sensorimotor cortex measured noninvasively with near-infrared optical imaging. Psychophysiology 40, 548–560.

Fransson, P., 2005. Spontaneous low-frequency BOLD signal fluctuations: an fMRI investigation of the resting-state default mode of brain function hypothesis. Hum. Brain Mapp. 26, 15–29.

Fries, P., 2009. Neuronal gamma-band synchronization as a fundamental process in cortical computation. Annu Rev Neurosci 32, 209–224.

Friston, K.J., 1998. The disconnection hypothesis. Schizophr Res 30, 115–125.

Friston, K.J., Frith, C.D., Liddle, P.F., Frackowiak, R.S., 1993. Functional connectivity: the principal-component analysis of large (PET) data sets. J Cereb Blood Flow Metab 13, 5–14.

Fruchterman, T.M.J., Reingold, E.M. 1991, "Graph Drawing by Force-Directed Placement", Software – Practice & Experience 21, 1129–1164.

Funane, T., Kiguchi, M., Atsumori, H., Sato, H., Kubota, K., Koizumi, H., 2011. Synchronous activity of two people's prefrontal cortices during a cooperative task measured by simultaneous near-infrared spectroscopy. J. Biomed. Opt. 16, 077011.

Gagnon, L., Cooper, R.J., Yücel, M.A., Perdue, K.L., Greve, D.N., Boas, D.A., 2012a. Short separation channel location impacts the performance of short channel regression in NIRS. NeuroImage 59, 2518–2528.

Gagnon, L., Yücel, M.A., Dehaes, M., Cooper, R.J., Perdue, K.L., Selb, J., Huppert, T.H., Hoge, R.D., Boas, D.A., 2012b. Quantification of the cortical contribution to the NIRS signal over the motor cortex using concurrent NIRS–fMRI measurements. NeuroImage 59, 3933–3940.

Gallagher, H.L., Frith, C.D., 2003. Functional imaging of “theory of mind”. Trends Cogn. Sci. 7, 77–83.

Gao, W., Zhu, H., Giovanello, K.S., Smith, J.K., Shen, D., Gilmore, J.H., Lin, W., 2009. Evidence on the emergence of the brain's default network from 2-week-old to 2-year-old healthy pediatric subjects. Proc. Natl. Acad. Sci. U. S. A. 106, 6790–6795.

Gao, W., Lin, W., 2012. Frontal parietal control network regulates the anti-correlated default and dorsal attention networks. Hum. Brain Mapp. 33. 192–202.

Gießing, C., Thiel, C.M., Alexander-Bloch, A.F., Patel, A.X., Bullmore, E.T., 2013. Human Brain

Functional Network Changes Associated with Enhanced and Impaired Attentional Task Performance. J. Neurosci. 33, 5903–5914.

Gilbert, C.D., Wiesel, T.N., 1983. Clustered intrinsic connections in cat visual cortex. J. Neurosci. 3, 1116–1133.

Glover, G.H., Li, T.Q., Ress, D., 2000. Image-based method for retrospective correction of physiological motion effects in fMRI: RETROICOR. Magn. Reson. Med. 44, 162–167

Greicius, M.D., Barad, M., Ueno, T., and Mackey, S.C., 2008. "Chronic pain remodels the brain's salience network: a resting-state fMRI study," in 14th International Meeting of the Organization for Human Brain Mapping Melbourne, Australia.

Greicius, M.D., Flores, B.H., Menon, V., Glover, G.H., Solvason, H.B., Kenna, H., Reiss, A.L., Schatzberg, A.F., 2007. Resting-state functional con¬nectivity in major depression: abnor¬mally increased contributions from subgenual cingulate cortex and tha¬lamus. Biol. Psychiatry 62, 429–437.

Greicius, M.D., Krasnow, B., Reiss, A.L., Menon, V., 2003. Functional connectivity in the resting brain: a network analysis of the default mode hypothesis. Proc. Natl. Acad. Sci. U. S. A. 100, 253–258. 19, 72–78.

Greicius, M.D., Srivastava, G., Reiss, A.L., Menon, V., 2004. Default-mode network activity distinguishes Alzheimer's disease from healthy aging: evidence from functional MRI. Proc. Natl. Acad. Sci. U.S.A. 101, 4637–4642.

Greicius, M.D., Supekar, K., Menon, V., Dougherty, R.F., 2009. Resting-state functional connectivity reflects structural connectivity in the default mode network. Cereb. Cortex 19, 72–78.

Gross, J., Schmitz, F., Schnitzler, I., Kessler, K., Shapiro, K., Hommel, B., Schnitzler, A., 2004.

Modulation of long-range neural synchrony reflects temporal limitations of visual attention in humans. Proc Natl Acad Sci U S A 101, 13050–13055.

Guillery, R.W., Sherman, S.M., 2002. Thalamic relay functions and their role in corticocortical communication: generalizations from the visual system. Neuron 33, 163–175.

Guionnet, S., Nadel, J., Bertasi, E., Sperduti, M., Delaveau, P., Fossati, P., 2012. Reciprocal Imitation: Toward a neural basis of social interaction. Cereb. Cortex. 22, 971–978.

Gusnard, D.A., Akbudak, E., Shulman, G.L., Raichle, M.E., 2001. Medial prefrontal cortex and self-referential mental activity: relation to a default mode of brain function. Proc. Natl. Acad. Sci. U. S. A. 98, 4259–4264.

Hagmann, P., Cammoun, L., Gigandet, X., Meuli, R., Honey, C.J., Wedeen, V.J., Sporns, O., 2008. Mapping the structural core of human cerebral cortex. PLoS Biol 6, e159.

Handwerker, D.A., Roopchansingh, V., Gonzalez-Castillo, J., Bandettini, P.A., 2012. Periodic changes in fMRI connectivity. Neuroimage 63, 1712–1719.

Hayasaka, S., Laurienti, P.J., 2010. Comparison of characteristics between region-and voxel-based network analyses in resting-state fMRI data, NeuroImage, 50, 499–508.

He, B.J., 2011. Scale-free properties of the functional magnetic resonance imaging signal during rest and task. J. Neurosci. 31, 13786–13795.

He, B.J., Raichle, M.E., 2009. The fMRI signal, slow cortical potential and consciousness. Trends Cogn. Sci. 13, 302–309.

He, B.J., Snyder, A.Z., Vincent, J.L., Epstein, A., Shulman, G.L., Corbetta, M., 2007. Breakdown of functional connectivity in frontopa¬rietal networks underlies behavioral deficits in spatial neglect. Neuron 53, 905–918.

He, B.J., Snyder, A.Z., Zempel, J.M., Smyth, M.D., Raichle, M.E., 2008. Electrophysiological correlates of the brain's intrinsic large-scale functional architecture. Proc. Natl. Acad. Sci. U.S.A. 105, 16039–16044.

He, B.J., Zempel, J.M., Snyder, A.Z., Raichle, M.E., 2010. The temporal structures and functional significance of scale-free brain activity. Neuron 66, 353–369.

Hedden, T., Van Dijk, K.R., Becker, J.A., Mehta, A., Sperling, R.A., Johnson, K.A., Buckner, R.L., 2009. Disruption of functional connectivity in clinically normal older adults harboring amyloid burden. J. Neurosci. 29, 12686–12694.

Hoge, R.D., Franceschini, M.A., Covolan, R.J.M., Huppert, T., Mandeville, J.B., Boas, D.A., 2005. Simultaneous recording of task-induced changes in blood oxygenation, volume, and flow using diffuse optical imaging and arterial spin-labeling MRI. Neuroimage 25, 701–707.

Homae, F., Watanabe, H., Nakano, T. and Taga, G., 2011. Large-scale brain networks underlying language acquisition in early infancy. Front. Psychology 2, 93.

Homae, F., Watanabe, H., Otobe, T., Nakano, T., Go, T., Konishi, Y., Taga, G., 2010. Development of global cortical networks in early infancy. J. Neurosci. 30, 4877–4882.

Honey, C.J., Kötter, R., Breakspear, M., Sporns, O., 2007. Network structure of cerebral cortex shapes functional connectivity on multiple time scales. Proc. Natl. Acad. Sci. U.S.A. 104, 10240–10245.

Honey, C.J., Sporns, O., Cammoun, L., Gigandet, X., Thiran, J.P., Meuli, R., Hagmann, P., 2009. Predicting human resting-state functional connectivity from structural connectivity. Proc. Natl. Acad. Sci. U. S. A. 106, 2035–2040.

Honey, C.J., Thesen, T., Donner, T.H., Silbert, L.J., Carlson, C.E., Devinsky, O., Doyle, W.K., Rubin, N., Heeger, D.J., Hasson, U., 2012. Slow cortical dynamics and the accumulation of information

over long time scales. Neuron 76, 423–434.

Horovitz, S.G., Braun, A.R., Carr, W.S., Picchioni, D., Balkin, T.J., Fukunaga, M., Duyn, J.H., 2009. Decoupling of the brain's default mode network during deep sleep. Proc. Natl. Acad. Sci. U.S.A. 106, 11376–11381.

Hoshi, Y., Kosaka, S., Xie, Y., Kohri, S., Tamura, M., 1998. Relationship between fluctuations in the cerebral hemoglobin oxygenation state and neuronal activity under resting conditions in man. Neurosci. Lett. 245, 147–150.

Hoshi, Y., Tamura, M., 1993. Detection of dynamic changes in cerebral oxygenation coupled to neuronal function during mental work in man. Neurosci. Lett. 150, 5–8.

Hohwy, J., 2009. The neural correlates of consciousness: New experimental approaches needed?, Consciousness and Cognition, 18, 428–438.

Hubel, D.H., Wiesel, T. N., 1962. Receptive Fields, Binocular Interaction And Functional Architecture In The Cat's Visual Cortex, Journal of Physiology 160, 106–154.

Hudetz, A.G., Biswal, B.B., Shen, H., Lauer, K.K., Kampine, J.P., 1998. Spontaneous fluctuations in cerebral oxygen supply. An introduction. Adv. Exp. Med. Biol. 454, 551–559.

Humphries, M.D., Gurney, K., 2008. Network ‘small-world-ness’: a quantitative method for determining canonical network equivalence. PLoS ONE 3, e0002051.

Huppert, T., Hoge, R., Dale, A., Franceschini, M., Boas, D., 2006a. Quantitative spatial comparison of diffuse optical imaging with blood oxygen level-dependent and arterial spin labeling-based functional magnetic resonance imaging. J. Biomed. Opt. 11, 064018.

Huppert, T., Hoge, R., Diamond, S., Franceschini, M., Boas, D., 2006b. A temporal comparison of BOLD, ASL, and NIRS hemodynamic responses to motor stimuli in adult humans, Neuroimage,

29, 368–382.

Hutchison, R.M., Womelsdorf, T., Allen, E.A., Bandettini, P.A., Calhoun, V.D., Corbetta, M., Della Penna, S., Duyn, J.H., Glover, G.H., Gonzalez-Castillo, J., Handwerker, D.A., Keilholz, S., Kiviniemi, V., Leopold, D.A., de Pasquale, F., Sporns, O., Walter, M., Chang, C., 2013. Dynamic functional connectivity: Promise, issues, and interpretations. Neuroimage. 80, 360–378.

Hutchison, R.M., Womelsdorf, T., Gati, J.S., Everling, S., Menon, R.S., 2012. Resting-state networks show dynamic functional connectivity in awake humans and anesthetized macaques. Hum Brain Mapp. http://dx.doi.org/10.1002/hbm.22058 (in press).

Ikegami, T., Taga, G., 2008. Decrease in cortical activation during learning of a multi-joint discrete motor task. Exp Brain Res 191, 221–236.

Inouye, T., Iyama, A., Shinozaki, K., Toi, S., Matsumoto, Y., 1995. Inter-site EEG relationships before widespread epileptiform discharges. Intern. J. Neuroscience 82, 143–153.

Jafri, M.J., Pearlson, G.D., Stevens, M., Calhoun, V.D., 2008. A method for functional network connectivity among spatially independent resting-state components in schizophrenia. Neuroimage 39, 1666–1681.

Jensen, O., Colgin, L.L., 2007. Cross-frequency coupling between neuronal oscillations. Trends Cogn. Sci. 11, 267–269.

Jeong, J., Gore, J.C., Peterson, B.S., 2001. Mutual information analysis of the EEG in patients with Alzheimer's disease. Clin Neurophysiol 112, 827–835.

Jöbsis, F.F., 1977. Noninvasive, infrared monitoring of cerebral and myocardial oxygen sufficiency and circulatory parameters. Science 198, 1264–1267.

John, O.P., Srivastava, S., 1999. The Big Five trait taxonomy: History, measurement, and theoretical

perspectives. Handbook of personality: Theory and research, 2, 102–138.

Johnston, J.M., Vaishnavi, S.N., Smyth, M.D., Zhang, D., He, B.J., Zempel, J.M., Shimony, J.S., Snyder, A.Z., Raichle, M.E., 2008. Loss of resting interhemispheric functional connectivity after complete section of the corpus callosum. J. Neurosci. 28, 6453–6458.

Jones, E.G., 2002. Thalamic circuitry and thalamocortical synchrony. Philos Trans R Soc Lond B Biol Sci 357, 1659–1673.

Jones, D.T., Vermuri, P., Murphy, M.C., Gunter, J.L., Senjem, M.L., Machulda, M.M., Przybelski, S.A., Gregg, B.E., Kantarci, K., Knopman, D.S., 2012. Non-stationarity in the ‘‘resting brain’s’’ modular architecture. PLoS ONE 7, e39731.

Kang, J., Wang, L., Yan, C., Wang, J., Liang, X., He, Y., 2011. Characterizing dynamic functional connectivity in the resting brain using variable parameter regression and Kalman filtering approaches. Neuroimage 56, 1222–1234.

Karim, H., Fuhrman, S.I., Sparto, P., Furman, J., Huppert, T., 2013. Functional brain imaging of multi-sensory vestibular processing during computerized dynamic posturography using near-infrared spectroscopy. Neuroimage 74, 318–325.

Karim, H., Schmidt, B., Dart, D., Beluk, N., Huppert, T., 2012. Functional near-infrared spectroscopy (fNIRS) of brain function during active balancing using a video game system. Gait & Posture, 35, 367–372.

Kato, T., Kamei, A., Takashima, S., Ozaki, T., 1993. Human visual cortical function duringphotic stimulation monitoring by means of near-infrared spectroscopy. J. Cereb. Blood Flow Metab. 13, 516–520.

Katura, T., Tanaka, N., Obata, A., Sato, H., Maki, A., 2006. Quantitative evaluation of interrelations

between spontaneous low-frequency oscillations in cerebral hemodynamics and systemic cardiovascular dynamics. NeuroImage 31, 1592–1600.

Kelly, A.M.C., Uddin, L.Q., Biswal, B.B., Castellanos, F.X., Milham, M.P., 2008. Competition between functional brain networks mediates behavioral variability. Neuroimage 39, 527–537.

Kennedy, D. P., Courchesne, E., 2008. The intrinsic functional organiza¬tion of the brain is altered in autism. Neuroimage 39, 1877–1885.

Kerns, J.G., Cohen, J.D., MacDonald, III A.W., Cho, R.Y., Stenger, V.A., Carter, C.S., 2004. Anterior cingulate conflict monitoring and adjustments in control. Science 303, 1023–1026.

Kinnison, J., Padmala, S., Choi, J.M., Pessoa, L., 2012. Network analysis reveals increased integration during emotional and motivational processing. J. Neurosci. 32, 8361–8372.

Kitzbichler, M.G., Henson, R.N.A., Smith, M.L., Nathan, P.J., Bullmore, E.T., 2011. Cognitive effort drives workspace configuration of human brain functional networks. J. Neurosci. 31, 8259–8270.

Kleinschmidt, A., Obrig, H., Requardt, M., Merboldt, K.D., Dirnagl, U., Villringer, A., Frahm, J., 1996. Simultaneous recording of cerebral blood oxygenation changes during human brain activation by magnetic resonance imaging and near-infrared spectroscopy. J. Cereb. Blood Flow Metab. 16, 817–826.

Kohno, S., Miyai, I., Seiyama, A., Oda, I., Ishikawa, A., Tsuneishi, S., Amita, T., Shimizu, K., 2007. Removal of the skin blood flow artifact in functional near-infrared spectroscopic imaging data through independent component analysis. J. Biomed. Opt. 12, 062111.

Lagopoulos, J., Malhi, G.S., Cahill, A.M., Lang, E.W., Mudalier, Y., Dorsch, N., Yam, A., Griffith, J., Mulvey, J., 2006. Cerebrovascular autoregulation as a neuroimaging tool. Acta Neuropsychiatrica 18, 100–104.

Latora, V., Marchiori, M., 2001. Efficient behavior of small-world networks. Phys. Rev. Lett. 87, 198701.

Laureys, S., Faymonville, M.E., Luxen, A., Lamy, M., Franck, G., Maquet, P., 2000. Restoration of thalamocortical connectivity after recovery from persistent vegetative state. Lancet 355, 1790–1791.

Lauritzen, M., Gold, L., 2003. Brain function and neurophysiological correlates of signals used in functional neuroimaging. J. Neurosci. 23, 3972–3980.

Leech, R., Kamourieh, S., Beckmann, C.F., Sharp, D.J., 2011. Fractionating the default mode network: distinct contributions of the ventral and dorsal posterior cingulate cortex to cognitive control. J. Neurosci. 31, 3217–3224.

Lennie, P., 2003. The cost of cortical computation. Curr. Biol. 13, 493–497.

Li, Z., Kadivar, A., Pluta, J., Dunlop, J., Wang, Z., 2012. Test-retest stability analysis of resting brain activity revealed by blood oxygen level-dependent functional MRI. J Magn Reson Imaging 36, 344–354.

Li, S. J., Li, Z., Wu, G., Zhang, M. J., Franczak, M., Antuono, P. G., 2002. Alzheimer disease: evaluation of a functional MR imaging index as a marker. Radiology 225, 253–259.

Liang, M., Zhou, Y., Jiang, T., Liu, Z., Tian, L., Liu, H., Hao, Y., 2006. Widespread functional disconnectivity in schizophrenia with resting-state functional magnetic resonance imaging. Neuroreport 17, 209–213.

Liu, Y., Liang, M., Zhou, Y., He, Y., Hao, Y., Song, M., Yu, C., Liu, H., Liu, Z., Jiang, T., 2008. Disrupted small-world networks in schizophrenia. Brain. 131(Pt 4), 945–961.

Liu, H., Liu, Z., Liang, M., Hao, Y., Tan, L., Kuang, F., Yanhong, Y., Xu, L., Jiang, T., 2006. Decreased

regional homogeneity in schizophrenia: a resting state functional magnetic resonance imaging study. Neuroreport 17, 19–22.

Liu, Y., Yu, C., Liang, M., Li, J., Tian, L., Zhou, Y., Qin, W., Li, K., Jiang, T., 2007. Whole brain functional connectivity in the early blind. Brain. 130(Pt 8), 2085–2096.

Logothetis, N.K., 2002. The neural basis of the blood-oxygen-level-dependent functional magnetic resonance imaging signal. Philos. Trans. R. Soc. Lond. B. Biol. Sci. 357, 1003–1037.

Logothetis, N.K., Pauls, J., Augath, M., Trinath, T., Oeltermann, A., 2001. Neurophysiological investigation of the basis of the fMRI signal. Nature 412, 150–157.

Lohmann, G., Margulies, D.S., Horstmann, A., Pleger, B., Lepsien, J., Goldhahn, D., Schloegl, H., Stumvoll, M., Villringer, A., Turner, R., 2010. Eigenvector centrality mapping for analyzing connectivity patterns in fMRI data of the human brain. PLoS One 5, e10232.

Lowe, M.J., Mock, B.J., Sorenson, J.A., 1998. Functional connectivity in single and multislice echoplanar imaging using resting-state fluctuations. Neuroimage 7, 119–132.

Lowe, M. J., Phillips, M. D., Lurito, J. T., Mattson, D. L., Dzemidzic, M., and Mathews, V. P., 2002. Multiple sclerosis: low-frequency temporal blood oxygen level-dependent fluc¬tuations indicate reduced functional connectivity – initial results. Radiology 224, 184–192.

Lu, C.M., Zhang, Y.J., Biswal, B.B., Zang, Y.F., Peng, D.L., Zhu, C.Z., 2010. Use of fNIRS to assess resting state functional connectivity. J. Neurosci. Meth. 186, 242–249.

Lui, S., Ouyang, L., Chen, Q., Huang, X., Tang, H., Chen, H., Zhou, D., Kemp, G. J., Gong, Q., 2008. Differential interictal activity of the precuneus/posterior cingulate cortex revealed by resting state functional MRI at 3T in generalized vs. partial seizure. J. Magn. Reson. Imaging 27, 1214–1220.

Macefield, V.G., 2009. Single-minded about heart failure. J Physiol 587, 2421.

Majeed, W., Magnuson, M., Hasenkamp, W., Schwarb, H., Schumacher, E.H., Barsalou, L., Keilholz, S.D., 2011. Spatiotemporal dynamics of low frequency BOLD fluctuations in rats and humans. Neuroimage 54, 1140–1150.

Maki, A., Yamashita, Y., Ito, Y., Watanabe, E., Mayanagi, Y., Koizumi, H., 1995. Spatial and temporal analysis of human motor activity using noninvasive NIR topography. Med. Phys. 22, 1997–2005.

Macey, P.M., Macey, K.E., Kumar, R., Harper, R.M., 2004. A method for removal of global effects from fMRI time series. Neuroimage 22, 360–366.

Mason, M.F., Norton, M.I., Van Horn, J.D., Wegner, D.M., Grafton, S.T., Macrae, C.N., 2007. Wandering minds: the default network and stimulus independent thought. Science 315, 393–395.

Massimini, M., Ferrarelli, F., Huber, R., Esser, S.K., Singh, H., Tononi. G., 2005. Breakdown of Cortical Effective Connectivity During Sleep. Science 30, 2228–2232.

McAuley, J.J., da Fontoura Costa, L., Caetano, T.S., 2007. Rich-club phenomena across complex network hierachies. Appl Phys Lett 91.

Mennes, M., Zuo, X.N., Kelly, C., Di Martino, A., Zang, Y.F., Biswal, B., Castellanos, F.X., Milham, M.P., 2011. Linking inter-individual differences in neural activation and behavior to intrinsic brain dynamics. Neuroimage 54, 2950–2959.

Menon, V., Adleman, N.E., White, C.D., Glover, G.H., Reiss, A.L., 2001. Error- related brain activation during a Go/NoGo response inhibition task. Hum. Brain Mapp. 12, 131–143.

Menon, V., Uddin, L.Q., 2010. Saliency, switching, attention and control: a network model of insula function. Brain Struct. Funct. 214, 655–667.

Mesquita, R.C., Francheschini, M.A., Boas, A.A., 2010. Resting state functional connectivity of the whole head with near-infrared spectroscopy. Biomed. Opt. Express 1, 324–336.

Mesulam, M.M., 1990. Large-scale neurocognitive networks and distributed processing for attention, language, and memory. Ann. Neurol. 28, 597–613.

Milgram S, 1967. The small-world problem. Psychology Today, 1, 61–67.

Miller, K.J., Sorensen, L.B., Ojemann, J.G., den Nijs, M., 2009. Power-law scaling in the brain surface electric potential. PLoS Comput. Biol. 5, e1000609.

Mitchell, J.P., Heatherton, T.F., Macrae, C.N., 2002. Distinct neural systems subserve person and object knowledge. Proc. Natl Acad. Sci. U. S. A. 99, 15238–15243.

Mitchell, J.P., Macrae, C.N., Banaji, M.R., 2006. Dissociable medial prefrontal contributions to judgments of similar and dissimilar others. Neuron 50, 655–663.

Mizuhara, H., Wang, L.Q., Kobayashi, K., Yamaguchi, Y., 2005. Long-range EEG phase synchronization during an arithmetic task indexes a coherent cortical network simultaneously measured by fMRI. Neuroimage 27, 553–563.

Mohammadi, B., Kollewe, K., Samii, A., Krampfl, K., Dengler, R., Munte, T. F., 2009. Changes of resting state brain networks in amyotrophic lateral sclerosis. Exp. Neurol. 217, 147–153.

Monk, C. S., Peltier, S. J., Wiggins, J. L., Weng, S. J., Carrasco, M., Risi, S., Lord, C., 2009. Abnormalities of intrinsic functional connectiv¬ity in autism spectrum disorders. Neuroimage 47, 764–772.

Morita-Tsuzuki, Y., Bouskela, E., Hardebo, J.E., 1992. Vasomotion in the rat cerebral micro-circulation recorded by laser-Doppler flowmetry. Acta Physiol. Scand. 146, 431–439.

Mormann, F., Lehnerts, K., David, P., Elger, C.E., 2000. Mean phase coherence as a measure for phase synchronization and its application to the EEG of epilepsy patients. Physica D, 144, 358–369.

Mountcastle, V.B., 1957. Modality and topographic properties of single neurons of cat's somatic

sensory cortex. J. Neurophysiol. 20, 408–34.

Moussa, M.N., Vechlekar, C.D., Burdette, J.H., Steen, M.R., Hugenschmidt, C.E., Laurienti, P.J., 2011. Changes in cognitive state alter human functional brain networks. Front. Hum. Neurosci. 5, 83.

Murphy, K., Birn, R.M., Bandettini, P.A., 2013. Resting-state fMRI confounds and cleanup. Neuroimage. 80, 349–359.

Murphy, K., Birn, R.M., Handwerker, D.A., Jones, T.B., Bandettini, P.A., 2009. The impact of global signal regression on resting state correlations: Are anti-correlated networks introduced? Neuroimage 44, 893–905.

Na, S.H., Jin, S.H., Kim, S.Y., Ham, B.J., 2002. EEG in schizophrenic patients: mutual information analysis. Clin Neurophysiol 113, 1954–1960.

Newman, M.E.J., 2003. The structure and function of complex networks. SIAM Rev. 45, 167–256.

Newman, M.E.J., 2004. Fast algorithm for detecting community structure in networks. Phys. Rev., E 69, 066133.

Newman, M.E.J., 2006. Modularity and community structure in networks. Proc. Natl. Acad. Sci. U. S. A. 103, 8577–8582.

Niessing, J., Ebisch, B., Schmidt, K.E., Niessing, M., Singer, W., Galuske, R.A., 2005. Hemodynamic signals correlate tightly with synchronized gamma oscillations. Science 309, 948–951.

Nir, Y., Mukamel, R., Dinstein, I., Privman, E., Harel, M., Fisch, L., Gelbard-Sagiv, H., Kipervasser, S., Andelman, F., Neufeld, M.Y., Kramer, U., Arieli, A., Fried, I., Malach, R., 2008. Interhemispheric correlations of slow spontaneous neuronal fluctuations revealed in human sensory cortex. Nat. Neurosci. 11, 1100–1108.

Obrig, H., Neufang, M., Wenzel, R., Kohl, M., Steinbrink, J., Einhaupl, K., Villringer, A., 2000.

Spontaneous low frequency oscillations of cerebral hemodynamics and metabolism in human adults. Neuroimage 12, 623–639.

Obrig, H., Villringer, A., 2003. Beyond the visible-imaging the human brain with light. J. Cereb. Blood Flow Metab. 23, 1–18.

Ogawa S, Lee TM, 1990 Magnetic resonance imaging of blood vessels at high fields: in vivo and in vitro measurements and image simulation. Magn Reson Med 16, 9 –18.

Ogawa S, Lee TM, Kay AR, Tank DW, 1990a. Brain magnetic resonance imaging with contrast dependent on blood oxygenation. Proc Natl Acad Sci USA 87, 9868 –9872.

Ogawa S, Lee TM, Nayak AS, Glynn P, 1990b. Oxygenation-sensitive contrast in magnetic resonance image of rodent brain at high magnetic fields. Magn Reson Med 14, 68–78.

Okada, E., Firbank, M., Schweiger, M., Arridge, S., Cope, M., Delpy, D., 1997. Theoretical and experimental investigation of near-infrared light propagation in a model of the adult head. Appl. Opt. 36, 21–31.

Okamoto, M., Dan, H., Sakamoto, K., Takeo, K., Shimizu, K., Kohno, S., Oda, I., Isobe, S., Suzuki, T., Kohyama, K., Dan, I., 2004. Three-dimensional probabilistic anatomical cranio-cerebral correlation via the international 10–20 system oriented for transcranial functional brain mapping. Neuroimage 21, 99–111.

Palva, J.M., Palva, S., 2012. Infra-slow fluctuations in electrophysiological recordings, blood-oxygenation-level-dependent signals, and psychophysical time series. Neuroimage 62, 2201–2211.

Pessoa, L., Gutierrez, E., Bandettini, P., Ungerleider, L., 2002. Neural correlates of visual working memory: fMRI amplitude predicts task performance. Neuron 35, 975–987.

Pessoa, L., Padmala, S., 2005. Quantitative prediction of perceptual decisions during near-threshold fear detection. Proc Natl Acad Sci U S A 102, 5612–5617.

Power, J.D., Cohen, A.L., Nelson, S.M., Wig, G.S., Barnes, K.A., Church, J.A., Vogel, A.C., Laumann, T.O., Miezin, F.M., Schlaggar, B.L., Petersen, S.E., 2011. Functional network organization of the human brain. Neuron 72, 665–678.

Raichle M., MacLeod A., Snyder A., Powers W., Gusnard D., Shulman G., 2001. A default mode of brain function. Proc. Natl. Acad. Sci. U. S. A. 98, 676–682.

Raichle, M.E., Mintun, M.A., 2006. Brain work and brain imaging. Annu Rev Neurosci 29, 449–476.

Raichle, M.E., Snyder, A.Z., 2007. A default mode of brain function: a brief history of an evolving idea. Neuroimage 37, 1083-1090; discussion 1097–1089.

Rabinovich, M.I., Friston, K.J., Varona, P. (Eds.), 2012. Principles of Brain Dynamics: Global State Interactions, 1st ed. The MIT Press.

Redcay, E., Dodell-Feder, D., Pearrow, M.J., Mavros, P.L., Kleiner. M., Gabrieli. J.D., Saxe. R., 2010. Live face-to-face interaction during fMRI: a new tool for social cognitive neuroscience. Neuroimage 50, 1639–1647.

Ress, D., Heeger, D.J., 2003. Neuronal correlates of perception in early visual cortex. Nat. Neurosci. 6, 414–420.

Reynolds, E.O., Wyatt, J.S., Azzopardi, D., Delpy, D.T., Cady, E.B., Cope, M., Wray, S., 1988. New non-invasive methods for assessing brain oxygenation and hemodynamics. Br. Med. Bull. 44, 1052–1075.

Ridderinkhof, K.R., Ullsperger, M, Crone, E.A., Nieuwenhuis, S., 2004. The role of the medial frontal cortex in cognitive control. Science 306, 443–447.

Rilling, J.K., Dagenais, J.E., Goldsmith, D.R., Glenn, A.L., Pagnoni, G., 2008. Social cognitive neural networks during in-group and out-group interactions. Neuroimage 41, 1447–1461.

Rilling, J.K., Sanfey, A.G., Aronson, J.A., Nystrom, L.E., Cohen, J.D., 2004. The neural correlates of theory of mind within interpersonal interactions. Neuroimage 22, 1694–1703.

Roche-Labarbe, N., Zaaimi, B., Berquin, P., Nehlig, A., Grebe, R., Wallois, F., 2008. NIRS-measured oxy- and deoxyhemoglobin changes associated with EEG spike-and-wave discharges in children. Epilepsia 49, 1871–1880.

Rubinov, M., Sporns, O., 2010. Complex network measures of brain connectivity: uses and interpretations. Neuroimage 52, 1059–1069.

Saager, R.B., Berger, A.J., 2008. Measurement of layer-like hemodynamic trends in scalp and cortex: implications for physiological baseline suppression in functional near infrared spectroscopy. J. Biomed. Opt. 13, 034017.

Sadaghiani, S., Hesselmann, G., Kleinschmidt, A., 2009. Distributed and antagonistic contributions of ongoing activity fluctuations to auditory stimulus detection. J Neurosci 29, 13410–13417.

Saito, D.N., Tanabe, H.C., Izuma, K., Hayashi, M.J., Morito, Y., Komeda, H., Uchiyama, H., Kosaka, H., Okazawa, H., Fujibayashi, Y., Sadato, N., 2010. “Stay tuned”: inter-individual neural synchronization during mutual gaze and joint attention. Front. Integr. Neurosci. 4, 127.

Salvador, R., Martinez, A., Pomarol-Clotet, E., Gomar, J., Vila, F., Sarro, S., Capdevila, A., Bullmore, E., 2008. A simple view of the brain through a frequency-specific functional connectivity measure. Neuroimage 39, 279–289.

Salvador, R., Martínez, A., Pomarol-Clotet, E., Sarró, S., Suckling, J., Bullmore, E., 2007. Frequency based mutual information measures between clusters of brain regions in functional magnetic

resonance imaging. Neuroimage 35, 83–88.

Salvador, R., Suckling, J., Coleman, M.R., Pickard, J.D., Menon, D., Bullmore, E., 2005a. Neurophysiological architecture of functional magnetic resonance images of human brain. Cereb Cortex 15, 1332–1342.

Salvador, R., Suckling, J., Schwarzbauer, C., Bullmore, E., 2005b. Undirected graphs of frequency-dependent functional connectivity in whole brain networks. Philos Trans R Soc Lond B Biol Sci 360, 937–946.

Sasai, S., Homae, F., Watanabe, H., Sasaki, A.T., Tanabe, H.C., Sadato, N., Taga, G., 2012. A NIRS-fMRI study of resting state network. Neuroimage 63, 179–193.

Sasai, S., Homae, F., Watanabe, H., Taga, G., 2011. Frequency-specific functional connectivity in the brain during resting state revealed by NIRS. Neuroimage 56, 252–257.

Schacter, D.L., Addis, D.R., Buckner, R.L., 2007. Remembering the past to imagine the future: the prospective brain. Nat. Rev. Neurosci. 8, 657–661.

Schilbach L., Wilms M., Eickhoff S.B., Romanzetti S., Tepest R., Bente G., Shah N.J., Fink G.R., Vogeley K., 2010. Minds made for sharing: initiating joint attention recruits reward-related neurocircuitry. J Cogn Neurosci. 22, 2702–2715.

Schroeter, M.L., Kupka, T., Mildner, T., Uludag, K., von Cramon, D.Y., 2006. Investigating the post-stimulus undershoot of the BOLD signal–a simultaneous fMRI and fNIRS study. Neuroimage 30, 349–358.

Schroeter, M.L., Schmiedel, O., von Cramon, D.Y., 2004. Spontaneous low-frequency oscillations decline in the aging brain. J Cereb Blood Flow Metab 24, 1183–1191.

Seeley, W.W., Allman, J.M., Carlin, D.A., Crawford, R.K., Macedo, M.N., Greicius, M.D., Dearmond,

S.J., Miller, B.L., 2007a. Divergent social functioning in behavioral variant fron¬totemporal dementia and Alzheimer disease: reciprocal networks and neu¬ronal evolution. Alzheimer Dis. Assoc. Disord. 21, S50–57.

Seeley, W.W., Crawford, R.K., Miller, B.L., Greicius, M.D., 2008. "Cortical neurodegeneration syndromes target human structural-functional covariance networks," in 14th International Meeting of the Organization for Human Brain Mapping Melbourne, Australia.

Seeley, W.W., Menon, V., Schatzberg, A.F., Keller, J., Glover, G.H., Kenna, H., Reiss, A.L., Greicius, M.D., 2007b. Dissociable intrinsic connectivity networks for salience processing and executive control. J Neurosci 27, 2349–2356.

Shehzad, Z., Kelly, A.M., Reiss, P.T., Gee, D.G., Gotimer, K., Uddin, L.Q., Lee, S.H., Margulies, D.S., Roy, A.K., Biswal, B.B., Petkova, E., Castellanos, F.X., Milham, M.P., 2009. The resting brain: unconstrained yet reliable. Cereb. Cortex 19, 2209–2229.

Sheline, Y. I., Raichle, M. E., Snyder, A. Z., Morris, J. C., Head, D., Wang, S., and Mintun, M.A., 2010. Amyloid plaques disrupt resting state default mode network connectivity in cognitively normal elderly. Biol. Psychiatry 67, 584–587.

Shmueli, K., van Gelderen, P., de Zwart, J.A., Horovitz, S.G., Fukunaga, M., Jansma, J.M., Duyn, J.H., 2007. Low-frequency fluctuations in the cardiac rate as a source of variance in the resting-state fMRI BOLD signal. Neuroimage 38, 306–320.

Shulman, G.L., McAvoy, M.P., Cowan, M.C., Astafiev, S.V., Tansy, A.P., d'Avossa, G., Corbetta, M., 2003. Quantitative analysis of attention and detection signals during visual search. J. Neurophysiol. 90, 3384–3397.

Shulman, R. G., Rothman, D. L., Behar, K. L. Hyder, F. 2004. Energetic basis of brain activity:

implications for neuroimaging. Trends Neurosci. 27, 489–495.

Siegel, M., Donner, T.H., Engel, A.K., 2012. Spectral fingerprints of large-scale neuronal interactions. Nat Rev Neurosci 13, 121–134.

Siegel, M., Donner, T.H., Oostenveld, R., Fries, P., Engel, A.K., 2008. Neuronal synchronization along the dorsal visual pathway reflects the focus of spatial attention. Neuron 60, 709–719.

Simons, J.S., Henson, R.N., Gilbert, S.J., Fletcher, P.C., 2008. Separable forms of reality monitoring supported by anterior prefrontal cortex. J. Cogn. Neurosci. 20, 447–457.

Smallwood, J., Beach, E., Schooler, J.W., Handy, T.C., 2008. Going AWOL in the brain: mind wandering reduces cortical analysis of external events. J. Cogn. Neurosci. 20, 458–469.

Smith, S.M., Miller, K.L., Moeller, S., Xu, J., Auerbach, E.J., Woolrich, M.W., Beckmann, C.F., Jenkinson, M., Andersson, J., Glasser, M.F., Van Essen, D.C., Feinberg, D.A., Yacoub, E.S., Ugurbil, K., 2012. Temporally-independent functional modes of spontaneous brain activity. Proc Natl Acad Sci U S A 109, 3131–3136.

Sorg, C., Riedl, V., Muhlau, M., Calhoun, V. D., Eichele, T., Laer, L., Drzezga, A., Forstl, H., Kurz, A., Zimmer, C., and Wohlschlager, A. M., 2007. Selective changes of resting-state networks in individuals at risk for Alzheimer's dis¬ease. Proc. Natl. Acad. Sci. U.S.A. 104, 18760–18765.

Sporns, O., 2013. Network attributes for segregation and integration in the human brain. Curr Opin Neurobiol. 23, 162–171.

Sporns, O., Honey, C.J., Kötter, R., 2007. Identification and classification of hubs in brain networks. PLoS One 2, e1049.

Spreng, R.N., Mar, R.A., Kim, A.S., 2009. The common neural basis of autobiographical memory, prospection, navigation, theory of mind, and the default mode: a quantitative meta-analysis. J.

Cogn. Neurosci. 21, 489–510.

Spreng, R.N., Sepulcre, J., Turner, G.R., Stevens, W.D., Schacter, D.L., 2013. Intrinsic architecture underlying the relations among the default, dorsal attention, and frontoparietal control networks of the human brain. J. Cogn. Neurosci. 25, 74–86.

Spreng, R.N., Stevens, W.D., Chamberlain, J.P., Gilmore, A.W., Schacter, D.L., 2010. Default network activity, coupled with the frontoparietal control network, supports goal-directed cognition. Neuroimage 53, 303–317.

Sridharan D., Levitin D.J., Menon V., 2008. A critical role for the right fronto-insular cortex in switching between central-executive and default-mode networks. Proc. Natl. Acad. Sci. U. S. A. 105, 12569–12574.

Steinbrink, J., Villringer, A., Kempf, F., Haux, D., Boden, S., Obrig, H., 2006. Illuminating the BOLD signal: combined fMRI–fNIRS studies. Mag. Res. Imaging 24, 495–505.

Steriade, M., Contreras, D., Curró Dossi, R., Nuñez, A., 1993. The slow (< 1 Hz) oscillation in reticular thalamic and thalamocortical neurons: scenario of sleep rhythm generation in interacting thalamic and neocortical networks. J Neurosci 13, 3284–3299.

Strogatz, S.H., 2001. Exploring complex networks. Nature 410, 268–276.

Strangman, G., Culver, J., Thompson, J., Boas, D., 2002. A quantitative comparison of simultaneous BOLD fMRI and NIRS recordings during functional brain activation. Neuroimage 17, 719–31.

Suda, M., Takei, Y., Aoyama, Y., Narita, K., Sato, T., Fukuda, M., Mikuni, M., 2010. Frontopolar activation during face-to-face conversation: an in situ study using near-infrared spectroscopy. Neuropsychologia 48, 441–447.

Sun, F.T., Miller, L.M., D'Esposito, M., 2003. Measuring interregional functional connectivity using

coherence and partial coherence analyses of fMRI data. Neuroimage 21, 647–658.

Supekar, K., Menon, V., Rubin, D., Musen, M., Greicius, M.D., 2008. Network analysis of intrinsic functional brain connectivity in Alzheimer's disease. PLoS Comput Biol 4, e1000100.

Tachtsidis, I., Leung, T., Tisdall, M., Devendra, P., Smith, M., Delpy, D., Elwell, C., 2008. Investigation of frontal cortex, motor cortex and systemic haemodynamic changes during anagram solving. Adv. Exp. Biol. 614, 21–28.

Taga, G., Konishi, Y., Maki, A., Tachibana, T., Fujiwara, M., Koizumi, H., 2000. Spontaneous oscillation of oxy- and deoxy-hemoglobin changes with a phase difference throughout the occipital cortex of newborn infants observed using noninvasive optical topography. Neurosci. Lett. 282, 101–104.

Taga, G., Watanabe, H. Homae, F., 2011. Spatiotemporal properties of cortical hemodynamic response to auditory stimuli in sleeping infants revealed by multi-channel NIRS. Phil. Trans. R. Soc. A 369, 4495–4511.

Takahashi, T., Takikawa, Y., Kawagoe, R., Shibuya, S., Iwano, T., 2011. Influence of skin blood flow on near-infrared spectroscopy signals measured on the forehead during a verbal fluency task. Neuroimage 57, 991–1002.

Tass, P., Rosenblum, M.G., Weule, J., Pikovski, A., Volkmann, J., Schnitzler, A., Freund, H.J., 1998. Detection of n:m Phase Locking from Noisy Data: Application to Magnetoencephalography. Phys. Rev. Lett. 81, 3291–3294.

Thomason, M.E., Dennis, E.L., Joshi, A.A., Joshi, S.H., Dinov, I.D., Chang, C., Henry, M.L., Johnson, R.F., Thompson, P.M., Toga, A.W., Glover, G.H., Van Horn, J.D., Gotlib, I.H., 2011. Resting-state fMRI can reliably map neural networks in children. Neuroimage 55, 165–175.

Tian, L., Jiang, T., Wang, Y., Zang, Y., He, Y., Liang, M., Sui, M., Cao, Q., Hu, S., Peng, M., Zhuo, Y., 2006. Altered resting-state functional connectivity patterns of anterior cingulate cortex in adolescents with attention deficit hyperactivity disorder. Neurosci. Lett. 400, 39–43.

Tognoli, E., Lagarde, J., DeGuzman, G.C., Kelso. J.A., 2007. The phi complex as a neuromarker of human social coordination. Proc. Natl. Acad. Sci. U.S.A. 104, 8190–8195.

Tomasi, D., Volkow, N.D., 2011a. Association between functional connectivity hubs and brain networks. Cereb. Cortex 21, 2003–2013.

Tomasi, D., Volkow, N.D., 2011b. Functional connectivity hubs in the human brain. Neuroimage 57, 908–917.

Tong, Y., Frederick, B., 2010. Time lag dependent multimodal processing of concurrent fMRI and near-infrared spectroscopy (NIRS) data suggests a global circulatory origin for low-frequency oscillation signals in human brain. Neuroimage 53, 553–64.

Tononi, G., Sporns, O., Edelman, G.M., 1994. A measure for brain complexity: relating functional segregation and integration in the nervous system. Proc. Natl. Acad. Sci. U.S.A. 91, 5033–5037.

Toronov, V., Franceschini, M., Filiaci, M., Fantini, S., Wolf, M., Michalos, A., Gratton, E., 2000. Near-infrared study of fluctuations in cerebral hemodynamics during rest and motor stimulation: temporal analysis and spatial mapping. Med. Phys. 27, 801–815.

Toronov, V., Webb, A., Choi, J., 2001. Investigation of human brain hemodynamics by simultaneous near-infrared spectroscopy and functional magnetic resonance imaging. Med. Phys. 28, 521–527.

Toyoda, H., Kashikura, K., Ikada, T., Nakashita, S., Honda, M., Yonekura, Y., Kawaguchi, H., Maki, A., Sadato, N., 2008. Source of nonlinearity of the BOLD response revealed by simultaneous fMRI and NIRS. Neuroimage 39, 997–1013.

Tzourio-Mazoyer, N., Landeau, B., Papathanassiou, D., Crivello. F., Etard, O., Delcroix, N., Mazoyer, B., Joliot, M., 2002. Automated anatomical labeling of activations in SPM using a macroscopic anatomical parcellation of the MNI MRI single-subject brain. Neuroimage 15, 273–289.

van den Heuvel, M.P., Hulshoff H.E., 2010. Exploring the brain network: A review on resting-state fMRI functional connectivity. Eur. Neuropsychopharmacol. 20, 519–534.

van den Heuvel, M.P., Mandl, R.C., Hulshoff Pol, H.E., 2008a. Normalized group clustering of resting-state fMRI data. PLoS ONE 3, e2001.

van den Heuvel, M.P., Mandl, R. C., Kahn, R. S., Hulshoff Pol, H.E., 2009. Functionally linked resting-state networks reflect the underlying structural connectivity architecture of the human brain. Hum. Brain Mapp. 30, 3127–3141.

van den Heuvel, M.P., Sporns, O., 2011. Rich-club organization of the human connectome. J. Neurosci. 31, 15775–15786.

van den Heuvel, M.P., Stam, C.J., Boersma, M., Hulshoff Pol, H.E., 2008b. Small-world and scale-free organization of voxel-based resting-state functional connectivity in the human brain. Neuroimage 43, 528–539.

van de Ven, V.G., Formisano, E., Prvulovic, D., Roeder, C.H., Linden, D.E., 2004. Functional connectivity as revealed by spatial independent component analysis of fMRI measurements during rest. Hum. Brain Mapp. 22, 165–178.

van der Zee, P., Arridge, S., Cope, M., Delpy, D., 1990. The effect of optode positioning on optical pathlength in near infrared spectroscopy of brain. Adv. Exp. Med. Biol. 277, 79–84.

Van Dijk, K.R., Hedden, T., Venkataraman, A., Evans, K.C., Lazar, S.W., Buckner, R.L., 2010. Intrinsic functional connectivity as a tool for human connectomics: theory, properties, and optimization. J.

Neurophysiol. 103, 297–321.

Van Essen, D.C., Anderson, C.H., Felleman, D.J., 1992. Information processing in the primate visual system: an integrated systems perspective. Science 255, 419–423.

Vanhaudenhuyse, A., Noirhomme, Q., Tshibanda, L.J., Bruno, M.A., Boveroux, P., Schnakers, C., Soddu, A., Perlbarg, V., Ledoux, D., Brichant, J.F., Moonen, G., Maquet, P., Greicius, M.D., Laureys, S., Boly, M., 2010. Default network connectivity reflects the level of consciousness in non-communicative brain-damaged patients. Brain 133, 161–171.

Varela, F., Lachaux, J.P., Rodriguez, E., Martinerie, J., 2001. The brainweb: phase synchronization and large-scale integration. Nat. Rev. Neurosci. 2, 229–239.

Villringer, A., Planck, J., Hock, C., Schleinkofer, L., Dirnagl, U., 1993. Near infrared spectroscopy (NIRS): a new tool to study hemodynamic changes during activation of brain function in human adults. Neurosci. Lett. 154, 101–104.

Vincent, J., Kahn, I., Snyder, A., Raichle, M., Buckner, R., 2008. Evidence for a frontoparietal control system revealed by intrinsic functional connectivity. J Neurophysiol 100, 3328–3342.

Vincent, J., Patel, G., Fox, M., Snyder, A., Baker, J., Van Essen, D., Zempel, J., Snyder, L., Corbetta, M., Raichle, M., 2007. Intrinsic functional architecture in the anaesthetized monkey brain. Nature, 447, 83–6.

Viswanathan, A., Freeman, R.D., 2007. Neurometabolic coupling in cerebral cortex reflects synaptic more than spiking activity. Nat. Neurosci. 10, 1308–1312.

Vogels, R., Spileers, W., Orban, G.A., 1989. The response variability of striate cortical neurons in the behaving monkey. Exp. Brain Res. 77, 432–436.

von der Malsburg, C., Phillips, W.A., Singer, W. (Eds.), 2010. Dynamic Coordination in the Brain:

From Neurons to Mind. The MIT Press.

Wagner, A.D., Schacter, D.L., Rotte, M., Koutstaal, W., Maril, A., Dale, A.M., Rosen, B.R., Buckner, R.L., 1998. Building memories: remembering and forgetting of verbal experiences as predicted by brain activity. Science 281, 1188–1191.

Waites, A. B., Briellman, R. S., Saling, M. M., Abbott, D. F., Jackson, G. D., 2006. Functional connectivity networks are disrupted in left tem¬poral lobe epilepsy. Ann. Neurol. 59, 335–343.

Wang, K., Jiang, T., Liang, M., Wang, L., Tian, L., Zhang, X., Li, K., Liu, Z., 2006a. Discriminative analysis of early Alzheimer's disease based on two intrinsically anti-correlated networks with resting-state fMRI. Med. Image Comput. Comput. Assist. Interv. Int. Conf. Med. Image Comput. Comput. Assist. Interv. 9, 340–347.

Wang, L., Zang, Y., He, Y., Liang, M., Zhang, X., Tian, L., Wu, T., Jiang, T., Li, K., 2006b. Changes in hippocampal connectivity in the early stages of Alzheimer's disease: evidence from resting state fMRI. Neuroimage 31, 496–504.

Wang, K., Liang, M., Wang, L., Tian, L., Zhang, X., Li, K., Jiang, T., 2007. Altered functional connectivity in early Alzheimer's disease: a resting-state fMRI study. Hum. Brain Mapp. 28, 967–978.

Wang, L., Zhu, C., He, Y., Zang, Y., Cao, Q., Zhang, H., Zhong, Q., Wang, Y., 2009. Altered small-world brain functional networks in children with attention-deficit/hyperactivity disor¬der. Hum. Brain Mapp. 30, 638–649.

Watts, D.J., Strogatz, S.H., 1998. Collective dynamics of 'small-world' networks. Nature 393, 440–442.

Wei, L., Duan, X., Zheng, C., Wang, S., Gao, Q., Zhang, Z., Lu, G., Chen, H., 2012. Specific frequency

bands of amplitude low-frequency oscillation encodes personality. Hum Brain Mapp. http://dx.doi.org/10.1002/hbm.22176 (in press).

Weng, S.J., Wiggins, J.L., Peltier, S.J., Carrasco, M., Risi, S., Lord, C., and Monk, C.S., 2010. Alterations of resting state functional connectivity in the default network in adolescents with autism spectrum disorders. Brain Res. 1313, 202–214.

White, B., Liao, S., Ferradal, S., Inder, T., Culver, J., 2012. Bedside optical imaging of occipital resting-state functional connectivity in neonates. Neuroimage 59, 2529–2538.

White, B., Snyder, A., Cohen, A., Petersen, S., Raichle, M., Schlaggar, B., Culver, J., 2009. Resting-state functional connectivity in the human brain revealed with diffuse optical tomography. Neuroimage 47, 148–156.

Whitfield-Gabrieli, S., Thermenos, H. W., Milanovic, S., Tsuang, M. T., Faraone, S. V., McCarley, R. W., Shenton, M. E., Green, A. I., Nieto-Castanon, A., LaViolette, P., Wojcik, J., Gabrieli, J. D., and Seidman, L. J., 2009. Hyperactivity and hypercon¬nectivity of the default network in schizophrenia and in first-degree relatives of persons with schizophre¬nia. Proc. Natl. Acad. Sci. U.S.A. 106, 1279–1284

Windischberger, C., Langenberger, H., Sycha, T., Tschernko, E., Fuchsjager-Mayerl, G., Schmetterer, L., Moser, E., 2002. On the origin of respiratory artifacts in BOLD-EPI of the human brain. Magn. Reson. Imaging 20, 575–582.

Wise, R.G., Ide, K., Poulin, M.J., Tracey, I., 2004. Resting fluctuations in arterial carbon dioxide induce significant low frequency variations in BOLD signal. Neuroimage 21, 1652–1664.

Wu, C.W., Lu, H., Stein, E.A., Chen, J., Yang, Y., 2008. Frequency specificity of functional connectivity in brain networks. Neuroimage 42, 1047–1055.

Yamada, T., Umeyama, S., Matsuda, K., 2009. Multidistance probe arrangement to eliminate artifacts in functional near-infrared spectroscopy. J. Biomed. Opt. 16, 06434.

Yu, C., Liu, Y., Li, J., Zhou, Y., Wang, K., Tian, L., Qin, W., Jiang, T., Li, K., 2008. Altered functional connectiv¬ity of primary visual cortex in early blindness. Hum. Brain Mapp. 29, 533–543.

Zang, Y. F., He, Y., Zhu, C. Z., Cao, Q. J., Sui, M. Q., Liang, M., Tian, L. X., Jiang, T. Z., Wang, Y. F., 2007. Altered baseline brain activity in children with ADHD revealed by resting-state func¬tional MRI. Brain Dev. 29, 83–91.

Zhang, Q., Brown, E.N., Strangman, G.E., 2007. Adaptive filtering to reduce global interference in evoked brain activity detection: a human subject case study. J. Biomed. Opt. 12, 064009.

Zhang, H., Duan, L., Zhang, Y., Lu, C., Liu, H., Zhu, C., 2011. Test–retest assessment of independent component analysis-derived resting-state functional connectivity based on functional near-infrared spectroscopy. Neuroimage 55, 607–615.

Zhang, Z., Lu, G., Zhong, Y., Tan, Q., Liao, W., Chen, Z., Shi, J., and Liu, Y., 2009a. Impaired perceptual networks in temporal lobe epilepsy revealed by resting fMRI. J. Neurol. 256, 1705–1713.

Zhang, Z., Lu, G., Zhong, Y., Tan, Q., Yang, Z., Liao, W., Chen, Z., Shi, J., and Liu, Y., 2009b. Impaired attention network in temporal lobe epilepsy: a resting FMRI study. Neurosci. Lett. 458, 97–101.

Zhang, D., Snyder, A.Z., Shimony, J.S., Fox, M.D., Raichle, M.E., 2010a. Noninvasive functional and structural connectivity mapping of the human thalamocortical system. Cereb Cortex 20, 1187–1194.

Zhang, H., Zhang, Y., Lu, C., Ma, S., Zang, Y., Zhu, C., 2010b. Functional connectivity as revealed by independent component analysis of resting-state fNIRS measurements. Neuroimage 51,

1150–1161.

Zhou, Y., Liang, M., Jiang, T., Tian, L., Liu, Y., Liu, Z., Liu, H., and Kuang, F., 2007. Functional dysconnectivity of the dor¬solateral prefrontal cortex in first-epi¬sode schizophrenia using resting-state fMRI. Neurosci. Lett. 417, 297–302.

Zhu, C. Z., Zang, Y. F., Cao, Q. J., Yan, C. G., He, Y., Jiang, T. Z., Sui, M. Q., and Wang, Y. F., 2008. Fisher discrimina¬tive analysis of resting-state brain func¬tion for attention-deficit/hyperactivity disorder. Neuroimage 40, 110–120.

Zhu, C. Z., Zang, Y. F., Liang, M., Tian, L. X., He, Y., Li, X. B., Sui, M. Q., Wang, Y. F., and Jiang, T. Z., 2005. Discriminative analysis of brain function at resting-state for attention-deficit/hyperactivity disor¬der. Med. Image Comput. Comput. Assist. Interv. Int. Conf. Med. Image Comput. Comput. Assist. Interv. 8, 468–475.

Zuo, X.N., Di Martino, A., Kelly, C., Shehzad, Z.E., Gee, D.G., Klein, D.F., Castellanos, F.X., Biswal, B.B., Milham, M.P., 2010a. The oscillating brain: complex and reliable. Neuroimage 49, 1432–1445.

Zuo, X.N., Kelly, C., Adelstein, J.S., Klein, D.F., Castellanos, F.X., Milham, M.P., 2010b. Reliable intrinsic connectivity networks: test–retest evaluation using ICA and dual regression approach. Neuroimage 49, 2163–2177.